Numerical modeling of abdominal aortic aneurysm expansion

Virag, Lana

University of Zagreb

FACULTY OF MECHANICAL ENGINEERING AND NAVAL ARCHITECTURE

Lana Virag

NUMERICAL MODELING OF ABDOMINAL AORTIC ANEURYSM EXPANSION

DOCTORAL DISSERTATION

Zagreb, 2017

UNIVERSITY OF ZAGREB
FACULTY OF MECHANICAL ENGINEERING AND NAVAL ARCHITECTURE

Lana Virag

NUMERICAL MODELING OF ABDOMINAL AORTIC ANEURYSM EXPANSION

DOCTORAL DISSERTATION

Supervisor: Igor Karšaj, Associate Professor

Zagreb, 2017

Sveučilište u Zagrebu

FAKULTET STROJARSTVA I BRODOGRADNJE

Lana Virag

NUMERIČKO MODELIRANJE RASTA ANEURIZME ABDOMINALNE AORTE

DOKTORSKI RAD

Mentor: izv. prof. dr. sc. Igor Karšaj

Zagreb, 2017.

BIBLIOGRAPHY DATA

UDC: 616.13-007:519.6

Keywords: abdominal aortic aneurysm, intraluminal thrombus, growth and remodeling, proteolytic activity, rupture risk factors

Scientific area: technical sciences

Scientific field: mechanical engineering

Institution: Faculty of Mechanical Engineering and Naval Architecture

Thesis supervisor: Assoc. Prof. Igor Karšaj

Number of pages: 144

Number of pages (in total): 152

Number of figures: 52

Number of tables: 6

Number of references: 195

Date of examination: February 10, 2017

Thesis defense commission:

Prof. Jurica Sorić – Chairman of defense commission

Jay D. Humphrey, John C. Malone Professor of Biomedical Engineering – member

Prof. Gerhard A. Holzapfel, PhD– member

Prof. Ivo Lovričević – member

Assoc. Prof. Igor Karšaj – supervisor

Archive: Faculty of Mechanical Engineering and Naval Architecture

ACKNOWLEDGMENTS

I would like to begin expressing my deepest gratitude to my supervisor, Professor Igor Karšaj for giving me the opportunity to participate in this interdisciplinary research, for guidance, patience and constant support. Special thanks goes to Prof Jay Humphrey and John Wilson, MD, PhD for their valuable advices, discussions and guidance throughout this work. My sincere thanks to the Committee members, Prof. Gerhard Holzapfel, Prof. Jurica Sorić and Prof. Ivo Lovričević for the helpful suggestions and for their time to read the Thesis.
I would also like to thank my colleagues and friends at the Faculty of Mechanical Engineering and Naval Architecture for creating an enjoyable and productive working environment.

Lana Virag
Zagreb, February 2017

SPECIAL ACKNOWLEDGMENT

I wish to express my deepest gratitude to the Croatian Science Foundation for supporting the research conducted in this Thesis under an Installation grant (I. Karšaj), and the projects "Multiscale Numerical Modeling of Material Deformation Responses from Macro- to Nanolevel" (J. Sorić) and "BioChemoMechanical Modeling of Aneurysmal Growth" (I. Karšaj).

Lana Virag
Zagreb, February 2017

Contents

List of figures

List of tables

Nomenclature

A_0^{VV}	Initial area of *vasa vasorum*
A_{tot}^{VV}	Total area of *vasa vasorum*
$\mathbf{C}$, $\mathbf{C}_{n(\tau)}^{k}$	Cauchy-Green tensors
$\mathbb{C}$	Tangent modulus
$\mathbb{C}_{sph}$	Volumetric part of tangent modulus
$\overline{\mathbb{C}}$	Isochoric part of tangent modulus
$\mathbb{C}_{act}$	Active part of tangent modulus
c_1^k , c_2^k c_3^k , c_e	Material parameters
D	Diffusion coefficient
$\mathbf{e}_\theta$	Unit vector in circumferential direction
$\mathbf{F}$, ${}_0^s\mathbf{F}$, $\mathbf{F}_{n(\tau)}^{k}$	Deformation gradients
$\overline{\mathbf{F}}$	Isochoric part of deformation gradient
G_h^k	Homeostatic pre-stretch of fiber *k*
$\mathbf{G}^k$	Pre-stretch tensor of constituent *k*
I_1	First invariant of Cauchy-Green tensor
I_4	Forth invariant of Cauchy-Green tensor
J	Jacobian
K_q^k	Rate-type parameter of mass removal of constituent *k*
K_σ^k	Rate-type parameter governing stress-driven mass production
$K_{plt,\phi}^f$	Correlation parameter between production of fibrin , amount of platelets and mass fraction of fibrin
K_N^{pls}	Correlation factor between plasmin and neutrophils in the ILT
K_f^{pls}	Amount of plasmin consumed per unit of fibrin
K_{EDP}^{pls}	Correlation parameter between plasmin and EDPs
K_{VV}^{pls}	Correlation parameter between plasmin and *vasa vasorum*
K_{EDP}^{VV}	Correlation factor that relates *vasa vasorum* growth per unit of EDPs per unit time

$K_{\max}^{aniso}$	Maximal measure of mechanical anisotropy
K_{t}^{aniso}	Correlation factor that relates anisotropy and age of luminal layer of thrombus
$K_{\tau_w}^{aniso}$	Correlation factor that relates anisotropy and change of wall shear stress
$K_{EDP,VV}^{WBC}$	Correlation factor that relates the proliferation of white blood cells with EDPs and neovascularization
k_1, k_2	Fibrin stiffness parameters
L	Axial force
M^k	Mass of constituent k
M_{crit}^{f}	Critical mass of fibrin
M_{wall}^{pls}	Mass of plasmin in the wall
M_{tot}^{EDP}	Total mass of elastin degradation products
M_{tot}^{N}	Total mass of leukocytes in the luminal layer
M_{tot}^{WBC}	Total mass of leukocytes in the wall
$\dot{m}^k$	Rate of production of constituent k
m_B^k	Basal production of constituent k
$\mathbf{m}^k$	Orientation of fiber k
P	Blood pressure
P_h	Homeostatic blood pressure
Q	Blood flow
Q_h	Homeostatic blood flow
Q^k	Percentage of initial mass of constituent k remaining in current time s
$q^k(s-\tau)$	Survival function of constituent k produced in time τ in time s
r_l	Luminal radius
r_i	Radius at the luminal/intimal interface
r_m	Radius at the intimal/medial interface
r_a	Radius at the medial/abluminal interface
r_o	Outer radius

r_{crit}	Critical radius for formation of luminal layer
r_L	The location of the source of the proteases
S	Growth and remodeling time
T_m	Maximal active stress
$\mathbf{t}$	Cauchy stress
$\mathbf{t}_{\mathrm{h}}^{k}$	Homeostatic Cauchy stress of constituent *k*
$\mathbf{t}^{k}$	Cauchy stress experienced by constituent *k*
t^{active}	Active stress contribution from smooth muscle contractility
$\mathbf{t}_{sph}$	Volumetric part of Cauchy stress
$\bar{\mathbf{t}}$	Isochoric part of Cauchy stress
W	Overall stored energy function
W^k	Stored energy function of constituent *k*
$\hat{W}^k$	Specific stored energy function of constituent *k*
W_{sph}	Volumetric part of stored energy function
$\overline{W}$	Isochoric part of stored energy function
w_q^f	Weighting function for degradation of fibrin
$w_{q,elas}^e$	Weighting factor between amount of elastase and degradation of elastin
$w_{q,MMP}^c$	Weighting factor between amount of MMP and degradation of collagen
α	Power parameter
β_m	Scaling parameter that controlled the degree of proportionality between elastin content and vasoactivity
ϕ^k	Mass fraction of constituent *k*
ϕ_{int} , ϕ_{med} , ϕ_{adv}	Volume fractions of intima, media and adventitia
λ	Fiber stretch
λ_{m}	Stretch at which the active stress is maximal
λ_0	Stretch at which the active stress is zero
μ	Blood viscosity
μ^f	Fibrin stiffness parameter

ρ	Wall density
ρ^{aniso}	Measure of mechanical anisotropy of luminal layer
τ	Arbitrary time
$\tau_{crit}^{i,1}$	Time at which a critical mass of fibrin was achieved
$\tau_{crit}^{i,2}$	Time at which the critical mass fraction of fibrin was reached
$\tau_{1/2}^{k}$	Half-life of constituent, cell or molecule *k*
$\tau_{i,0}$	Time at which the current luminal layer was formed
τ_{w}	Wall shear stress
$\tau_{w,h}$	Homeostatic wall shear stress

Biochemical terms and definitions

Staining

TUNEL – a method for detecting DNA fragmentation by labeling the terminal end of nucleic acids; stains dying cells

RANTES – is a activation protein; abbreviation for 'regulated on activation, normal T cell expressed and secreted'; stains platelets

SPIO and USPIO – magnetic resonance imaging contrast agents used to improve the visibility of internal body structures, two types of iron oxide contrast agents: superparamagnetic iron oxide (SPIO) and ultrasmall superparamagnetic iron oxide (USPIO).

Molecules and cells

angiotensin II (Ang-II) – hormone that causes vasoconstriction and a subsequent increase in blood pressure

Apolipoprotein E (Apo-E) – produced by macrophages, transports lipoproteins, fat-soluble vitamins, and cholesterol into the lymph system and then into the blood. In the field of immune regulation, a growing number of studies point to Apo-E's interaction with many immunological processes, including suppressing T-cell proliferation, macrophage functioning regulation etc.

α1-antitrypsin (α1-AT) – is a protease inhibitor, it inhibits a wide variety of proteases, protects tissues from enzymes of inflammatory cells, especially neutrophil elastase

α2-antiplasmin (α2-AP) – a serine protease inhibitor (serpin) responsible for inactivating plasmin

Cathepsin G – plays an important role in eliminating intracellular pathogens and breaking down tissues at inflammatory sites, as well as in anti-inflammatory response

EDP – Elastin degradation products

FDP – Fibrin degradation product

fXIIa, fXIIIa – activated fibrin stabilizing factors, enzymes of the blood coagulation system that crosslink fibrin. Deficiency of these factors affects clot stability

IL – Interleukins are a group of cytokines (secreted proteins and signal molecules) expressed by white blood cells (leukocytes). The function of the immune system depends in a large part on interleukins. Seventeen types of interleukins exist

interferon-γ (IFN-γ) – is a cytokine (cell signaling protein) that is critical for innate and adaptive immunity against viral, some bacterial and protozoal infections. IFNγ is an important

activator of macrophages. Aberrant IFNγ expression is associated with a number of autoinflammatory and autoimmune diseases. The importance of IFNγ in the immune system stems in part from its ability to inhibit viral replication directly, and most importantly from its immunostimulatory and immunomodulatory effects

JNK, pJNK – c-Jun N-terminal kinase, activated by Inflammatory signals, changes in levels of reactive oxygen species, ultraviolet radiation, protein synthesis inhibitors, and a variety of stress stimuli, JNK1 is involved in apoptosis, neurodegeneration, cell differentiation and proliferation, inflammatory conditions and cytokine production

LE – leukocyte elastase, enzyme that degrades elastin

Macrophages – large white blood cells that engulf and digest cellular debris, foreign substances, microbes, cancer cells, and anything else that does not have the types of proteins specific to healthy body cells on its surface in a process called phagocytosis. Found in all tissues

MMP – matrix metalloproteinases are proteases involved in the cleavage of cell surface receptors, the release of apoptotic ligands (such as the FAS ligand), and chemokine/cytokine inactivation. MMPs are also thought to play a major role in cell behaviors such as cell proliferation, migration (adhesion/dispersion), differentiation, angiogenesis, apoptosis, and host defense. Collectively, these enzymes are capable of degrading all kinds of extracellular matrix proteins, but also can process a number of bioactive molecules. Latent forms are called proMMPs

NGAL – Neutrophil gelatinase associated lipocalin, NGAL is involved in innate immunity by sequestrating iron that in turn limits bacterial growth

PAI-1 – plasminogen activator inhibitor-1 also known as endothelial plasminogen activator inhibitor or serpin E1 is a protein that in humans is encoded by the SERPINE1 gene. Elevated PAI-1 is a risk factor for thrombosis and atherosclerosis

RBC – red blood cells, erythrocytes

TFG-β – Transforming growth factor beta is a multifunctional cytokine, secreted by many cell types, including macrophages. Activation of TGF-β complexes leads to the activation of different downstream substrates and regulatory proteins, inducing transcription of different target genes that function in differentiation, chemotaxis, proliferation, and activation of many immune cells

TIMP –tissue inhibitors of metalloproteinases; comprise a family of four protease inhibitors: TIMP1, TIMP2, TIMP3 and TIMP4

TNF-α – Tumor necrosis factor is a cell signaling protein (cytokine) involved in systemic inflammation. It is produced chiefly by activated macrophages, although it can be produced by many other cell types. The primary role of TNF is in the regulation of immune cells

tPA – tissue plasminogen activator, similar to uPa, but found on endothelial cells, the cells that line the blood vessels. As an enzyme, it catalyzes the conversion of plasminogen to plasmin

uPA – urokinase, also known as urokinase-type plasminogen activator (uPA), was originally isolated from human urine, and it is also present in the blood and in the extracellular matrix of many tissues. The primary physiological substrate of this enzyme is plasminogen, which is an inactive form of the serine protease plasmin. Activation of plasmin triggers a proteolytic cascade that, depending on the physiological environment, participates in thrombolysis or extracellular matrix degradation

WBC – white blood cells, also called leukocytes, are the cells of the immune system that are involved in protecting the body against both infectious disease and foreign invaders. Types of white blood cells can be classified into the five main types: neutrophils, eosinophils, basophils, lymphocytes, and monocytes. These types are distinguished by their physical and functional characteristics.

Biochemical processes

Anoikis is a form of programmed cell death that occurs in anchorage-dependent cells when they detach from the surrounding extracellular matrix (ECM). (from Ancient Greek ἀπόπτωσις "falling off") is a process of programmed cell death that occurs in multicellular organisms. Biochemical events lead to characteristic cell changes (morphology) and death.

Abstract

Abdominal aortic aneurysm (AAA) is a dilatation of aorta characterized by loss of functional elastin and smooth muscle cells, as well as enhanced production of collagen. The majority of AAAs includes an intraluminal thrombus (ILT) that decreases peak wall stress; however, it also degrades aortic wall, thus reducing its strength. Aneurysm rupture has a high mortality rate. To help clinicians predict rupture, growth and remodeling models have been developed. Nevertheless, in hitherto conducted studies effect of ILT has been neglected.

The doctoral thesis includes detailed biochemomechanical overview of the thrombus-laden aneurysms. Based on this review a new comprehensive growth and remodeling ILT model interconnected with kinematics of the aneurysmal aortic wall has been developed. The majority of parameters were chosen to fit experimental results and showed a great potential to predict behavior of AAAs. The remaining parameters were studied parametrically, describing most common rupture or stabilization risk factors. Changes in dilatation rates were compared to clinical observations, and insight into their influences on aneurysmal changes was given. The results also emphasize the necessity to include biochemical and biomechanical influences of ILT on the wall when predicting AAA outcome (rupture, continuous growth or stabilization).

Finally, the 3-D growth and remodeling theory of aortic wall was implemented into finite element analysis program (*FEAP*), which enables simulation of more realistic aneurysm geometries – axially symmetric (fusiform) and non-symmetric (intracranial aneurysm). Results for fusiform aneurysms obtained by 3-D finite elements were compared to membrane element results available in literature. A great potential to model saccular aneurysms, and advantage of 3-D to 2-D elements was shown.

The aim of AAA growth modeling is to increase understanding of aneurysm pathophysiology (e.g., "staccato" expansion), and to determine reliable rupture risk and stabilization factors.

Keywords: abdominal aortic aneurysm, intraluminal thrombus, growth and remodeling, proteolytic activity, rupture risk factors

Prošireni sažetak

Uvod

Aneurizma abdominalne aorte (AAA) je kronični degenerativni poremećaj, trajno i nepovratno lokalizirano proširenje aorte i čest uzrok smrti kod starijih osoba. Iako sam proces nastanka AAA nije poznat, poznati su rizični faktori poput muškog spola, starosne dobi, pušenja, hipertenzije, plućnih bolesti i bolesti krvožilnog sustava. U posljednja dva desetljeća znatno se povećao broj otkrivenih slučajeva aneurizmi u svijetu, djelomično zbog većeg broja aneurizama (uslijed duže životne dobi i starenja stanovništva te povećanog broja pušača), ali i zbog napretka dijagnostičkih uređaja. Naime, AAA je asimptomatska bolest (zbog čega se otkriva slučajno), sve dok se ne zakomplicira rupturom ili embolijom, komplikacijama koje dovode do smrti i često se krivo dijagnosticiraju kao infarkt. Ruptura aneurizme abdominalne aorte je četrnaesti najčešći uzrok smrti u Sjedinjenim Američkim Državama, deseti kod muškaraca [1].

Promjer zdrave aorte ovisi o godinama, spolu, tjelesnoj masi pacijenta te položaju promatranog presjeka aorte. Smanjuje se od ulaska u trbušnu šupljinu prema ilijačnim arterijama. Kod muškaraca starijih od 65 godina vanjski promjer infrarenalne abdominalne aorte kreće se između 15 i 24 mm. S obzirom da ne postoji jedna vrijednost za promjer aorte te se on mijenja sa srčanim ciklusom, a širenje krvnih žila može biti uzrokovano i povećanim protokom krvi ili hipertenzijom, značenje „proširena aorta“ nije jednoznačno definirano. Upravo se iz tog razloga AAA definira ili kao infrarenalna aorta s promjerom većim od 30 mm, ili kao 50%-tno proširenje u odnosu na neki bliski presjek.

Liječenje AAA svodi se na operativni zahvat, a trenutno jedini kriteriji za slanje pacijenta na operaciju je maksimalni promjer aneurizme veći od 5-5,5 cm i iskustvo liječnika. Dodatni kriterij, ako je dostupan, je brzina rasta aneurizme. Rast od 1 cm godišnje povezuje se s visokom opasnosti od rupture, za razliku od uobičajene brzine rasta od 2 mm godišnje. Podatak o brzini rasta aneurizme dostupan je u slučajevima kada je otkrivena aneurizma manja od 5 cm te pacijentu nije preporučena operacija, nego redovito praćenje ultrazvukom ili CT-om. Istraživanja su pokazala da, iako je rizik od rupture zasigurno povezan s maksimalnim promjerom, korištenje samo tog pokazatelja za odlučivanje o odlasku na operaciju ne samo da može dovesti do nepotrebnih operativnih zahvata u slučaju stabilnih velikih aneurizmi, nego može isključiti neke potrebne (aneurizme promjera manjeg od 5 cm kod kojih je došlo do rupture). Studije su pokazale da u 10-24% slučajeva aneurizme manje od 5 cm dožive rupturu, ali i da 25-54% aneurizmi većih od 7,1 cm ne rupturira, [2]. Također,

kod žena češće dolazi do rupture malih aneurizmi nego kod muškaraca, ali kod većih aneurizmi nema razlika.

Stijenka aorte sastoji se od tri sloja: intime, medije i adventicije. Svaki od slojeva ima različiti udio konstituenata koji daju krutost stijenci: kolagena, elastina i glatkih mišićnih stanica. Unutarnja površina stijenke nije u direktnom doticaju s krvi, nego je prekrivena slojem endotelnih stanica. Te stanice izlučuju vazokonstriktore i vazodilatatore, čime omogućuju održavanje homeostatskih uvjeta kod zdrave aorte, ali i sprečavaju aktivaciju molekula iz krvi u stijenci krvne žile. U 80% AAA dolazi od oštećenja endotelnih stanica, zbog čega krv dolazi u dodir s kolagenom i stvara se intraluminalni tromb (ILT) [3,4]. U slučajevima kada je oštećen endotel ILT nastaje uslijed poremećene hemodinamike, odnosno stvaranja vrtlogâ tijekom sistole, te njihovog propagiranja i disipacije tijekom dijastole. Vrtlozi stvaraju područja s visokim posmičnim naprezanjima u lumenu pogodnim za aktivaciju trombocita te područja s niskim posmičnim naprezanjima na stijenci aorte gdje je omogućeno skupljanje aktiviranih trombocita na oštećenim endotelnim stanicama ([5–7]). Početna faza nastanka ILT-a može se opisati aktiviranjem trombocita, pretvaranjem fibrinogena u fibrin pomoću trombina i stvaranjem fibrinske mreže u kojoj crvene i bijele krvne stanice ostaju zarobljene [8]. Ovakva je struktura tipična za dio intraluminalnog tromba uz tok krvi, taj sloj ILT naziva se luminalni sloj. S obzirom da je u kontaktu s krvi, luminalni sloj je prepoznatljive crvene boje i proteolitički je najaktivniji. Obično je širok oko 2 mm jer je ograničen dubinom do koje krv može prodrijeti kroz fibrinsku mrežu. Daljnjim povećanjem promjera aneurizme raste i ILT pa nastaju dijelovi tromba koji su dovoljno daleko od krvi, odnosno nastaje medijalni sloj koji može biti debeo i nekoliko centimetara. U ovom žućkastom sloju odumiru stanice koje su bile zarobljene u luminalnom sloju i fibrinska mreža se razgrađuje pa nastaju kanalići (*cannaliculi*) čija se površina povećava od lumena prema stijenci [9]. U velikim aneurizmama fibrin se može razgraditi do granice da mreža postaje neorganizirana ili čak djelomično u obliku tekućine [10,11]. Taj smeđi dio tromba zove se abluminalni sloj. Očito svaki od tri sloja tromba karakteriziraju drugačija biokemijska i mehanička svojstva ([12,13]). Primjerice, u luminalnom sloju nalaze se upalne stanice iz krvi (npr. T-limfociti), dok ostala dva sloja sadrže mnogo manje stanica i molekula. Upalne stanice u luminalnom sloju izlučuju proteolitičke enzime, matriks metaloproteaze, u latentnom obliku (proMMP). Ukoliko te stanice prodru u stijenku aorte te budu aktivirane plazminom razgrađuju kolagen i elastin, što stijenku čini slabijom i podložnom razvoju aneurizme. Osim u luminalnom sloju, upalne stanice nalaze se i u mediji te adventiciji. Naime, aorta je najveća krvna žila u ljudskom tijelu, te se dijelovi zdrave aorte koji su najviše udaljeni od lumena

opskrbljuju kisikom pomoću mreže kapilara koje se zovu *vasa vasorum*. U slučaju aneurizme površina *vase vasorum* se višestruko poveća, što uz povećani dotok kisika za posljedicu ima i povećani broj upalnih stanica koje proizvode proMMP ([14,15]). To znači da difuzija proteaza i kisika nije jednosmjerna, već ima dva izvora (dio iz tromba blizak lumenu te dio iz same stijenke).

Istraživanja mehaničkih svojstava tromba počinju radom iz 1944. godine [16] te traju još i danas, npr. [8]. Inzoli et al. [17] prvi su predložili mogućnost da ILT može služiti kao mehanička zaštita stijenke AAA od prevelikih naprezanja. Taj je rad potaknuo mnoga istraživanja, većina od kojih su to potvrdila (npr. [18]), ali i neka koja sumnjaju u mogućnost poroznog tromba da smanji naprezanja u stijenci (primjerice [19]). Dok npr. Meyer et al. [20] tvrde da tromb koji je potpuno povezan sa stijenkom aorte može smanjiti naprezanja u stijenci, međutim u slučaju da je ILT samo djelomično spojen pojavljuju se koncentracije naprezanja.S druge strane, prema kliničkom iskustvu, do rupture najčešće dolazi upravo na mjestu najvećeg tromba. Lako je zaključiti da stvaranje intraluminalnog tromba može imati veliki utjecaj u procesu razgradnje dijelova izvanstaničnog matriksa, a time i na rast i razvoj AAA.

Cilj istraživanja je razviti teoriju koja može opisati rast aneurizmi kao i promjenu građe ILT i stijenke aorte (G&R) koja će dovesti do boljeg razumijevanja utjecaja tromba na rast aneurizme, kao i same patofiziologije AAA. Primjerice, istraživanja u kojima se pratio rast aneurizmi pokazala su da neke AAA rastu kontinuirano (23%), neke „*staccato*“, odnosno imaju periode tijekom kojih ne rastu (65%), dok su neke stabilne (12%) [21–23]. Razlozi za različiti način razvoja aneurizmi trenutno su nepoznati.

Konačni cilj istraživanja na području G&R aneurizmi jest smanjiti broj smrti uzrokovanih nepotrebnim operacijama velikih, stabilnih aneurizmi kao i broja ruptura malih aneurizmi koje ne bi bile liječene. Drugim riječima, cilj je simulirati budući razvoj aneurizme i procijeniti hoće li doći do rupture, stabilizacije ili stabilnog rasta. Time bi se pomoglo liječniku odlučiti koji je način liječenja AAA za pacijenta najprikladniji: operacija ili redovito praćenje napretka rasta.

Trenutno stanje istraživanja

Dosad su razvijeni G&R modeli zdrave arterije, G&R modeli aneurizme u kojima se biokemijski utjecaj uzima kroz preddefinirane funkcije, a mehanički utjecaj potpuno zanemaren. Dosad nitko nije proučavao sveobuhvatni biokemijski i biomehanički ('biokemomehanički') utjecaj intraluminanog tromba na razvoj aneurizme. Također su

razvijeni i modeli koji opisuju samo razvoj tromba, koji se događa na manjim vremenskim skalama u odnosu na rast aneurizme (za nastanak tromba potrebne su sekunde, a AAA raste tijekom godina).

Zdrava krvna žila

Razvijeni su razni konstitutivni modeli koji služe za promatranje procesa deformiranja krvnih žila, a većina ih se temelji na različitim oblicima slobodne energije. Kao najbolja aproksimacija pokazali su se anizotropni hiperelastični modeli izneseni u [24,25]. U njima se uzima u obzir ponašanje izvanstaničnih dijelova (elastin, kolagen, glatke mišićne stanice) koji daju krutost stijenci, kao i slojeva krvne žile (intime, medije i adventicije). No s druge strane vrlo važno svojstvo krvnih žila, ovisnost o prethodnom opterećenju, nije uzeto u obzir kod prethodno spomenutih modela. Ti oblici ponašanja mogu se opisati mehanizmima rasta i restrukturiranja (growth and remodeling - G&R).

Rodriguez et al. [26] potaknuli su istraživanja na području matematičkog modeliranja rasta, odnosno promjena u masi, i restrukturiranja, tj. promjene mikrostrukture, mekih tkiva. Modeli moraju uzeti u obzir vrlo kompleksnu mehaniku krvnih žila, kompozitnu strukturu, kao i aktivno djelovanje glatkih mišićnih stanica i pasivno anizotropno hiperelastično ponašanje. Razlikujemo dva pristupa G&R modeliranju. Prvi je kinematički pristup [27,28] gdje se G&R samo opisuje, ali ne ulazi se u uzroke takvog ponašanja. Drugi je pristup prema Humphrey & Rajagopal [29] u kojem je predložen model temeljen na opisu promjena i proizvodnje odnosno razgradnje izvanstaničnih dijelova stijenke žile kao posljedice promjene normalnih vrijednosti vanjskog opterećenja. Ovaj drugi pristup do sada je bio primijenjen samo za membranski model stijenke, [30] i [31]. Iako su ograničeni na membransku teoriju i njena ograničenja, ti modeli nam daju bitne informacije o mehanizmima G&R (npr. ovisnost o naprezanju, o koncentraciji vazodilatatora i vazokonstriktora). Isti pristup može se primijeniti i za trodimenzijske modele na osnosimetričnoj geometriji, kao u radovima [32–34]. Za razliku od membranskih modela, 3-D formulacija omogućuje praćenje radijalnih promjena pojedinih konstituenata kao i molekula (npr. dušični oksid, endotelin-I, MMP), no s tim se javlja i potreba za eksperimentalnim metodama koje će potvrditi te gradijente i dati povratnu informaciju G&R modelima.

Bolesna krvna žila

Hiperelastični modeli mogu vrlo dobro opisati ponašanje stijenke aneurizme, ali pri tome još nitko nije uzeo u obzir mikrostrukturnu građu. Veliki doprinos razvoju modela AAA daju

jednoosni ([35]) i dvoosni [4] pokusi na ljudskim AAA. Volokh & Vorp [36] predložili su matematički model za rast i predviđanje rupture AAA. Njihova pretpostavka je da tanka sferna ljuska opterećena tlakom može opisati ponašanje aneurizme. U Rodriguez et al. [37] su usporedili prethodno spomenute modele s izotropnim opisanim preko polinomne funkcije i dvije porodice kolagenih vlakana. Opći zaključak je da modeli temeljeni na strukturi trebaju biti napravljeni iz histoloških podataka, a ne preko krivulja rastezanja. Rissland et al. [38] napravili su analizu rezultata iz [4] pomoću modela s kolagenih vlaknima orijentiranim u dva smjera te su zaključili da anizotropni model daje pouzdanije rezultate. Za obradu istih rezultata Feruzzi et al. [39] koriste konstitutivne relacije s četiri familije kolagenih vlakana uzimajući u obzir mikrostrukturu, što čini rezultate toga rada vrlo primjenjivima kod modela rasta i restrukturiranja (G&R) u abdominalnoj aorti.

Prvi G&R model za opisivanje evolucije AAA, ali koji ne uključe intraluminalni tromb, je prezentiran u Watton et al. [40]. U tom radu je stijenka modelirana kao dvoslojna cilindrična membrana. Razmatrali su nastanak osnosimetrične, kao i asimetrične aneurizme uz ograničavanje rasta aneurizme na posteriornoj strani na kojoj se nalazi kralježnica. Ovaj je rad potaknuo niz istraživanja ([41–43]) koji se razlikuju u konstitutivnim funkcijama i njihovoj implementaciji. U Wilson et al. [43] (membranski model) je sugerirano da su G&R parametri o kojima ovisi obnavljanje kolagena (npr. brzina produkcije i razgradnje, krutost, preddeformacije) ključni za rupturu, ravnotežu ili stabilan rast aneurizme.

Popularno je i razmatranje utjecaja hemodinamike na rast aneurizme, tzv. *fluid-structure-growth* (FSG), primjerice [44]. Međutim, niti jedan od ovih modela ne uključuje direktno sveobuhvatni utjecaj intaluminanog tromba na aneurizmu.

Modeliranje intraluminalnog tromba

S druge strane, modeli razvijeni za opisivanje nastanka i razvijanja tromba ne bave se njegovim utjecajem na krvnu žilu, nego isključivo zgrušnjavanjem krvi (tj. stvaranjem fibrina, fibrinogenezom), mehaničkim svojstvima fibrina te njegovom razgradnjom pomoću plazmina (fibrinolizom). Takvi modeli mogu se podijeliti na intrinzične i ekstrinzične pristupe [45–47], te sve popularnije hibridne formulacije ([48–53]). Intrinzični i ekstrinzični pristupi pokušavaju opisati promjene u koncentraciji i aktivaciji osnovnih hemostatskih faktora na makrorazini pomoću brojnih (obično oko 50) diferencijalnih jednadžbi. Hibridna formulacija spaja diskretni Pottsov model za trombocite, crvene i bijele krvne stanice na mikrorazini s kontinuum modelom strujanja krvi na makrorazini u pokušaju iskorištavanja prednosti oba modela: točnost prvog i brzinu drugog.

Unatoč svim naporima do danas nije uložen veći napor za otkrivanje vremenskog razvoja krvnog ugruška unutar AAA. Koristeći dostupne eksperimentalne rezultate Karšaj et al. [54] predlažu prvi takav model pomoću spregnute teorije smjesa (*constrained mixture theory*) gdje opisuju složene kinetičke promjene različitih skala (minute kod stvaranja fibrina do tjedana i mjeseci kod stvaranja kolagena). Glavni nedostatak ovog rada je ograničenje na 0-D problem.

Ciljevi i hipoteze istraživanja

Cilj istraživanja je razvoj numeričkog modela rasta i restrukturiranja aneurizme koja sadrži intraluminalni tromb. Opis vremenski promjenjive raspodjele proteaza u radijalnom smjeru kroz tromb i stijenku aorte omogućuje simulaciju rasta aneurizme te određivanja sklonosti rupturi. Očekujemo da će model dovesti do boljeg razumijevanja patofiziologije aneurizmi.

Hipoteze istraživanja su:

1. tromb direktno utječe na tijek rasta AAA i vjerojatnost pojave rupture, i to:
   a. mehanički - tromb preuzima dio naprezanja i time pruža mehaničku zaštitu stijenci aorte,
   b. biokemijski - nastankom tromba stvaraju se enzimi koji razgrađuju pojedine konstitutente stijenke aorte i na taj način joj degradiraju mehanička svojstva,
2. osim u trombu, enzimi koji utječu na rast AAA stvaraju se i u stijenci, mijenjaju mehanička mehanička svojstva i smanjuju čvrstoću stijenke.

Biokemomehanički pregled

ILT je veoma kompleksna fibrinska struktura koja se za razliku od ostalih krvnih ugrušaka i tromba unutar aneurizmi u drugom dijelovima tijela ne razgrađuje, a fibrinska vlakna se ne zamjenjuju kolagenom, kao što je slučaj pri liječenju ozljeda [55]. Smatra se da ključnu ulogu pri stvaranju ILT-a ima hemodinamika koja uzrokuje oštećenje endotelnog sloja. Stvaraju se područja pogodna za aktivaciju trombocita iz krvi te područja pogodna za njihovo nakupljanje i stvaranje fibrina (fibrinogenezu), a time i stvaranje fibrinske mreže u koju se potom zapliću crvene i bijele krvne stanice. Fibrinska mreža nastaje stabilizacijom i povezivanjem fibrinskih vlakana pomoću aktiviranog faktora XIII. S druge strane, fibrinsku mrežu razgrađuje plazmin, Zanimljivo, istraživanja su pokazala da gušća, manje porozna fibrinska mreža pokazuje veći otpor fibrinolizi (razgradnji fibrina) [56]. Proces zgrušnjavanje krvi i fibrinolize su detaljno opisani u nekoliko preglednih članaka [57–59], kao i nekolicini novijih članaka [60–62].

Osim razumijevanja strukture tromba, bitna su istraživanja mehaničkih svojstava tromba koja počinju radom [16] te traju još i danas. Bitniji napredak u istraživanjima svojstva ILT-a

je krenuo s ultrazvučnim mjerenjima u [63], gdje je pokazano su da ILT doživljava nelinearne deformacije. Najkvalitetniji rezultati prikazani su u [8], u kojem su ispitana mehanička i histološka svojstva sva tri sloja tromba. U radu su definirali četiri faze starosti tromba koje se razlikuju po svojstvima fibrina i histologiji. Također, pokazali su da su intermedijalni i abluminalni sloj izotropni, što ne mora vrijediti za luminalni sloj te da vlačna krutost opada radijalno, ali raste starenjem. Ashton et al. [64] su pokazali suprotno ponašanje kompresijske krutosti, odnosno da je kompresijska krutost abluminalnog sloja znatno veća od iste luminalnog i intermedijalnog sloja.

ILT unutar AAA karakteriziraju jedinstvena biokemijska i biomehanička svojstva koja su različita od vrijednosti dobivenih za tromb u ostalim dijelovima tijela. S obzirom na nemogućnost zacjeljivanja i konstantno obnavljanje stanične aktivnosti u luminalnom dijelu, on je mogući izvor kronične upale stijenke aorte. Stoga za razumijevanje i modeliranje utjecaja tromba na rast AAA nije dovoljno poznavati samo njegovu strukturu i mehanička svojstva, nego i heterogenu sintezu, skladištenje i otpuštanje relevantnih biomolekula (npr. neutrofila, makrofaga i limfocita). Neutrofili u luminalnom sloju tromba mogu lučiti interleukin-8, koji je kemotaktičan za neutrofile, te količine neutrofila u ILT-u mogu biti i 12 puta veće nego u krvi [65]. Oni također mogu otpuštati matriks metaloproteinaze MMP-8 i MMP-9 (enzime koji razgrađuju proteine – kolagen i elastin u stijenci aorte) te aktivator plasminogena uPA (čijom aktivacijom nastaje plazmin koji razgrađuje fibrin, a dodatno i aktivira latentne oblike MMP-ova) [66]. Unutar AAA zabilježene su povećane razine proteinaza, kao i smanjene razine inhibitora proteinaza (TIMP-1 i TIMP-2) u usporedbi sa zdravim tkivom [66,67]. Osim plazmina, latentne oblike proteinaza (proMMP) aktiviraju ostale proteinaze te reaktivni oblici kisika i dušikov oksid [67].

Zbog heterogene strukture tromba i lokalizacije stanične aktivnosti na luminalni sloj, pokazano je da stijenka aorte ispod koje je tanki tromb ($\leq$ 1.0 cm) ima znatno veće razine aktivnosti proteinaza i omjera aktivnog MMP-9 i inhibitora TIMP-1 u odnosu na stijenku ispod debljeg tromba [66]. Pad stanične aktivnosti uočen je i od luminalnog sloja prema medijalnom i abluminalnom sloju tromba. Medijalni i abluminalni sloj karakterizira nedostatak stanica i sve manje organizirana fibrinska mreža u procesu razgradnje. Dijelovi abluminalnog sloja najbliži stijenci mogu biti čak potpuno razgrađeni i u obliku tekućine (*liquid interphase*) [64,68]. Zbog nedostatka stanica u ovim slojevima nije moguća sinteza proteina, međutim uslijed fibrinolize moguće je otpuštanje biomolekula koje su se vezale za fibrin tijekom koagulacije. Zbog toga mjerenja proteolitičke aktivnosti u ovim slojevima dosta variraju vremenski i prostorno pa istraživanja mogu pokazati različite rezultate (npr. [69] i .

[10]). Otpuštanje vezanih latentnih proteinaza u prisutnosti plazmina povećava razgradnju susjedne stijenke. Uzimajući u obzir da proteolitički enzimi i molekule koje utječu na rast AAA vjerojatno mogu prolaziti kroz propusni tromb konvekcijom i difuzijom [9], razumijevanje i modeliranje tromba postaje još kompleksnije. Dodatni problem predstavljaju teškoće pri dobivanju uzoraka ljudskog tkiva pa su životinjski modeli vrlo korisni.

Osim biokemijskog sastava tromba za razumijevanje AAA bitne su i promjene u stijenci aorte. Aneurizmatična stijenka aorte ispod koje nema tromba ima manje upalnih stanica, manji površinu *vase vasoruma* i više elastičnih vlakana i glatkih mišićnih stanica koje sporije odumiru [70] u usporedbi sa stijenkom ispod koje se nalazi tromb. Osim toga, postoje znatne razlike u izvanstaničnom matriksu (npr. svojstva kolagena) i staničnom sastavu. Gubitak elastina uzrokuje smanjenje aksijalne potpore i dovodi do produživanja, odnosno izvijanja aorte, koje može uzrokovati dodatno oštećenje endotelnih stanica, poremetiti strujanje krvi i uzrokovati abnormalna naprezanja [11]. U slučaju kada naprezanja lokalno nadvise čvrstoću stijenke dolazi do rupture [71]. Međutim, i naprezanja i čvrstoća stijenke su izrazito heterogeni. Također, oštećenje tromba indirektno dovodi do rupture jer omogućuje obnovljenu staničnu aktivnost i razgradnju stijenke aorte [72].

Modeli rasta i restrukturiranja

Za pravilno numeričko G&R modeliranje moramo znati kako se deformira stijenka krvne žile, kako nastaje i raste tromb unutar AAA te promjene u sastavu i mehaničkim svojstvima stijenke i tromba. Međutim, treba imati na umu da rast tromba utječe na deformiranje stijenke, ali i da je ograničen upravo rastom aneurizme. Stoga, razvijen je numerički model koji uzima u obzir:

a. ponašanje tri sloja stijenke krvne žile povezano s razmatranjem rasta i restrukturiranja (G&R) na mikrorazini,
b. nastanak, stvaranje slojeva i ponašanje intraluminalnog tromba,
c. međudjelovanje tromba i stijenke, odnosno difuziju proteinaza (MMP) kroz ILT i stijenku aorte.

Trodimenzijski materijalni model zdrave abdominalne arterije temeljen na teoriji prema Humphrey & Rajagopal [29], odnosno prema numeričkom modelu iz [34], je prilagođen za opisivanje aneurizmatične stijenke aorte. Osnovna teorija temelji se na spregnutoj teoriji smjesa i teoriji evoluirajućih konfiguracija. Pri modeliranju čvrstoće stijenke aorte uzeti su u obzir samo mehanički bitni dijelovi (elastin, više familija kolagenih vlakana i glatke mišićne stanice). Pretpostavka je da svaki od konstituenata u svakom trenutku ima svoju prirodnu

konfiguraciju u kojoj nije napregnut. Svaka nova generacija konstituenata ugrađuje se u trenutnu konfiguraciju smjese (tj. stijenku aorte) s preddeformacijom. Promjena mase pojedinih konstituenata značajno utječe na raspodjelu naprezanja. Za razliku od teorije za zdravu stijenku, aneurizme karakterizira smanjenje mase elastina i apoptoza mišićnih stanica, dok masa kolagena znatno raste. To za posljedicu ima i stanjenje medije, te zadebljanje intime i adventicije.

Temeljem biokemomehaničkog pregleda razvijen je model za opisivanje nastanka intraluminalnog tromba (ILT) i prostorno-vremenske promjene njegove strukture i mehaničkih svojstava prilikom rasta aneurizme pod osnovnom pretpostavkom o konstantnom unutarnjem promjeru pri konstantnom opterećenju. Treba primijetiti da se zbog te pretpostavke u svakom vremenskom koraku u kojem aneurizma raste stvara novi dio luminalnog sloja tromba. Model također opisuje i proizvodnju enzima koji nastaju tijekom tih procesa (MMP). Opažanja da se tromb sastoji od različitih mehanički bitnih dijelova (fibrin, crvene krvne stanice, produkti degradacije fibrina, praznine) potaknuli su nas na upotrebu teorije smjesa. Modeliran je nastanak fibrina pomoću biokemijskih reakcija, pri čemu će fibrinska vlakna biti položena u konfiguraciju smjese (tromba) s određenom deformacijom. Razgrađeni fibrin u dubljim slojevima tromba djelomično se pretvara u produkte degradacije fibrina, a djelomično, uslijed djelovanja makrofaga, zajedno s odumrlim krvnim stanicama ostavlja praznine. Ovo razmatranje se poklapa s idejom spregnutih smjesa već izloženom u prvom koraku.

Biokemijski utjecaj tromba na stijenku definiran je difuzijom proteinaza. Proteinaze imaju dva izvora: luminalni sloj tromba te mediju i adventiciju u stijenci, što komplicira njezino modeliranje. Važnost pojedinog izvora mijenja se tijekom vremena: primjerice, luminalni sloj koji se nalazi blizu stijenke ima znatno veći utjecaj na njezinu razgradnju od proteinaza izlučenih iz upalnih stanica u samoj stijenci, ali kod velike aneurizme koja sadrži tromb debeo nekoliko centimetara proteinaze proizvedene u luminalnom sloju su daleko od proteina koje razgrađuju i gotovo da nemaju utjecaj na njih, [29,30]. S druge strane, biomehanički utjecaj tromba opisan je preuzimanjem dijela naprezanja.

Rezultati

Trodimenzijalni model aneurizmatične aorte je primijenjen prvo na cilindričnu geometriju, bez modela tromba. S obzirom da bez modela tromba nije poznata vremensko-prostorna raspodjela proteinaza (elastaza i kolagenaza), degradacija je elastina predefinirana kao funkcija vremena. Za ovakav slučaj je aneurizme dobiveno da je stabilizacija moguća samo u

slučaju da kolagena vlakna očvršćuju, a produkcija mase konstituenata je dovoljno velika. Model rasta i restrukturiranja stijenke je također implementiran u programski paket za konačne elemente (*FEAP*), što je omogućilo simulacije aksijalno simetričnih (fuziformnih) i nesimetričnih (sakularnih) aneurizmi. Implementacija je validirana na cilindričnoj geometriji za zdravu aortu (adaptacija na promjenu tlaka i protoka) sa semi-analitičkim rješenjem. Rezultati za fuziformne aneurizme su uspoređeni s membranskim modelom iz literature [73]. Rezultati se dobro poklapaju, a dodatno je pokazano da pretpostavke membranskih konačnih elemenata ne vrijede nužno za problem rasta aneurizme. Prvi rezultati za sakularne aneurizme daju obećavajuće rezultate. Također je za cilindričnu geometriju opisan biokemijski utjecaj tromba na stijenku aneurizme, dok se mehanički utjecaj zanemario. Time je izbjegnuto da razgradnja elastina ovisi samo o vremensko-prostornim koordinatama, nego prostorna funkcija količine elastaza. Međutim, zbog visokih računalnih zahtjeva, ali i ograničenosti dostupnih eksperimentalnih podataka o cirkularnim i aksijalnim mehaničkim i histološkim promjenama, za prvu aproksimaciju je modelirana aneurizma koja sadrži tromb na cilindričnoj geometriju pomoću semi-analitičkom rješenja.

Model tromba unosi niz parametara, od kojih se dio ne može odrediti direktno iz eksperimenata. Veći dio tih parametara je određen parametarskim istraživanjima, na način da rezultati simulacije opišu ponašanje primijećeno eksperimentima. Primjerice, vremensko-prostorno struktura i mehanička svojstva tromba se poklapaju sa rezultatima iz Tong et al. [8], rast površine *vase vasorum* se može usporediti povećanjem površine s upalim stranicama iz Vorp et al. [74], a za težinske faktore korištena su istraživanja s eksperimentima na životinjama (npr. [75,76]). Model je pokazao velike mogućnosti, a ishod rasta aneurizme (ruptura, kontinuirani rast ili stabilizacija) više nije ovisio samo o svojstvima kolagena, nego i o svojstvima tromba. Aneurizma koja sadrži tromb može rasti bez rupture čak ako i kolagen ne očvršćuje.

Za parametre za koje su eksperimenti pokazali da značajno variraju od pacijenta do pacijenta (npr. proteolitička aktivnost luminalnog sloja tromba) napravljena je parametarska analiza. Promjenom vrijednosti određenih parametara modela su simulirane razlike u razvoju aneurizme kod pušača i nepušača, žena i muškaraca, pacijenata s normalnim krvnim tlakom i pacijenata s arterijskom hipertenzijom. Primjerice, pušači imaju znatno povećanu krutost stijenke, razinu upalnih stanica i aktivnost trombocita u odnosu na nepušače [77]. Nakon prestanka pušenja potrebno je 5-10 godina da bi se te razine vratile na razinu nepušača [78]. Uzimajući u obzir te razlike, dobiveno je da aneurizme kod pušača rastu 0,05 cm/god brže nego kod nepušača, što se u potpunosti poklapa s kliničkim opažanjima [79]. Slični su

rezultati dobiveni i za razlike u spolu, starosti te krvnom tlaku. Također, s obzirom da dosadašnji G&R modeli bez tromba nisu uspjeli objasniti stepeničasti način rasta aneurizme, a prvi zastoj u rastu je dobiven pomoću ovog modela aneurizme koja sadrži tromb, postoji mogućnost da je upravo tromb, odnosno velika razlika u proteolitičkoj aktivnosti tromba u odnosu na stijenku, razlog povremenom prestanku rasta aneurizme ili ponovnom početku rasta nakon stabilizacije.

Zaključak

Računalna biomehanika sve se više koristi za istraživanje kompleksnih procesa vaskularnog zdravlja i bolesti. Prijašnji G&R modeli aneurizme abdominalne aorte (npr. [43,44]) dali su nam značajan uvid u bolest, ali nisu uzeli u obzir biokemomehanički utjecaj intraluminalnog tromba na aneurizmatičnu stijenku. Ti bi utjecaji mogli biti ključni za evoluciju, predviđanje rasta i klinički ishod aneurizme.

Pored svih prednosti ovog modela prve generacije, sveobuhvatni model ograničen je na cilindričnu geometriju, koja ne dopušta lokalna proširenja. Također, pretpostavka da tromb popunjava prostor od stijenke do lumena ne dopušta rast tromba vođen hemodinamikom, kao što se vjerojatno događa *in vivo*. Ovi ograničavajući faktori potrebni su dok se ne razviju konačni elementi koji mogu opisati modele rasta i restrukturiranja. Krajnji je cilj razviti model koji opisuje rast i interakciju između krvi, tromba i stijenke (*fluid-solid-growth*).

Prijašnja istraživanja rasta i restrukturiranja su pokazala da krutost kolagena ima dominantnu ulogu kod predviđanja kliničkog ishoda (tj. prestanak rasta, kontinuirani rast ili ruptura) kod aneurizama koje ne sadrže tromb. Istraživanja u ovom radu to su potvrdila, ali dodatno sugeriraju i druge faktore koji imaju bitnu ulogu kod aneurizama s trombom. Rezultati pokazuju sposobnost tromba da nosi dio naprezanja, ali i da utječu na obnovu izvanstaničnog matriksa u stijenci putem proteolize. Naravno, potrebni su eksperimenti za određivanje određenih G&R parametara modela, idealno bi bilo za svakog pacijenta zasebno.

Također su pokazani i načini kako najvažniji rizični faktori za rupturu i terapeutske strategije utječu na evoluciju aneurizme i vjerojatnost rupture. Rezultati simulacije izvrsno se poklapaju s kliničkim promatranjima, intuicijom i prošlim G&R modelima koji imaju kompleksniju geometriju, ali ne uzimaju u obzir tromb. Primjerice, prosječna brzina rasta je cca 2 mm/god, dok je brzina rasta kod koje se predviđa ruptura oko 10 mm/god. Simulacije aneurizmi kod pušača uzrokuju povećanje brzine rasta za približno 0,43 mm/god, a kod pacijenata s arterijskom hipertenzijom oko 0,22 cm/god po 10 mmHg. Oba rezultata su opažena i klinički [79]. Nadalje, model je predvidio veću vjerojatnost rupture kod žena, a

uvodi hipotezu da mehaničko stanje aneurizme (npr. količina preostalog elastina, istegnutost kolagena) značajno utječe na mogućnost adaptacije AAA na promjene i oštećenja. Očvršćenje kolagena može pomoći stabilizaciji aneurizme (kao što je pokazano ranije u [73]), ali to ne mora biti dovoljno u slučaju visoke proteolitičke aktivnosti ili nagle promjene krvnog tlaka. Smanjivanje proteolitičke aktivnosti luminalnog sloja tromba u modelu također smanjuje rizik od rupture. Prema tome, tromb se ne bi smio zanemarivati tijekom predviđanja razvoja AAA u budućim eksperimentalnim i računalnim istraživanjima.

Zbog nedostatka eksperimentalnih podataka o molekularnim raspodjelama i heterogenostima mehaničkih svojstava u aksijalnom i cirkularnom smjeru aneurizme, proširivanje modela na 3-D neće biti jednostavno. Stoga zaključujemo da će biti potrebna pažljiva, integrirana razmatranja razvoja mehaničkih, kemijskih i bioloških svojstava biološki aktivne, slojevite strukture intraluminalnog tromba o prirodnoj AAA kako bi se povećao potencijal računalnih modela koji će nam pomoći identificirati i poboljšati faktore rupture rizika (ili, jednako važno, promicati stabilizacijske faktore), osigurati dijagnostiku pacijenta te specifično i intervencijsko planiranje, te u konačnici poboljšati klinički ishod.

Originalni znanstveni doprinos

1. Razvoj numeričkog modela koji opisuje:
   a. nastajanje aneurizme abdominalne aorte uzimajući u obzir radijalne promjene u strukturi stijenke aorte,
   b. nastanak i radijalne promjene u strukturi intraluminalnog tromba,
2. Implementacija modela u konačne elemente u programski paket *FEAP* koja će omogućiti provjeru hipoteza dobivenih na 1-D geometriji te analiza biokemijskog utjecaja tromba na stijenku aorte dobivena korištenjem povezivanjem *Matlaba* i *FEAP*a.
3. Modeliranjem interakcije tromba i stijenke omogućeno je praćenje utjecaja tromba na rast AAA te sklonost rupturi,
4. Uz početna ograničenja postavljena na model, moguće je potvrditi ili opovrgnuti utjecaj do sada predloženih rizičnih i stabilizacijskih faktora na tijek razvoja AAA.

Ključne riječi: aneurizma abdominalne aorte, intraluminalni tromb, rast i restrukturiranje, proteolitička aktivnost, faktori rizika od rupture

1. Introduction

1.1. Motivation

Abdominal aortic aneurysm (AAA, Figure 1.1) is a focal dilatation of infrarenal abdominal aorta with diameter larger than 30 mm, and a common cause of death among the elderly. Although the pathogenesis is still not well understood, some of the known development risk factors are male gender, age, smoking, hypertension, and cardiovascular and pulmonary diseases. AAA is asymptomatic disease; however, complications such as dissection, rupture, and embolization can lead to death. Nevertheless, our ability to predict whether a specific lesion will arrest, continue to enlarge either slowly or rapidly, or ultimately rupture remains wanting. Clinical interventions thus continue to be based primarily on the maximum dimension or expansion rate of the lesion, despite the observation that many small lesions rupture whereas larger lesions may remain asymptomatic, [2].

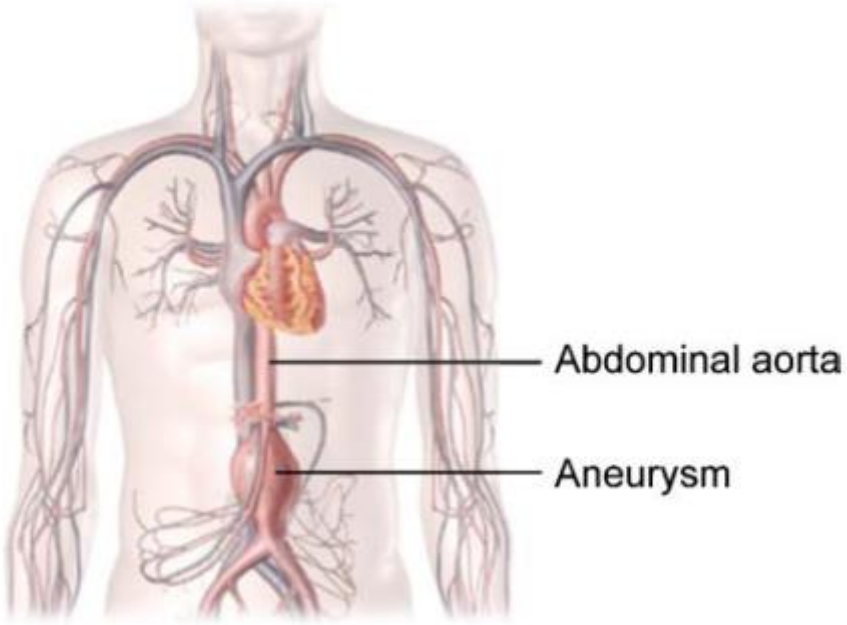

Figure 1.1: Abdominal aortic aneurysm, from [80]

The arterial wall is a composite structure organized in layers – intima, media, and adventitia (Figure 1.2). These layers entail different structural components such as smooth muscle cells, elastic fibers, and fibrillar collagens, and other cells (e.g., endothelial) and molecules. Endothelial cells at the inner surface of the vessel excrete vasoconstrictors and vasodilators, and thus maintain homeostasis in healthy aorta. They also provide a non-thrombogenic surface. Damage of endothelium in 80% of AAAs allows formation of an

intraluminal thrombus (ILT, Figure 1.3), [3,81]. The first phase of thrombus formation is characterized by loose fibrin networks entrapping the erythrocytes and leukocytes, [82]. This structure is typical for luminal layer of the thrombus. As it is in direct contact with the blood, it is proteolitically the most active. It is usually ~2 mm thick, which may be limited by the depth to which blood components can penetrate into the fibrin mesh. Parts of thrombus further away from the lumen (medial and abluminal layers) are characterized by disrupted erythrocytes and degradation of fibrin, [9]. All layers of ILT are histologically and mechanically distant, [13,82]. For example, luminal layer contains abundance of inflammation cells (e.g., T-lymphocytes), whereas medial and abluminal layers are mostly devoid of cells and molecules. Inflammation cells in luminal layer excrete proteolytical enzymes (matrix metalloproteinases, MMPs) that degrade collagen and elastin, thus weakening the aortic wall.

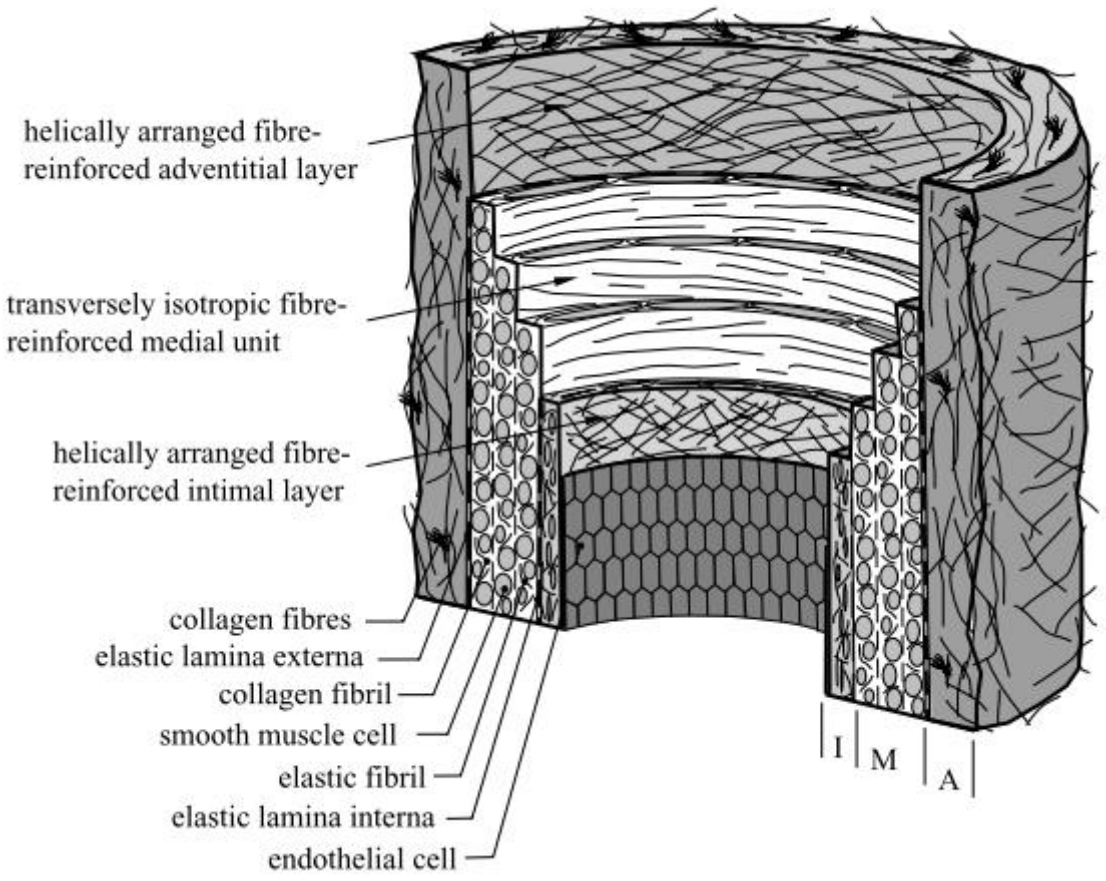

Figure 1.2: Layered structure of aortic wall, from [25]

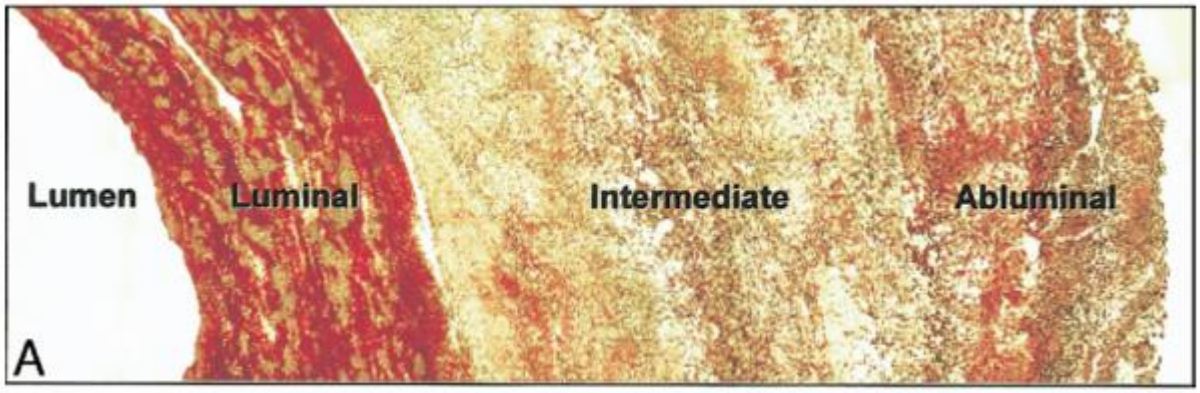

Figure 1.3: Layered structure of intraluminal thrombus, from [83]

Conversely, Inzoli et al [17]) were first to suggest that ILT can mechanically shield aneurysmal wall. Therefore, intraluminal thrombus could significantly influence AAA expansion and rupture. The objective of proposed research is development of growth and remodeling (G&R) model of thrombus-laden aneurysms that will lead to better understanding of aneurysm pathophysiology. For example, several follow-up studies showed that some AAAs grow continuously (23%), the majority (65%) grow stepwise ('*staccato*'), i.e., periods of growth alter with periods of non-growth, whereas some are stable (12%), [21]. Possible reasons for this variability in growth patterns are currently unknown. The ultimate objective of computational modelling of aneurysmal G&R is to help clinicians predict rupture risk, i.e. to decrease the number of unnecessary treatments of large, stable aneurysms, as well as number of ruptures of small AAAs that would not be treated.

1.2. Literature review

Various constitutive models for description of artery behavior have been proposed, the majority are free energy-based. Anisotropic hyperelastic models proved to capture the behavior the best, [24]. They consider deformation of structurally important constituents (elastin, collagen, smooth muscle), and arterial layers (intima, media, adventitia). However, they do not take into account dependence of current stress state on previous loading. This phenomenon can be described by growth and remodeling models (G&R). Rodriguez et al. ([26]) were first to model growth (change in mass) and remodeling (change in structure) of soft tissues. Such modeling is made challenging by the intrinsic complexities of arterial mechanics, including its composite make-up and associated active smooth muscle contractility plus nonlinear, anisotropic, pseudo-elastic passive behaviors over finite deformations. Two approaches for G&R modeling have been suggested. The 'kinematic

growth' approach [27,28] focuses primarily on the consequences of growth and remodeling (G&R), not the underlying mechanisms. Humphrey and Rajagopal [29] proposed a fundamentally different approach, one based on changes in the rates and extents of cellular and extracellular matrix turnover in response to perturbations of mechanical stimuli from normal values. This approach was used in several studies ([30,31]) restricted to membrane formulations, however, they provide insight to the G&R mechanisms (i.e. dependence on the stress state and the concentration of vasoconstrictor/vasodilatator ratio in the wall). The same approach can be applied to 3-D formulation, as is [32–34]. The advantages of a 3-D framework include the ability to account for effects of gradients in wall composition and distribution of molecules (e.g., NO, endothelin-1, MMPs). Nevertheless, this arises the need for experimental methods that will confirm these gradients and provide feedback to G&R models. To summarize, G&R models of healthy arteries and aneurysms without thrombus have been developed. Biochemomechanical influence of ILT on AAA expansion has been completely neglected in these studies.

As the word itself implies, *biomechanics* requires an understanding and description of both the biological and the mechanical aspects of a system. In this thesis both of these aspects in regards to intraluminal thrombus in abdominal aortic aneurysms have been highlighted. What remains, however, is a merging of the two into a computational framework capable of quantifying and predicting how the biology and mechanics interrelate. For example, hyperelasticity may be used to describe a thrombus at a given instant, but such a description could just as easily be assigned to a non-living polymer gel. What distinguishes the metabolically active thrombus from the inanimate gel is the ability of the incorporated platelets and cells to actively change the mass and interconnectedness of the fibrin matrix over time, that is, to grow and remodel. A G&R approach to modeling biological systems thus has the potential to describe *evolving* mechanical properties (e.g., mass, stiffness, failure criteria) over physiologically relevant timeframes as a function of local biological, chemical, and mechanical factors such as cellular content, proteinase levels, and hemodynamic loads. Ultimately, this is the challenge facing the clinician – not only determining immediate risk of rupture, but also risk over the subsequent months to years so that the timing of follow-up with re-imaging or surgical intervention may be selected appropriately for a given patient.

The first G&R model to describe AAA evolution was presented by Watton et al. [40] in 2004. They modeled the wall as a two layered cylindrical membrane described by a constrained mixture [118], with structural properties determined by the nonlinearly elastic collagen and elastin. They considered the development of both axisymmetric and asymmetric

aneurysms caused by prescribed focal degradations of elastin, with potential limitation of posterior expansion due to the spine. This G&R framework was later extended to include fluid-solid-growth (FSG) modeling by Watton et al. [44] in 2009.

More recent models [99, 100, 120, 121] also employed the concept of evolving constrained mixtures to investigate AAA mechanics, but with different constitutive functions and implementations. For example, instead of using a "recruitment stretch" to characterize when collagen becomes engaged mechanically, they used the concept of a "deposition stretch" to model incorporation of pre-stressed fibers within the *in vivo* geometry. Since new fibers are always added at a prescribed homeostatic deposition stretch, the wall as a whole can re-establish a homeostatic state provided that the forces favoring expansion (e.g., intravascular pressure and degradation of extracellular matrix) do not exceed the capacity of the wall to produce new material. Wilson et al. [100] suggested that the range of potential clinical endpoints (arrest, continued expansion, or rupture) depended primarily on G&R parameters governing collagen turnover (e.g., production rates, degradation rates, deposition stretch, and stiffness). A more detailed review of past finite element studies of AAA wall stress and growth and remodeling can be found in Humphrey and Holzapfel [2], and a review of the need for fluid-solid-growth (FSG) models of AAAs can be found in Humphrey and Taylor [1].

Yet, current models of aneurysmal G&R do not include directly the biochemical effects of intraluminal thrombus. For example, the aforementioned release of plasmin in a particular region of the ILT may activate available proMMPs and lead to a local change in the G&R parameter controlling the degradation rate of collagen. At the same time, the now active MMPs could activate latent TGF-β that had been sequestered in the extracellular matrix, and thereby increase the G&R parameter governing growth factor mediated collagen production. There is, therefore, a pressing need for development of biochemomechanical constitutive models to correlate the spatiotemporal activity of key proteinases and mediators (e.g., plasmin, MMPs, elastase, TGF- β, TIMPs) produced and activated by the ILT and wall with the governing G&R parameters that control the turnover of the primary load-bearing constituents within the wall, most notably, collagen, elastin, and smooth muscle. Given the inherent complexities in the biology and mechanical modeling, advances will likely need to proceed stepwise, building from lumped parameter models towards eventual multiscale, multiphysics models. Towards this end, an initial schema (Figure 1.4) outlining the interactions of key contributors likely affecting the growth and remodeling of thrombus-laden AAAs is presented. Indeed, the ability to identify and measure such lumped parameters non-

invasively and patient-specifically (e.g., leukocyte content of the ILT by USPIO (iron oxide contrast agents; ultrasmall superparamagnetic iron oxide) uptake or collagenase activity in the wall by MMP-targeted MRI agents) is increasingly becoming available to provide the necessary data to inform the next generation of biochemomechanical G&R models of AAAs.

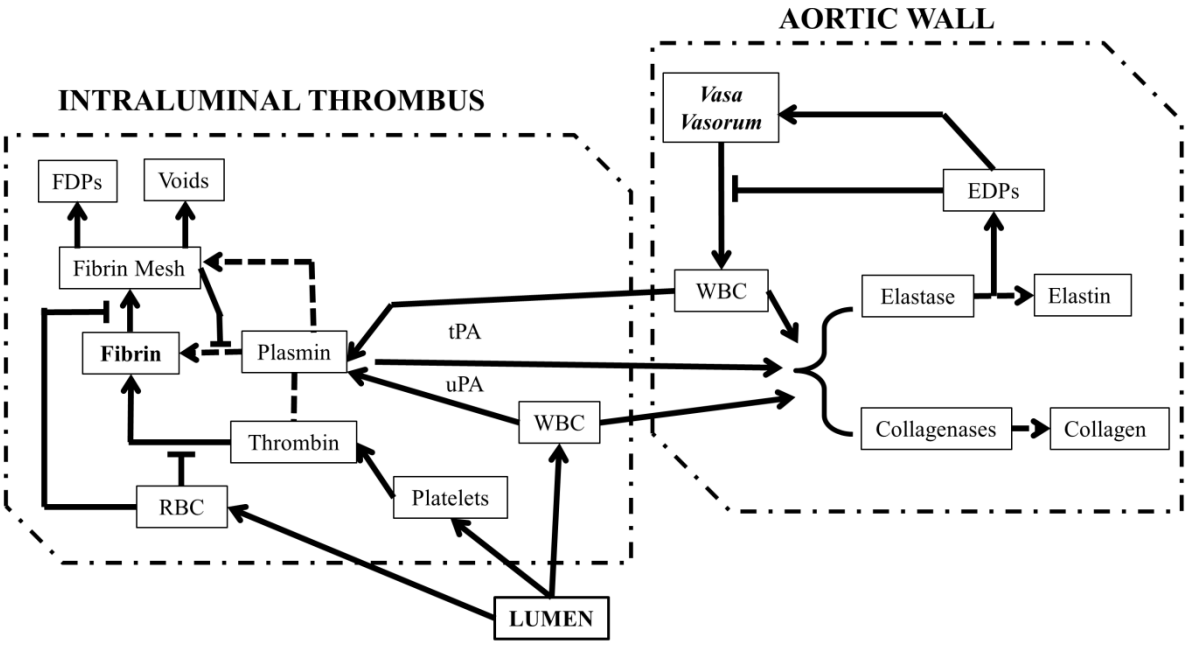

Figure 1.4: Schematic representation of effectors of the biochemomechanics of an evolving AAA from [84]. A solid black arrow indicates 'increases the amount or activity', a dashed black line indicates 'degrades', and a solid line indicates 'modulates the effect', WBC: white blood cell, RBC: red blood cell, EDP: elastin degradation products, FDP: fibrin degradation products

1.3. Objectives and Thesis hypothesis

The objective of proposed research is development of numerical growth and remodeling model of thrombus-laden aneurysm. Description of the temporal changes in radial distribution of proteinases throughout thrombus and aortic wall will allow us to simulate the growth of aneurysm, and determine rupture risk. The model is expected to increase comprehension of aneurysm pathophysiology.

The hypotheses motivating the proposed research are:

1. thrombus directly influences expansion pattern and rupture risk:
   a. mechanically – thrombus reduces peak wall stress, and thus mechanically shields aortic wall,

b. biochemically – formation of ILT introduces enzymes that degrade certain constituents of the aortic wall, and therefore change their mechanical properties,

2. enzymes that influence AAA expansion are produced in the aortic wall as well; they change mechanical properties and weaken the wall.

1.4. Thesis outline

Chapter 1

The first chapter provides the introduction to the Thesis, in which the motivation and Thesis objectives have been defined. The literature review provided in this Chapter additionally clarifies the motivation and objectives of the Thesis.

Chapter 2

This chapter describes growth and remodeling model of healthy and aneurysmal aortic wall used in this Thesis. For aortic wall the already existing model based on constrained mixture theory was adapted. Simplified aneurysm without thrombus was parametrically studied. Additionally, implementation of the model into finite elements and its verifications are presented, Implementation of growth and remodeling model of the aortic wall enables us to model realistic geometries.

Chapter 3

The third chapter covers biochemomechanical overview of abdominal aortic aneurysms. It includes description of structure of both; aneurysmal aortic wall and intraluminal thrombus, review of mechanical testing on these two structures, as well as cascade of biochemical processes responsible for aneurysm evolution. A special attention was given to the biochemical reaction in the thrombus and interaction between the thrombus and aortic wall.

Chapter 4

Based on biochemomechanical overview presented in Chapter 3 models for formation and maturation of intraluminal thrombus and interaction between thrombus and wall were derived. The analysis of biochemical influence of thrombus (neglecting mechanical effects) on cylindrical geometry using *Matfeap* was performed, while full biochemomechanical effects were studied using semi-analytical method. The validation of new models and their possibilities to retrieve clinical observations such as evolution of structure and mechanical

properties during aneurysm expansion is shown in the fourth chapter. Also, the importance of modelling thrombus for predicting aneurysm outcome is presented.

Chapter 5

Effects of the important rupture risk factors, such as smoking, hypertension, thrombus thickness, age and sex, on the aneurysm evolution have been studied in Chapter 5. Additionally, influence of stabilization factors has been investigated.

Chapter 6

The final Chapter summarizes the obtained results and provides recommendations for further research.

2. Growth and remodeling of aortic wall

2.1. Methodology

Growth and remodeling (G&R) of the aortic wall was described using a continuum-based constrained mixture model [29]. Specifically, the wall was assumed to behave initially as a constrained mixture of isotropic elastin, four predominant families of oriented collagen fibers, and circumferential smooth muscle (active and passive contribution). Structurally significant elastin was assumed to be produced only during perinatal development, not maturity. Note that the aging of elastin is described not only by its mechanical properties, but also with its initial mass and pre-stretch. The initial state in these simulations corresponds to a 40-year-old patient, see Table 1. Hence, only the collagen and smooth muscle were allowed to turnover as the lesion enlarged. Original constituents *k* (elastin, four families of collagen fibers and smooth muscle cells) were incorporated within the wall at a pre-stretch $\mathbf{G}^k(0)$ at G&R time $\tau = 0$, while new materials were incorporated within extant matrix at each time step $\tau \in (0, s]$ via a deposition stretch $\mathbf{G}^k(\tau)$; see Figure 2.1 for the associated kinematics. The figure a shows schema of configurations (dark circles / ellipses) and deformations (**F** or **G**) relevant to aortic G&R for times $\tau \in [0,s]$. Note that time $\tau = 0$ denotes the beginning of the simulation when the aged aorta suffers an instantaneous but minimal loss of elastin; time τ is a generic instant at which new constituents are produced and incorporated within the ILT or aneurysmal wall. Time $\tau = s$ is the current computational time at which quantities are interpreted. Note, too, that the natural configurations are stress-free and unique for each constituent. Herein it is assumed that $\mathbf{G}^k(\tau)$ was constant for all τ, though it may vary in disease.

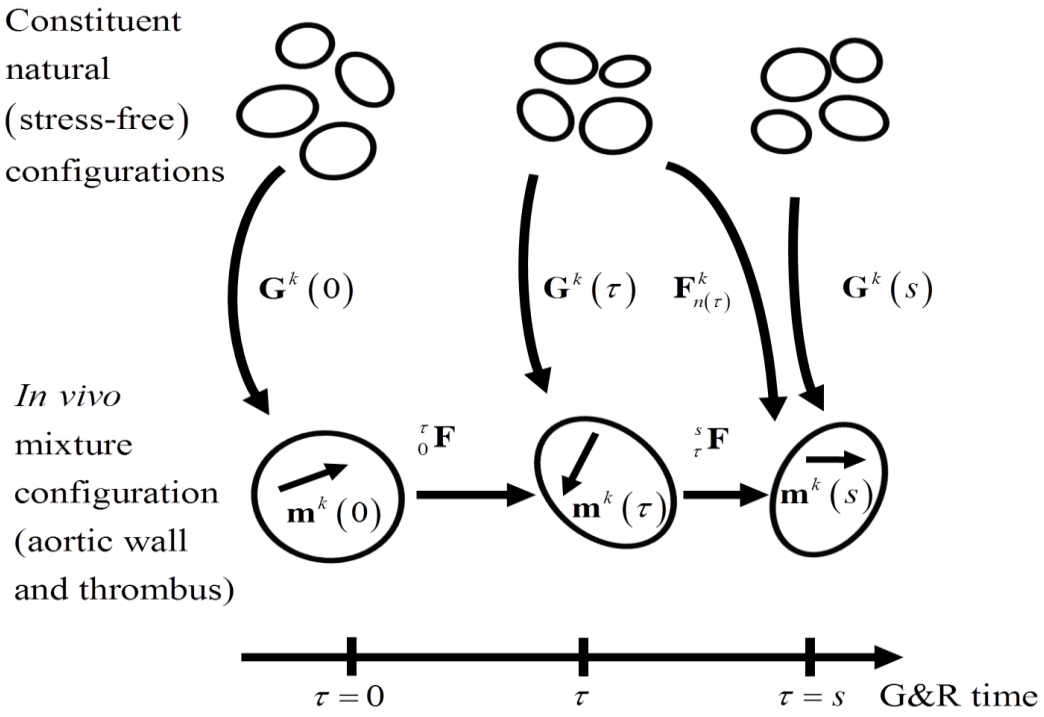

Figure 2.1: Schema of configurations and deformations relevant to aortic G&R, adopted from [33]

The turnover of collagen and smooth muscle was defined by rates of production $\dot{m}^k$ and degradation. The latter was described using survival functions $q^k(s-\tau)$ that accounted for the percentage of constituent *k* produced at past time τ that remained at current time s. The mass of each constituent *k* thus evolved according to its individual production and removal rates, namely [29]

$$M^k(s) = M^k(0)Q^k(s) + \int_0^s \dot{m}^k(\tau)\, q^k(s-\tau)\, \mathrm{d}\tau\,, \tag{1}$$

where $M^k(s)$ and $M^k(0)$ are total (point-wise) masses of constituent k at current time s and initial time 0, respectively. The survival function q^k was modeled consistent with a first order decay, that is,

$$q^k(s-\tau) = \exp\left(-\int_\tau^s K_q^k(\tilde{\tau})\,\mathrm{d}\tilde{\tau}\right), \tag{2}$$

where K_q^k is a rate-type parameter for mass removal. Note that $Q^k(s)$ represents a survival function's special case, at $\tau = 0$, such that $Q^k(s) = q^k(s-0)$.

It is assumed that G&R of the aortic wall is driven, in large part, by deviations in wall stress from a homeostatic target $\left\|\mathbf{t}_{\mathrm{h}}^{k}\right\|$, which represents the norm of the homeostatic Cauchy stress tensor. The mechanobiologically driven rate of mass production $\dot{m}^{k}\left(\tau\right)$ of each constituent *k* was thus defined as a function of the basal production rate m_{B}^{k} and changes in Cauchy stress $\mathbf{t}^{k}$ relative to the homeostatic value:

$$\dot{m}^{k}\left(\tau\right)=m_{B}^{k}\left(1+K_{\sigma}^{k}\frac{\left\|\mathbf{t}^{k}\left(\tau\right)\right\|-\left\|\mathbf{t}_{h}^{k}\right\|}{\left\|\mathbf{t}_{h}^{k}\right\|}+K_{C}^{k}\frac{\tau_{w}\left(\tau\right)-\tau_{w,h}}{\tau_{w,h}}\right). \tag{3}$$

K_{σ}^{k} and K_{C}^{k} are rate parameters governing constituent level stress-driven mass production and gain-type rate parameters responsible for constrictor-mediated changes, respectively; τ_{w} and $\tau_{w,h}$ are wall shear stress in the instant τ and homeostatic value of wall shear stress.

The Cauchy stress **t** within the aortic wall (mixture) was calculated under the assumption of a constrained mixture by first determining the overall stored energy function $W=\sum_{k}W^{k}$, where

$$\mathbf{t}=\frac{2}{\det(\mathbf{F})}\mathbf{F}\frac{\partial W}{\partial\mathbf{C}}\mathbf{F}^{T}+t^{\text{active}}\mathbf{e}^{SMC}\otimes\mathbf{e}^{SMC}, \tag{4}$$

with $\mathbf{F}$ the overall deformation gradient (which can be related to constituent-specific deformation gradients via the kinematics shown in Figure 2.1), $\mathbf{C}=\mathbf{F}^{\mathrm{T}}\mathbf{F}$ is the right Cauchy-Green tensor, and t^{active} is the active stress contribution from smooth muscle contractility (in the direction of smooth muscle; for axially symmetrical geometry they remain circumferential, however in non-symmetric geometry they might re-orient). Moreover, the constituent-specific stored energy functions W^{k} was given by (see section 4 in Baek et al. [85]),

$$W^{k}(s)=\frac{M^{k}(0)}{\sum_{k}M^{k}(s)}\hat{W}^{k}\left(\mathbf{C}_{n(0)}^{k}(s)\right)Q^{k}(s)+\int_{0}^{s}\frac{\dot{m}^{k}\left(\tau\right)}{\sum_{k}M^{k}(s)}\hat{W}^{k}\left(\mathbf{C}_{n(\tau)}^{k}(s)\right)q^{k}(s-\tau)\,\mathrm{d}\tau\,, \tag{5}$$

with $\mathbf{C}_{n(\tau)}^{k}(s)$ the right Cauchy-Green tensor for constituent *k*, calculated by $\mathbf{C}_{n(\tau)}^{k}(s)=\left(\mathbf{F}_{n(\tau)}^{k}(s)\right)^{\mathrm{T}}\mathbf{F}_{n(\tau)}^{k}(s)$, where $\mathbf{F}_{n(\tau)}^{k}(s)$ is the deformation gradient from the natural configuration to the current configuration at time s for constituent k produced at time τ (see Figure 2.1).

Collagen and smooth muscle were modeled as fiber-like structures without significant compressive stiffness, as in most prior G&R models. The stored energy function per unit mass for the smooth muscle-dominated behavior was defined as in Humphrey and Rajagopal [29]

$$\hat{W}^{SMC} = \frac{c_2^{SMC}}{4c_3^{SMC}}\left[\exp\left(c_3^{SMC}(I_4-1)^2\right)-1\right], \tag{6}$$

with c_2 and c_3 material parameters and I_4 the fourth (pseudo)invariant of right Green-Cauchy tensor ($I_4 = \mathbf{m}^k(\tau)\mathbf{C}^k_{n(\tau)}\left(\mathbf{m}^k(\tau)\right)^T$, with $\mathbf{m}^k(\tau)$ being orientation of the constituent *k*). Collagen may reorient out of the cylindrical plane in aneurysms [86], but radially reoriented fibers were not included because experimental data are lacking. In this case, elastin would bear all of the compressive radial stress. Because elastin is significantly lost as an AAA evolves, unrealistic radial stresses would result as the elastin content approached zero. Noting that glycosaminoglycans / proteoglycans typically associate with collagen fibers and can contribute to the overall compressive stiffness of the extracellular matrix, a neo-Hookean component to the stored energy function that described the (proteoglycan-augmented) collagen-dominated behavior was added, such that

$$\hat{W}^c = c_1^c\left(\mathrm{tr}\left(\mathbf{C}_{n(\tau)}\right)-3\right)+\frac{c_2^c}{4c_3^c}\left[\exp\left(c_3^c(I_4-1)^2\right)-1\right], \tag{7}$$

with corresponding material parameters c_1^c, c_2^c c_3^c (for details see chapter 4.1.). Values were chosen to fit the original exponential stored energy function while simultaneously ensuring an equivalent homeostatic stress at the deposition stretch $G_h^c = 1.08$, [87].

Active stress contribution from smooth muscle cells was considered to be (as in [88])

$$t^{active}(s) = T_m\phi^{SMC}(s)\left(1-e^{-C(s)^2}\right)\lambda^{SMC(\mathrm{active})}(s)\left[1-\left(\frac{\lambda_M-\lambda^{m(active)}(s)}{\lambda_M-\lambda_0}\right)^2\right]. \tag{8}$$

In the equation (8) T_m is the maximum actively generated stress, λ_M is the circumferential stretch at which active stress is maximum, λ_0 is the circumferential stretch at which active stress goes to zero, ϕ^{SMC} mass fraction of muscle cells, $C(s)$ is the net ratio of vasoconstrictors/vasodilators, and $\lambda^{m(active)}(\tau) = \frac{\lambda^{SMC}(\tau)}{\lambda^A(\tau)}$. This is slightly modified from the original model [89] , where $\lambda^{m(active)}$ was defined as $\lambda^{m(active)}(\tau) = \frac{r^{SMC}(\tau)}{r^A(\tau)}$ with r being radius. In general, the geometry does not need to stay axially symmetric, and thus radius is not

necessarily defined. The model was, therefore, extended for more general geometries by replacing the ratio of radii with stretch. Note that for cylindrical geometry the value of active stress is not changed by this modification. Stretch λ^A evolves via a first order rate equation, similar to original model

$$\frac{\mathrm{d}\lambda^A(\tau)}{\mathrm{d}s} = K^{act}\left[\lambda^{SMC}(\tau) - \lambda^A(\tau)\right], \tag{9}$$

where $\lambda^{\mathrm{A}}(0) = \lambda^{\mathrm{SMC}}(0)$ in a healthy artery.

2.2. Semi-analytical solution and *FEAP*

This model has been implemented in two software packages: *Matlab* and finite element analysis program *FEAP*.

In the case of an axisymmetric cylinder maintained at a fixed *in vivo* length, deformation gradient ${}^{s}_{\tau}\mathbf{F}$ that quantifies mappings within *in vivo* mixture configurations between arbitrary time τ and current time s can be easily calculated analytically as ${}^{s}_{\tau}\mathbf{F} = \begin{bmatrix} \partial r(s)/\partial r(\tau) & 0 & 0 \\ 0 & r(s)/r(\tau) & 0 \\ 0 & 0 & 1 \end{bmatrix} = \begin{bmatrix} J(s)r(\tau)/J(\tau)r(s) & 0 & 0 \\ 0 & r(s)/r(\tau) & 0 \\ 0 & 0 & 1 \end{bmatrix}$ (see [33] for more details). Thus, as long as geometry remains cylindrical and the deformation depends on the radius alone, finite element method is not necessary for obtaining results; this simpler sub-class of 3D problems allows a "semi-analytical" solution. Such 1D problems are clinically relevant for particular arteries, including common carotids, basilar artery, and aorta, e.g., during arterial adaptation to new blood pressure or flow. As it still requires radial discretization and iterative procedure to satisfy equilibrium, this semi-analytic solution was calculated using *Matlab*.

In contrast, implementation of the proposed theory for a general 3-D geometry (e.g., modeling growth of local dilatation during AAA evolution) requires finite element analysis. *FEAP* was used for finite element analysis; it is a general purpose finite element analysis program with fully open source code. The *FEAP* program includes options for defining one, two, and three dimensional meshes, defining a wide range of linear and nonlinear solution algorithms, graphics options for displaying meshes and contouring solution values, an element library for linear and nonlinear solids, thermal elements, two and three dimensional frame (rod/beam) elements, plate and shell elements, and multiple rigid body options with joint interactions. Constitutive models include linear and finite elasticity, viscoelasticity with

damage, and elasto-plasticity. It also allows user to define a new material, as was done within this work.

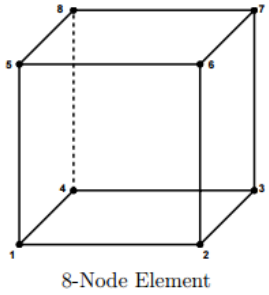

Figure 2.2: 8-node hexahedral element, from *FEAP* User Manual

For our simulations 8-node hexahedral element was used, Figure 2.2, with 3 degrees of freedom at each node. Solid mechanics elements in *FEAP* are available based on displacement, mixed, and enhanced strain formulations. A finite element formulation which is free from locking at the incompressible or nearly incompressible limit may be developed from a mixed variational approach using the Hu-Washizu variational principle. In the principle, displacements appear up to first derivatives, while the stresses and strains appear without any derivatives. Accordingly, the continuity conditions that may be used in finite element approximations are C^0 for the displacements and C^{-1} for the stresses and strains (a C^{-1} function is one whose first integral will be continuous). Appropriate interpolations for each element are thus:

$$\mathbf{u}(\xi) = N_I(\xi)\mathbf{u}^I(t) \tag{10}$$

$$\boldsymbol{\sigma}(\xi) = \phi_\alpha(\xi)\boldsymbol{\sigma}^\alpha(t) \tag{11}$$

$$\boldsymbol{\varepsilon}(\xi) = \psi_\alpha(\xi)\boldsymbol{\varepsilon}^\alpha(t) \tag{12}$$

where $\phi_\alpha(\xi)$ and $\psi_\alpha(\xi)$ are interpolations which are continuous in each element but may be discontinuous across element boundaries. The parameters $\boldsymbol{\sigma}^\alpha$ and $\boldsymbol{\varepsilon}^\alpha$ are not necessarily nodal values and, thus, may have no direct physical meaning.

A mixed approximation may now be used to describe the pressure and the volume change in each element. Accordingly, it is assumed

$$p(\xi) = \phi_\alpha(\xi)\, p^\alpha(t) \tag{13}$$

$$\theta(\xi) = \phi_\alpha(\xi)\theta^\alpha(t) \tag{14}$$

where it is noted that the same approximating functions are used for both pressure and volume. If the material is isotropic linear elastic, the use of the same functions will permit an exact satisfaction of the constitutive equation at each point of the domain of an element. For other situations, the constitutive equation may be approximately satisfied.

Traditionally, finite strain finite element formulations employs deviatoric split of deformation gradient. However, several studies (e.g., [90–92]) suggested that although volumetric-isochoric split of the deformation gradient, and thus stored energy function, can be justified and systematically derived for isotropic materials, in the case of anisotropic material description decomposition must be executed with care in order not to violate certain physical requirements. Thus, this fiber-reinforced hyperelastic material was compared to results obtained by volumetric-isohoric split and formulation without split.

In the volumetric-isochoric split formulation the total stored energy function W can be written in decoupled form as

$$W = W_{sph} + \overline{W}, \tag{15}$$

where W_{sph} is spherical (volumetric) part and $\overline{W}$ is the elastic contribution due to isochoric distortions. The distortional elastic contribution was calculated as

$$\overline{W}^k = \frac{c_2^k}{4c_3^k}\exp\left(c_3^k(\mathbf{m}\overline{\mathbf{C}}\mathbf{m}^{\mathrm{T}} - 1)^2\right), \tag{16}$$

with $\overline{\mathbf{C}} = \overline{\mathbf{F}}^{\mathrm{T}}\overline{\mathbf{F}}$ and $\overline{\mathbf{F}} = J^{-1/3}\mathbf{F}$; while c_2^k and c_3^k are stiffness material parameters.

On the other hand, formulation without split does not include decomposition of stored energy function and total stored energy is defined simply as

$$W^k = \frac{c_2}{4c_3}\exp\left(c_3(\mathbf{m}\mathbf{C}\mathbf{m}^{\mathrm{T}} - 1)^2\right). \tag{17}$$

Similarly, stress and tangent modulus in case of volumetric-isochoric split were calculated as $\mathbf{t} = \mathbf{t}_{sph} + \overline{\mathbf{t}} + \mathbf{t}_{act}$ and $\mathbb{C} = \mathbb{C}_{sph} + \overline{\mathbb{C}} + \mathbb{C}_{act}$ (for more details see [93]).

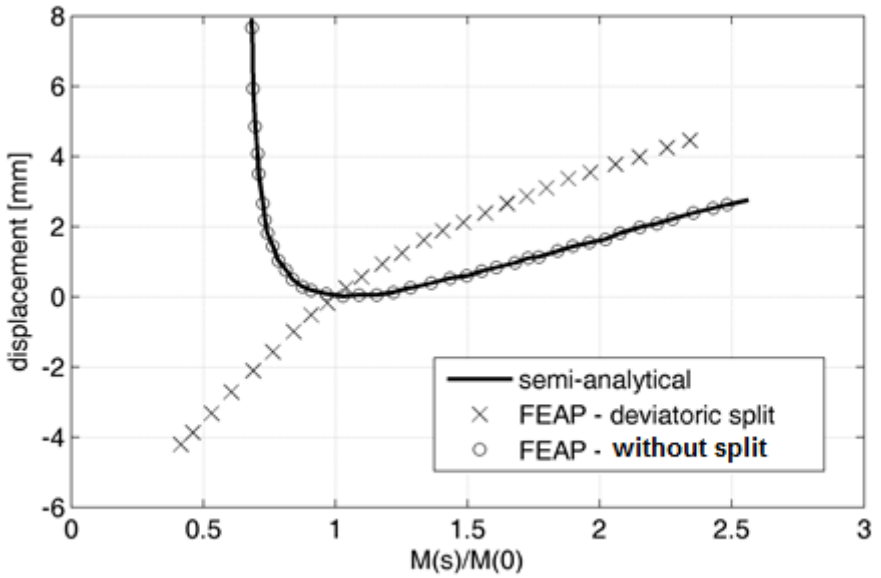

Figure 2.3: Comparison of results obtained by semi-analytic method, and deviotoric split and formulation without split in *FEAP*

Not only formulation without split proved to eliminate certain numerical instabilities, but the results were considerably more accurate. For example, Figure 2.3 shows comparison of evolution of radial displacements of cylindrical artery with no turnover of collagen and smooth muscle, and uniform change of mass of elastin calculated by *FEAP* with deviatoric delineation (cross sign) and formulation without split (plus sign), as well as semi-analytical solution (solid line) for case of uniform changes in mass.

In this example masses of collagen and smooth muscle were kept constant ($m_B^k = 0$, $K_q^k = 0$) to eliminate integrals from equations (1) and (5), while elastin was produced (for $M(s)/M(0) > 1$) or degraded (where $M(s)/M(0) < 1$). Degradation of elastin is typical for aging, and thus it would be expected that artery dilates with loss of elastin [94]. Semi-analytical solution showed steep increase in radius with degradation of elastin, whereas with its production radius first slightly decreased before slowly increasing. Results obtained by *FEAP* with deviatoric split implementation demonstrate unexpected shrinkage of artery when losing elastin. However, solution from formulation without split implemented in *FEAP* demonstrated full agreement with semi-analytical solution.

This might be explained by the fact that the inclusion of the isochoric part of the deformation in the expressions related to the fibers causes the stresses in the fiber to be not of a one-dimensional nature. The analysis provided in [90] suggests that the fiber-related terms in the energy are to be formulated using the complete deformation tensor $\mathbf{C}$, while the

volumetric-isochoric split should be applied to the matrix part (i.e. elastin) only. For more details also see [92].

2.3. Equilibrium equations and geometry

While this new G&R framework can, and eventually should, be implemented in simulations based on patient-specific geometries and with fluid-solid-growth coupling [95], it is first important to verify and test a new constitutive model in a geometrically simple case. Hence, similar to many prior G&R studies of AAAs [44,73], the first focus was on a simple axisymmetric geometry for illustrative purposes and to gain initial insights. Given differences in time scales between the cardiac cycle and the evolution of a lesion, a quasi-static motion of the lesion was considered whereby

$$\mathrm{div}\left(\mathbf{t}\right)=\mathbf{0}\,, \tag{18}$$

which, for an axisymmetric cylindrical geometry, reduces to

$$P=\int_{r_l}^{r_i}\left(t_{\theta\theta}-t_{rr}\right)\frac{\mathrm{d}r}{r}+\int_{r_i}^{r_m}\left(t_{\theta\theta}-t_{rr}\right)\frac{\mathrm{d}r}{r}+\int_{r_m}^{r_a}\left(t_{\theta\theta}-t_{rr}\right)\frac{\mathrm{d}r}{r}+\int_{r_a}^{r_o}\left(t_{\theta\theta}-t_{rr}\right)\frac{\mathrm{d}r}{r}\,, \tag{19}$$

where P is the luminal pressure distending the vessel and r_l, r_i, r_m, r_a, r_o are radii at the following interfaces: lumen/ILT, ILT/intima, intima/media, media/adventitia, adventitia/outer surface. Similarly, the overall axial force L was computed as:

$$L=\pi\left(\int_{r_l}^{r_i}\left(2t_{zz}-t_{\theta\theta}-t_{rr}\right)\frac{\mathrm{d}r}{r}+\int_{r_i}^{r_m}\left(2t_{zz}-t_{\theta\theta}-t_{rr}\right)\frac{\mathrm{d}r}{r}+\int_{r_m}^{r_a}\left(2t_{zz}-t_{\theta\theta}-t_{rr}\right)\frac{\mathrm{d}r}{r}+\int_{r_a}^{r_o}\left(2t_{zz}-t_{\theta\theta}-t_{rr}\right)\frac{\mathrm{d}r}{r}\right). \tag{20}$$

The overall procedure for solution is best appreciated via a flow chart below.

1. *Zeroth time step – homeostasis*
READ input file with data for homeostasis from semi-analytic solution
LOOP until convergence of Augmented Lagrange scheme
    UPDATE geometry
    GET deformation gradient ${}^{s}_{0}\mathbf{F}$
    LOOP over integration points until convergence of the Newton-Raphson scheme
        CALL user material (umat) subroutine
        INPUT deformation gradient ${}^{s}_{0}\mathbf{F}$
        READ history variables
        CALCULATE constituents' masses and orientations, stresses
        WRITE to history fields masses, orientations, deformation gradient, stress
        OUTPUT: stress $\boldsymbol{\sigma}$, tangent modulus □
    END LOOP (equilibrium)
END LOOP (Augmented Lagrange)
WRITE data

2. *Growth and remodeling*
LOOP for time
UPDATE geometry
GET deformation gradient ${}^{s}_{0}\mathbf{F}$
LOOP over integration points until convergence of Augmented Lagrange scheme
LOOP until convergence of the Newton Raphson scheme
CALL user material (umat) subroutine
INPUT deformation gradient ${}^{s}_{0}\mathbf{F}$
READ history variables
CALCULATE mass production, fiber orientations
LOOP for time (from 0 to current)
CALCULATE survival functions, stored energy function
END LOOP (time)
CALCULATE masses, stress
WRITE to history fields masses, orientations, deformation gradient, stress
OUTPUT stress $\boldsymbol{\sigma}$, tangent modulus $\mathbb{C}$
END LOOP (equilibrium)
END LOOP (Augmented Lagrange)
WRITE data
END LOOP (time)

2.4. Parameter values

Similar to previous implementations of constrained mixture models for arterial G&R [31,34,96], the constitutive relations and parameters were classified by level of consensus and function (Table 1). All parameters that were measured easily (such as arterial geometry and volumetric flowrates [8]) were classified as "observed". In contrast, "bounded" parameters were less well-known and either defined via a parametric study [31].

Table 1: Parameter values used for G&R of aortic wall. Note: 'h' denotes homeostatic.

Class	Role	Parameter value	Eq. #	Refs.
Observed	Physical constants	$\rho = 1050\ \mathrm{kg\,m^{-3}}$, $\mu = 0.0037\ \mathrm{Pa\cdot s}$, $r_i = 9.925\ \mathrm{mm}$	See [34]	[87]
	Initial loading	$P_h = 104\ \mathrm{mmHg}$, $\tau_{w,h} = 0.5\ \mathrm{Pa}$, $t_h = 100\ \mathrm{kPa}$		[87]
	Composition by layer	$\phi_{\mathrm{int}} = 0.16$, $\phi_{\mathrm{med}} = 0.52$, $\phi_{\mathrm{adv}} = 0.32$; $\phi^{c}_{\mathrm{int}} = 1$, $\phi^{e}_{\mathrm{med}} = 0.55$, $\phi^{c}_{\mathrm{med}} = 0.25$, $\phi^{SMC}_{\mathrm{med}} = 0.20$, $\phi^{e}_{\mathrm{adv}} = 0.25$, $\phi^{c}_{\mathrm{adv}} = 0.75$		[34,97]

	Homeostatic kinetics	$\tau_{1/2}^{c} = \tau_{1/2}^{SMC} = 70$ days	(2)	[87,98, 99]
	Passive elasticity	$c_1^c = 0.025$ MPa, $c_2^c = 498.2$ kPa, $c_3^c = 23.52$ $c_2^{SMC} = 25.9$ kPa, $c_3^{SMC} = 3.5$, $c_e = 134.96$ kPa	e.g., (16)	[8,97]
Bounded	Pre-stretches	$G_{\Theta\Theta}^{e} = G_{zz}^{e} = 1.2$, $G_h^{SMC} = 1.2$, $G_h^{c} = 1.08$, $G^{\mathrm{f}} = 1.08$	See Figure 2.1	[96]
	SMC activation	$T_{\mathrm{m}}(0) = 300$ kPa, $\beta_m = 0.75$, $\lambda_{\mathrm{m}} = 2$, $\lambda_0 = 0.4$	(8)	[96]
	Production	$K_\sigma^c = 3$, $K_\sigma^{SMC} = 3$	(3)	[31]

2.5. Simplified aneurysm without ILT (semi-analytical method)

AAAs are characterized by a much greater elastin degradation than aging alone. The resulting dilatation is considered aneurysmal when the diameter increases by 50% over baseline. Clinicians consider AAAs expanding ≤ 2 mm/year to be stable, whereas aneurysms that expand ≥1 cm/year are at high risk for rupture. Given that functional elastin and smooth muscle are almost completely lost during the development of an AAA, collagen turnover has a fundamental role in the endpoint of AAA progression: stable growth, cessation of growth, or rupture. Prior G&R investigations have explored parametrically the effects of key aspects of collagen turnover on AAA progression, including rates of production, half-life, deposition stretch, and stiffness [73]. Notably, these properties of collagen turnover may vary from healthy remodeling to AAAs.

Stored energy function per unit mass for collagen and SMC are defined as in [29]:

$$\hat{W}^k = \frac{c_2^k}{4c_3^k}\left[\exp\left(c_3^k (I_4 - 1)^2\right) - 1\right] \tag{21}$$

where c_2 and c_3 are material parameters and I_4 is forth invariant of right Green-Cauchy tensor ($I_4 = \mathbf{m}^k(\tau)\mathbf{C}_{n(\tau)}^k\left(\mathbf{m}^k(\tau)\right)^T$, with $\mathbf{m}^k(\tau)$ being orientation of the constituent k.

As a result, three cases for collagen stiffness in AAAs were considered: softening, remaining constant, or stiffening. Softening and stiffening of collagen was considered to be functions of

the homeostatic stiffness and the ratio of current and initial stretch (e.g., $c_3^k(s) = c_3^k(0)\lambda^k(s)/\lambda^k(0)$ for stiffening, inverse ratio for softening). Note that for maintenance in healthy aorta, $c_3^k(s) = c_3^k(0)$; therefore, stiffness is constant in maintenance as expected.

Since AAAs can expand from an initial 2 cm diameter to > 7 cm, strains measured from the homeostatic configurations can be much larger than in aging healthy aorta. For elastin, which does not undergo turnover, these strains may be fully experienced; however, for collagen and smooth muscle, ongoing turnover helps to prevent overloading, particularly considering the exponential nature of their strain energy function Eq. (16). Nevertheless, in rapidly progressing aneurysms, collagen and smooth muscle may still be at risk of mechanical failure. Thus, failure criteria of 6 MPa for collagen and 0.15 MPa for SMC [100] were implemented. Note that this increased risk of fibers mechanically failing in the G&R model is consistent with the clinical observation that rapidly growing lesions are more likely to rupture, while slower expansion allows adequate time for ECM turnover.

In many prior G&R models, collagen and smooth muscle have been modeled as fiber-like structures without significant compressive stiffness. Proteoglycan and glycosaminoglycan content, which may contribute to compressive stiffness of the ECM, also have usually been ignored. Furthermore, while collagen content in aneurysms may re-orient out of the cylindrical plane [86], adequate experimental guidance is lacking; therefore, radial reorientation has not been incorporated into this G&R model. As a result, elastin must bear all compressive radial stress. However, since elastin is significantly lost in AAA development, unrealistic radial stresses are predicted as elastin content approaches zero. Therefore, two hypotheses for modeling the aneurysmal wall were considered:

First, limiting the loss of elastin to 5-15% of its initial mass and keeping the stored energy function in Eq. (2), though allowing, smooth muscle to be degraded completely; with Eq. (49)

.

Second, allowing the complete degradation of elastin and introducing a Neo-Hookean component to the collagen stored energy function, such that,

$$\hat{W} = c_1^*\left(\mathrm{tr}\left(\mathbf{C}_{n(\tau)}\right)-3\right)+\frac{c_2^*}{4c_3^*}\left[\exp\left(c_3^*(I_4-1)^2\right)-1\right]. \tag{22}$$

Values of material parameters c_1^*, c_2^* c_3^* in Eq. (22) are slightly changed in comparison to ones from Eq. (21) by arbitrarily prescribing c_1^* and computing best-fit values of c_2^* and c_3^* to fit

the original exponential stored energy function (21) while ensuring the an equivalent homeostatic stress at the deposition stretch $G_h^c = 1.08$.

These newly proposed constitutive rules for variable collagen stiffness and stored energy were then applied to investigate AAA progression without thrombus (i.e., with elastolysis driven only by an initial degradation and time-dependent decay).

Concept 1: exponential stored energy function

To study the effects of collagen and elastin turnover in AAAs using the original stored energy function for collagen, four different parameters that potentially effect outcome were investigated: percentage of remaining initial elastin , changes in the material stiffness of the collagen fiber, rates of stress-mediated production of collagen (parameter K_σ in Eq.(3)), and rates of degradation of elastin (half-life of elastin $\tau_{1/2}^e$). Eight cases were simulated using parameters shown in Table 2; outer diameter of the lesion over time is shown in Figure 2.4

Note the increasing propensity for unstable expansion with decreasing collagen stiffness (cases 1-3). In fact, in all cases exhibiting stabilization, collagen stiffens (cases 1, 7, and 8). However, case 6 demonstrates that rupture may still occur despite collagen stiffening if collagen production (K_σ value) is sufficiently low. Nevertheless, not even increased collagen production and reduced elastin degradation rate (and thus reduced expansion rate of the AAA) prevent rupture if collagen stiffness remains constant (cases 4 and 5).

Table 2: Sets of parameter values used to simulate AAA without thrombus using concept 1

Case #	**Elastin survived, %**	**Collagen stiffness**	**Rate of production K_σ**	**Elastin half-life $\tau_{1/2}^e$**
1	15	Stiffening	3	1 year
2	15	Constant	3	1 year
3	15	Softening	3	1 year
4	15	Constant	3	2 years
5	15	Constant	4	2 years
6	15	Stiffening	2	1 year
7	10	Stiffening	3	1 year
8	10	Stiffening	4	3 year

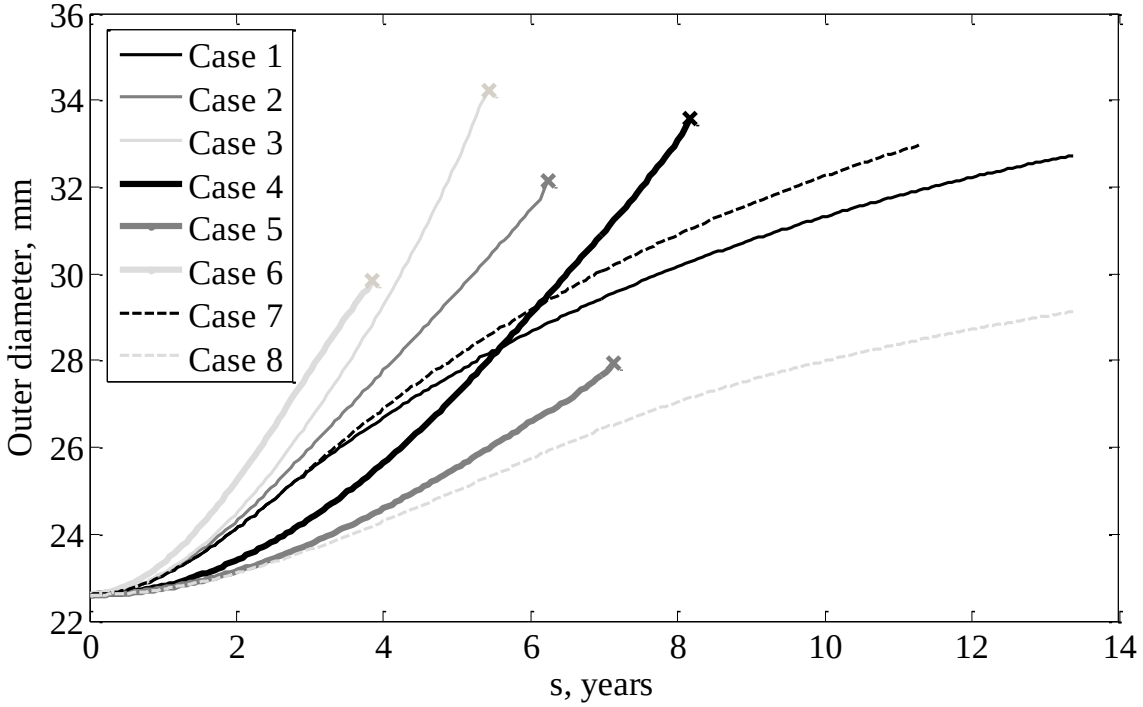

Figure 2.4: Temporal changes in outer diameter of AAA for eight cases defined by Table 2; aneurysm ruptures at the end of simulation are marked with "x"

Interestingly, for the cases simulated, neither percentage of remaining nor its half-life affected the ultimate outcome (rupture vs. stabilization), but rather only altered the final diameter and rate at which the outcome was achieved. This is consistent with Cyron et al. ([101]), who predicted collagen production and half-life to be the primary determinants of stability margin in the G&R of idealized AAAs.

In conclusion, elastin degradation rate and final mass of elastin have no influence on outcome of AAA growth. Similarly to [73], softening and unchanged stiffness tend to result in rupture, while stiffening of collagen can lead to stabilization of aneurysm. However, unlike conclusions in mentioned study, stabilization only occurs if there is sufficient production of collagen. "Sufficient collagen production" could be expected to be a certain combination of rate of its production and rate of elastin degradation (its half-life); however that is not the focus of this study. Moreover, the study in [73] was performed on membrane finite element model, meaning it was capable of computing axial changes of axisymmetric fusiform AAA. Note that after bulging axially oriented collagen can bear load in radial direction as well. On the other hand, being a membrane model, it is unable of capturing radial changes. Therefore, some differences are to be expected, while general behavior should be the same.

An example of the changes in mass of key load-bearing components of the wall is shown in Figure 2.5 (for case 8 in which elastin mass reduces to 15% while smooth muscle continues to decrease toward zero). Black line represents elastin, dark gray line SMC, and light gray line collagen. As elastin and SMCs are lost, increasing stress drives increased collagen production.

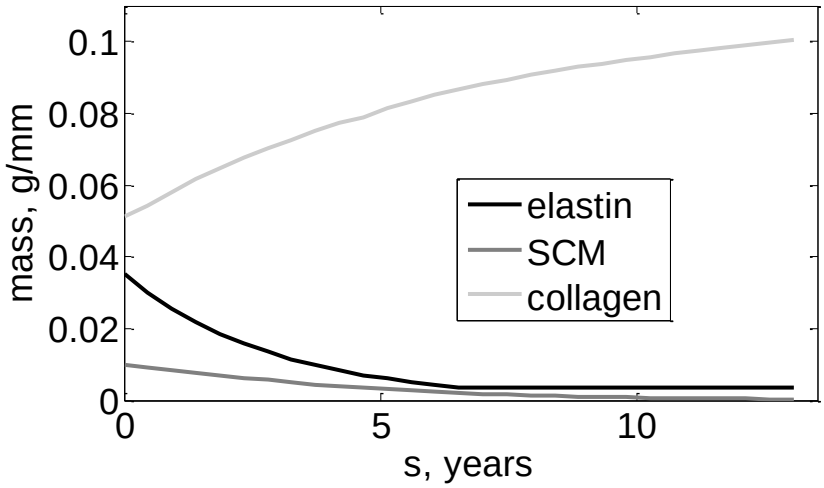

Figure 2.5: Temporal changes in masses of constituents

As a consequence of these mass variations, thicknesses of the layers of the aortic wall also change. Although whole-wall thickness only mildly reduced to 85% of the initial value (results not shown), normalized thickness (ratio of current thickness of the layer and current whole-wall thickness) predicts intimal thickening with medial loss (see Figure 2.6, black line represents intima, pale gray line media, and dark gray line adventitia).

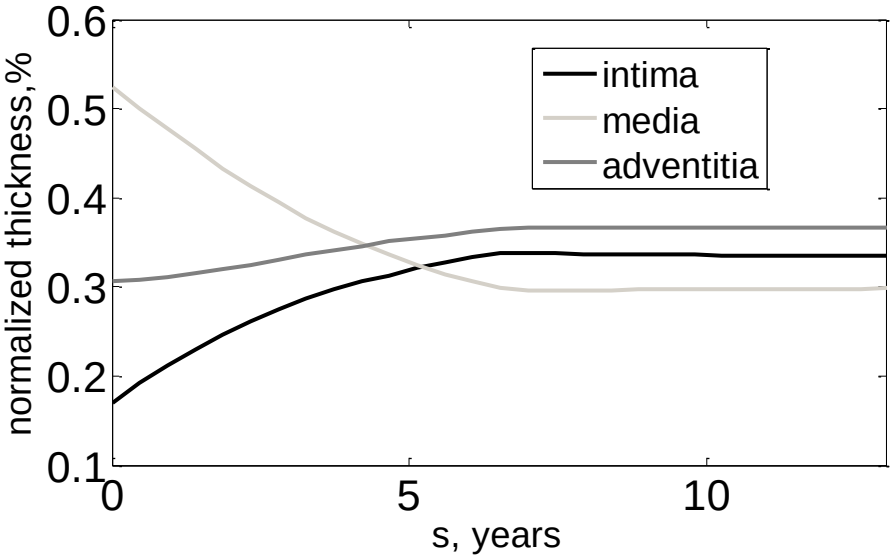

Figure 2.6: Temporal changes in normalized thicknesses of layers in case 8

Concept 2: complete degradation of elastin

Alternatively, to allow for complete degradation of elastin, a new stored energy function for collagen that includes both Neo-Hookean and exponential components (Eq. (22)) was considered. As discussed in Methods, new sets of material parameters were selected for six cases outlined in Figure 2.6.

Table 3: Examples of parameter values in modified stored energy function (Eq. (22)). RMSE denotes root mean square error.

#	c_1^*, MPa (chosen)	c_3^*, - (fitted)	c_2^*, MPa (calculated)	RMSE
1	0.001	22.06	0.5576	9.64e-5
2	0.005	22.29	0.5470	4.85e-4
3	0.01	22.59	0.5341	9.77e-4
4	0.025	23.52	0.4982	2.49e-3
5	0.05	25.15	0.4467	5.17e-3
6	0.1	28.8	0.3653	1.11e-2

Similar to Concept 1, smaller values of c_1^* (up to 0.025 MPa) allow for arrest of AAA expansion provided sufficient collagen production and stiffening. The value of production rate necessary for arresting expansion increases with increased isotropy. For values of c_1^* higher than 0.025, however, arrest is not likely, even with high stress-mediated production of collagen. In this case, the aneurysms may continue to expand with or without rupture.

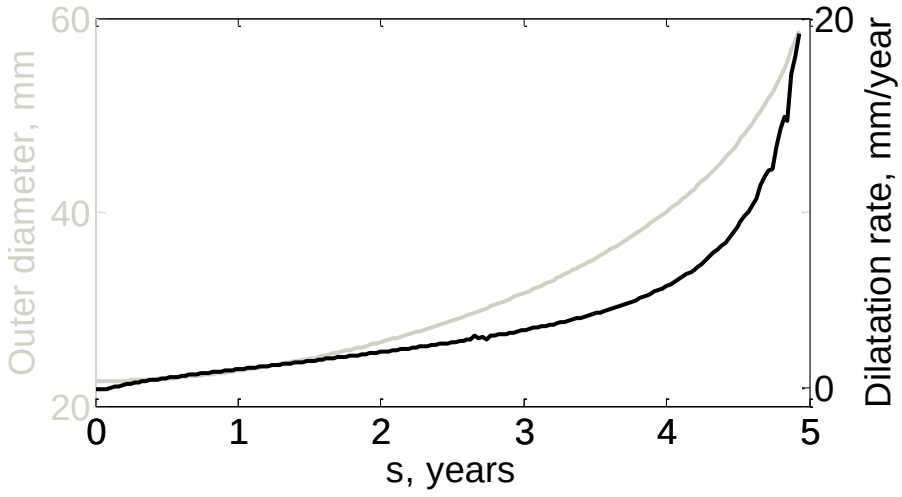

Figure 2.7: Temporal changes in dilatation (gray line) and rate of dilatation (black line) of AAA for modified stored energy function for collagen

Note that for $c_1^* = 0.025$ MPa, $K_\sigma = 2$ and half-life of elastin of 2 years, the aneurysm enlarges to 60 mm before rupturing (see Figure 2.7), while for Concept 1, the lesion ruptures at only 35 mm (see Figure 2.7). Furthermore, the dilatation rate in Figure 2.7 remains less than about 5 mm/year before sharply increasing before rupture to greater than 1 cm/year (a clinical value believed to represent high rupture risk)., Thus, Concept 2 appears to be more representative of actual AAAs than Concept 1 and will be used for the following thrombus-laden AAA simulations. Yet, what might account physiologically for the isotropic Neo-Hookean contribution to this modified storage energy function. Possibilities might include an increase in nonfibrillar collagen (e.g., collagen V), other isotropic materials such as proteoglycans and glycosaminoglycans, or remnant fragments of elastin (or even new non-lamellar elastin) capable of bearing small loads. Future experiments would be useful for further insight.

2.6. Implementation into finite element code

Several attempts of implementation of G&R models into finite element codes have been conducted. The model was first implemented in the membrane finite elements that allow modeling enlargement of axisymmetric (fusiform) aneurysms [85]. Using the membrane model geometrical changes and expansion rates during the aneurysm growth for different kinetic parameters were studied [102], as was the importance of initial aortic properties and collagen turnover on the evolution of fusiform AAAs without thrombus [43,73]. Furthermore, a computational framework coupling vascular G&R with blood flow simulation in a 3D patient-specific geometry was presented in [95].

Nevertheless, albeit undoubtedly useful, membrane models are incapable of capturing distributions in radial direction. Radial distributions of stresses and masses could be important for the evolution of aneurysms, as it is known that aneurysmal wall is not degraded uniformly, nor is the mass in the wall is produced evenly. The radial differences in masses are even greater in thrombus-laden aneurysms [103], and thus for modeling biochemical influence of thrombus on the aneurysmal wall more accurately the mean values might not suffice, and it would be necessary to calculate their radial distributions. Additionally, membrane model might not be the best approximation for the thick walled, multilayered arteries. Hence, there is

a pressing need for extension of the constrained mixture framework to reliable 3D finite elements capable of modeling the evolution of biochemical and mechanical properties. This process is quite challenging, as the formulation must allow large changes in mass while enforcing the incompressibility constraint during transient motions, as well as take into account evolving mechanical properties.

The first G&R implementation into 3D finite-element code [93] confronted a variety of numerical problems including instabilities and divergence of solutions with increased G&R time, management of computational requirements for storing histories of kinetics and motions, very high CPU expense and difficulties with enforcing isochoric responses.

2.6.1. Adaptation of healthy aorta to changes in blood flow and pressure

Before application of the G&R model to fusiform and saccular aneurysms it is necessary to verify implementation. This was done for examples for which semi-analytical solutions exist, i.e. geometry stays cylindrical, such as change in blood flow or pressure.

It has been shown that if both wall shear stress and circumferential stress are returned to homeostatic values after perturbations in blood flow and pressure, given by $Q = \varepsilon Q_h$ and $P = \gamma P_h$, then stress-mediated G&R must produce specific changes in geometry. For example, when blood flow is 10% below its homeostatic (normal) value, $\varepsilon = 1.1$ and it is expected that inner radius and thickness should both change as $1.1^{1/3} = 1.0323$ of homeostatic values. For an aorta with inner radius 1 cm, terminal displacement would amount to 0.323 mm. Both semi-analytical and finite element simulations agreed with membrane theory, as can be seen in Figure 2.8.

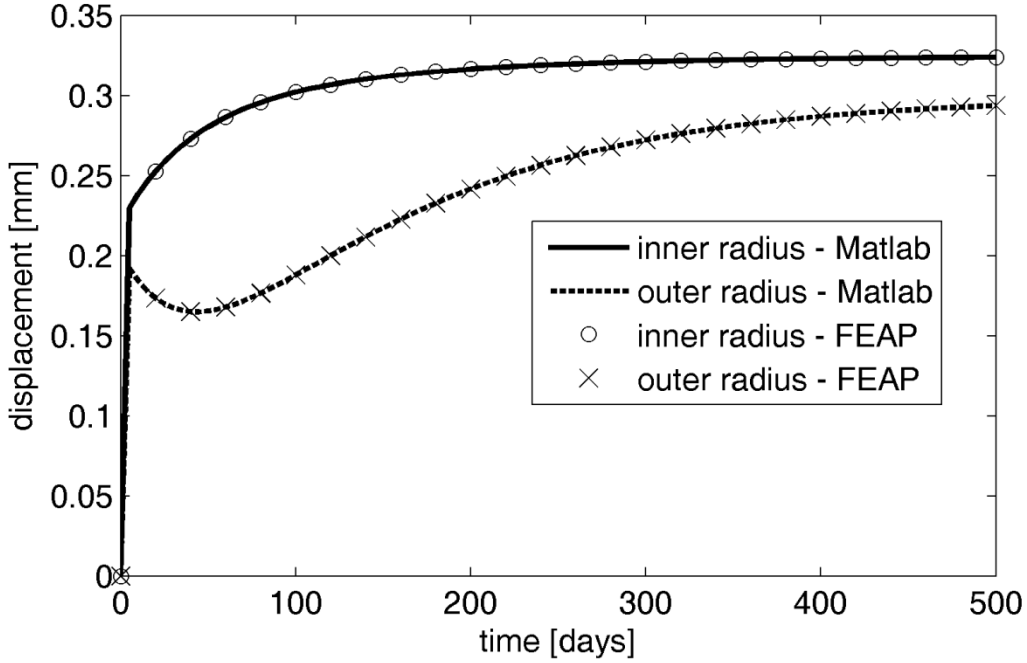

Figure 2.8: Evolution of displacements of inner and outer radius obtained by semi-analytical solution (lines) and FEM (markers) after 10% increase in blood flow

Similarly, after an abrupt and sustained alteration in pressure, relevant to study of hypotension or hypertension, the most empirically observed response by the arterial wall to is change of thickness of the wall, however no long-term dilatation/shrinkage of blood vessel was observed [104,105]. For instance, after 20% abrupt decrease in blood pressure, the vessel immediately shrinks due to change in loading; however, growth and remodeling processes quickly ensure the inner radius returns almost to the initial value (Figure 2.9). Conversely, in hypertension (30% increase in blood pressure in Figure 2.9), it dilates at first, but after adaptation to the new sustained pressure, inner radius returns to approximately homeostatic value. Solid and dashed lines represent displacements obtained semi-analytical solution at inner and outer radii, respectively, whereas circle and cross markers are results attained using *FEAP*. Note that the finite element results match semi-analytical ones perfectly.

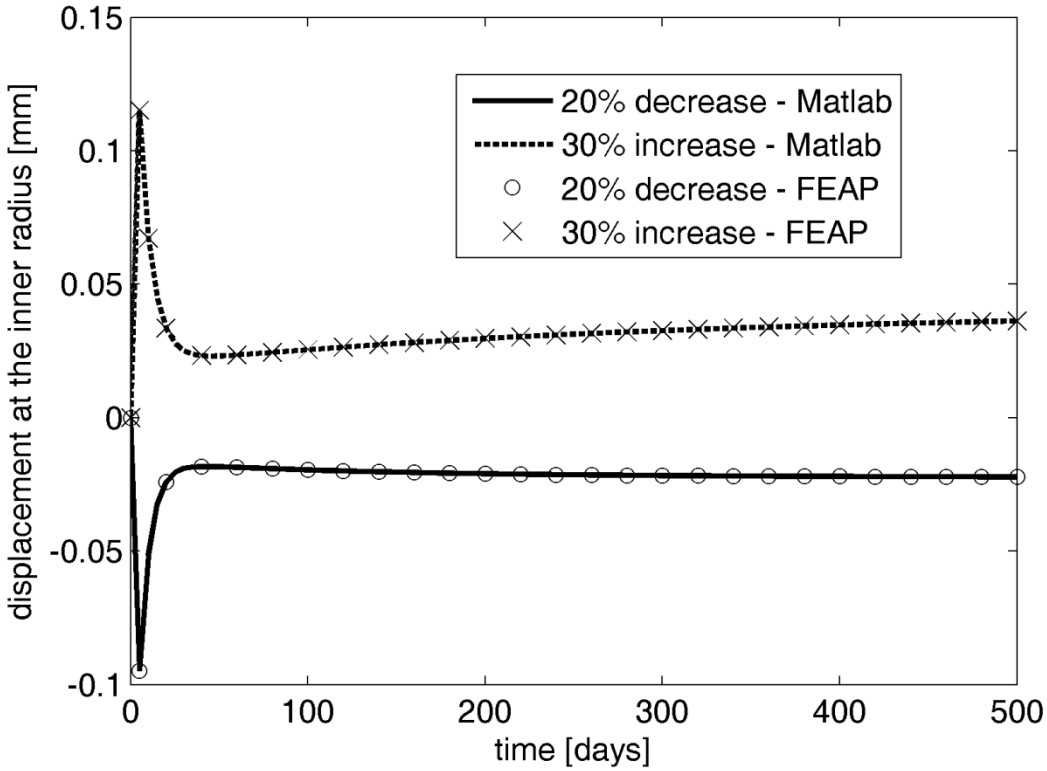

Figure 2.9: Evolution of radial displacement at the inner radius for 20% decrease and 30% increase in blood pressure obtained by semi-analytical solution (lines) and FEM (markers)

2.6.2. Fusiform aneurysms (axisymmetric)

Since verification can be performed solely on cylindrical geometry, where deformation gradient remains diagonal, it does not verify either the implementation or the model itself when axial of circumferential changes are introduced. However, this 3D finite element model should recover the behavior of fusiform membrane model from [43,73] for change in different kinetic parameters. As mentioned earlier, membrane model calculates only mean values or important variables (wall stress, constituent masses, orientations), and there are some differences in implementation (e.g. mass production function, active stress), so it should not be expected that the results would be identical.

Geometry and boundary conditions

In order to avoid numerous assumptions about microstructure (mass fractions of constituents), mechanical parameters (stiffness), orientations and pre-stretches of fibers of the already aneurysmal wall, simulations always start from healthy artery with well-known parameters. Abdominal part of healthy aorta can be represented by a cylinder (see Figure 2.10). For

simulation of fusiform aneurysm, due to axial symmetry, only one small section (e.g., 1°) can be used with applied symmetry boundary conditions on the sides. This will significantly reduce computational demands of the model. Computation demands can further be reduced by noting symmetry in "loading", i.e. elastin degradation (for clarification see section below), thus symmetry boundary conditions are enforced on the upper side as well. Bottom side is a starting point of iliac bifurcation, which cannot move axially.

Aorta is loaded with blood pressure on the luminal side. Boundary conditions and loading are shown in Figure 2.10.

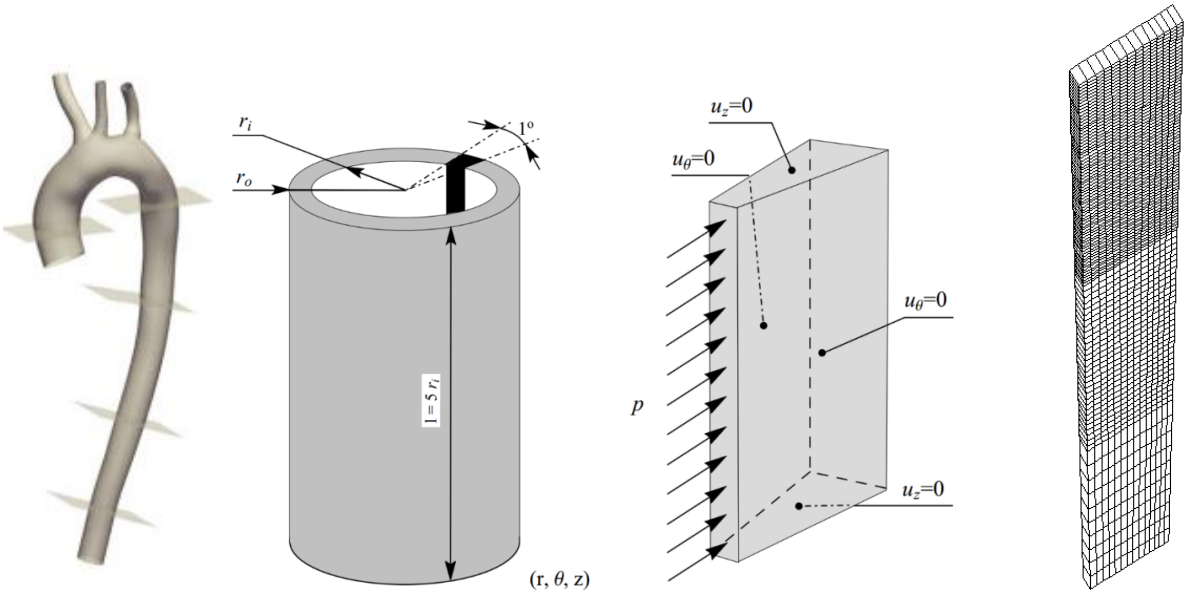

Figure 2.10: Model of real abdominal aorta from CT scan, initial geometry, computational model with boundary conditions, and mesh used for modeling fusiform aneurysms

Geometrical and structural changes

Fusiform aneurysm was simulated by local degradation of elastin, i.e. Gaussian spatio-temporal function, similar to [43] (see equations 2.2 and 2.3). Figure 2.11 shows local degradation of elastin in time. Loss of elastin is governing aneurysm growth, i.e., bulging is expected at places where microstructure is changing (approximately at axial location > 40 mm). Further away from local elastin loss (at axial location closer to 0) aorta should remain healthy (and unchanged). The mesh is created accordingly: upper part is discretized with finer mesh, and lower part with coarser finite element mesh (see Figure 2.10).

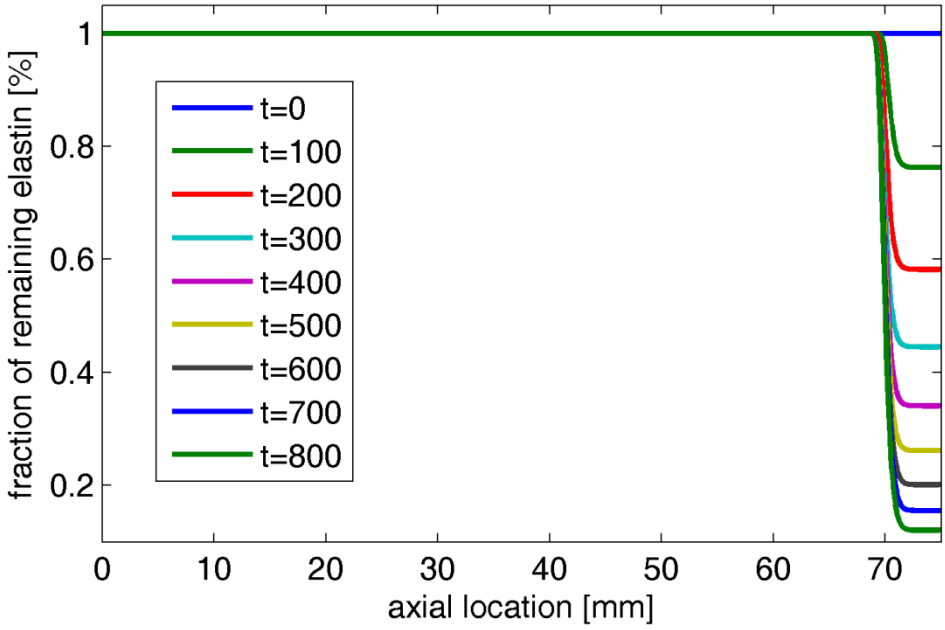

Figure 2.11: Degradation of elastin at different axial locations and in different time steps

Example of geometrical changes at some point during AAA growth is shown in Figure 2.12. Simulation started from healthy aorta approximated by cylindrical geometry (gray rectangle in Figure 2.12).

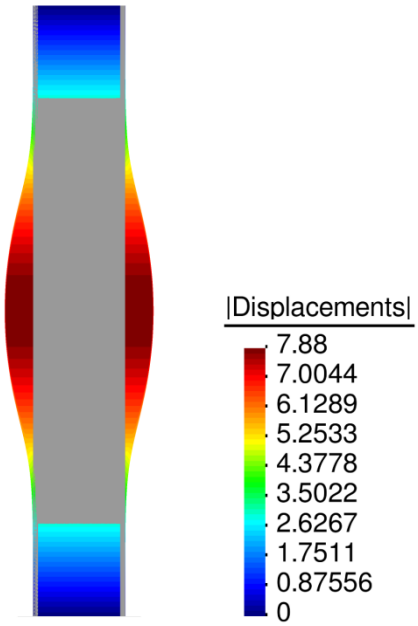

Figure 2.12: Radial displacements of fusiform aneurysm. Note: gray cylinder represents initial, healthy geometry

Besides changes of constituent masses, mechanically important are also orientations of collagen fibers. Since fusiform aneurysm is axially symmetric, axial and circumferentially oriented fibers practically do not re-orient. However, as can be seen in Figure 2.13, helically oriented fibers, initially at ±45° re-orient about 10° at the aneurysm apex towards circumferential direction. This was also experimentally observed by researches from TU Graz (personal communication). Additionally, note that orientation changes radially, which cannot be taken into account in membrane finite elements.

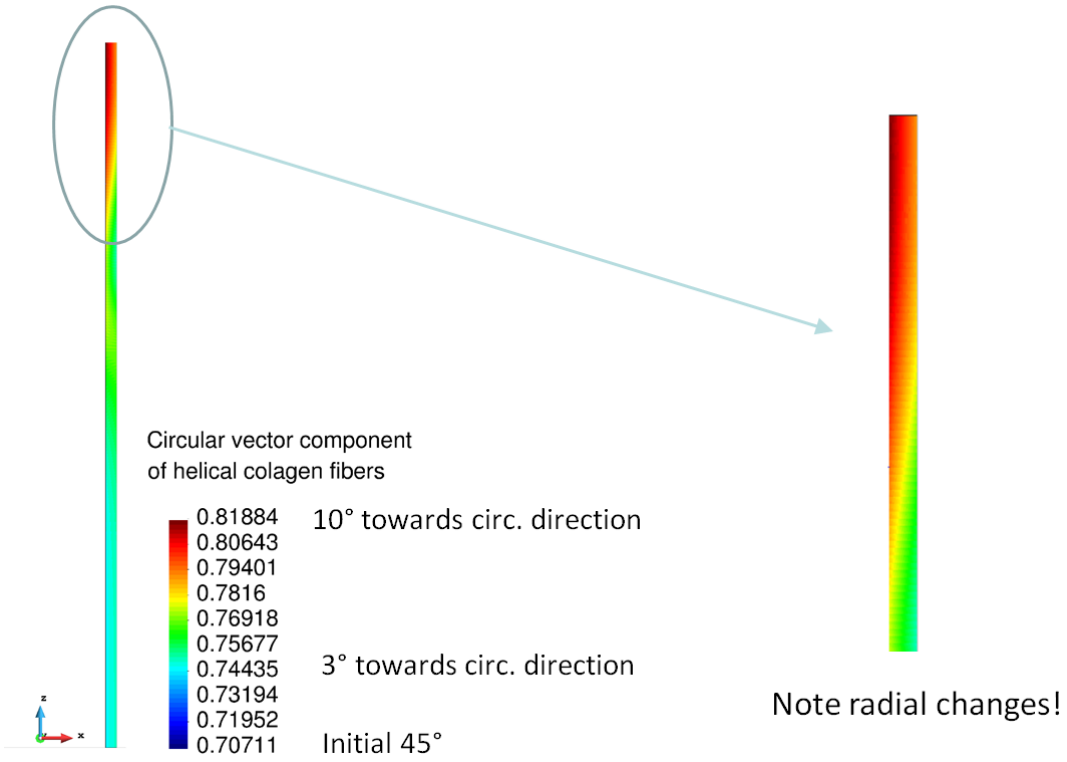

Figure 2.13: Orientations of helical collagen fibers at the time of AAA rupture

Collagen mass production

Computational results using membrane model [73] suggested that stabilization of AAA expansion could be achieved by increased collagen production This was later confirmed using animal models; reestablishment of the endothelial lining that led to the suspension of proteolysis, and the reconstitution of new aortic wall has been associated with the stabilizing effect on rat AAAs [106]. This is to be expected, since higher production of collagen leads to thicker aortic wall and lower pre-stretch experienced by collagen fibers. This necessarily causes lower stress, and thus slower expansion of AAA.

The results obtained by 3-D finite elements show that increased collagen production, modeled by increasing K_σ^c in Eq. (3), indeed decreases AAA expansion rate (Figure 2.14).

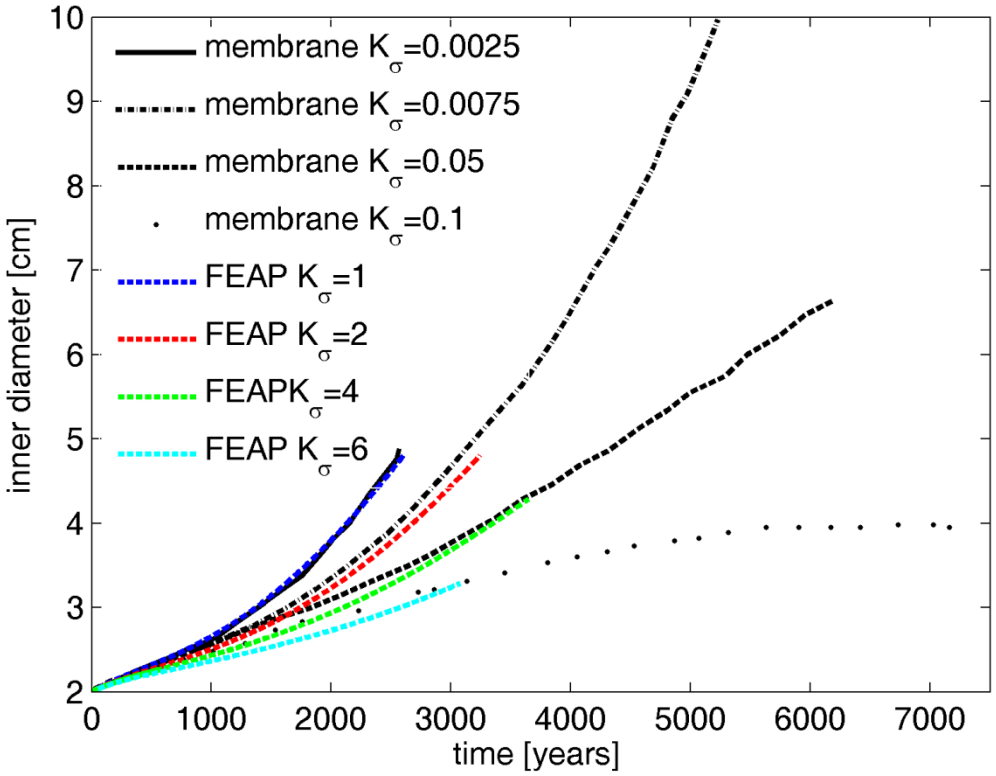

Figure 2.14: Temporal variations in diameter of developing AAAs with different gain parameters for stress-mediated mass production of collagen

Figure 2.14 shows comparison of evolution of diameter of developing aneurysms with different K_σ^c obtained with membrane model (results taken from [73]) and using 3-D elements in FEAP. Note that values of parameter K_σ^c differ between models due to different formulation of mass (density) production. The predicted evolutions roughly coincide, however due to numerical instabilities three simulations run in FEAP terminated before reaching rupture criterion (i.e., stress higher that 460 kPa).

Pre-stretch of collagen

Because collagen is the principal remaining load-bearing constituent of the aneurysmal wall, its properties must play a fundamental role in the natural history of the lesion without thrombus. Besides rate of production, one of the possible important mechanical properties of collagen is pre-stretch at which collagen is deposited into extracellular matrix. Temporal

variations of maximum diameter of aneurysms with different pre-stretches are shown in Figure 2.15. Stiffness (c_2^c in Eq. (7)) is assumed to reset in order to establish the same homeostatic stress, and thus to ensure homeostatic maintenance. This means that the aneurysm with the lowest pre-stretch at which collagen deposits in the ECM is the stiffest.

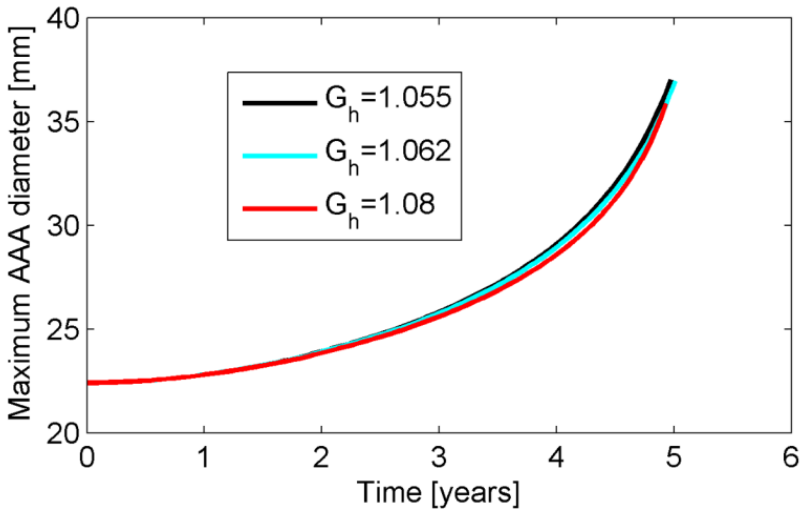

Figure 2.15: Evolution of maximum diameter of AAAs with different deposition pre-stretches

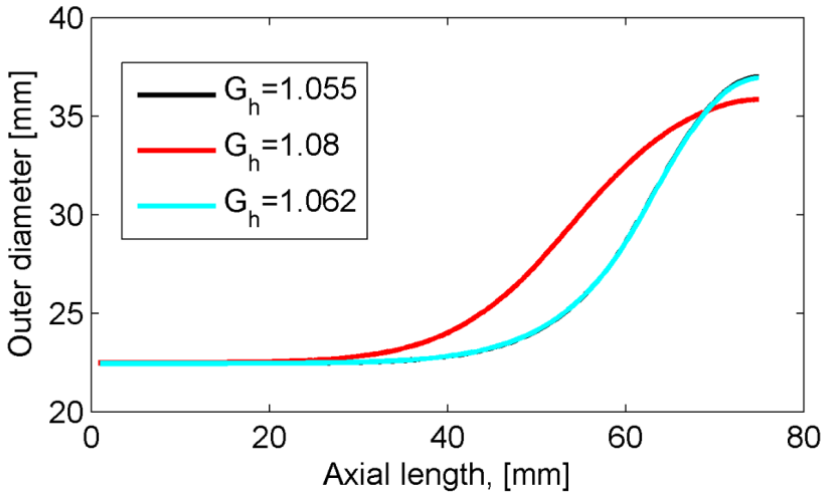

Figure 2.16: Geometries of AAAs with different deposition pre-stretches at the time of rupture

From Figure 2.15 could be concluded that collagen pre-stretch is not an important factor for AAA growth, since all the diameter evolutions are very similar. However, if aneurysm geometries at the time of rupture are compared (Figure 2.16), one can notice that although

maximum diameter is the same, the volume of aneurysmal sac is not. This can be explained by the fact that stiffness of aneurysm with deposition pre-stretch of 1.08 is lower than the aneurysm with deposition pre-stretch of 1.055. Since it is more compliant, it provides less resistance to expansion of "healthy" parts of aorta, i.e. parts where elastin is not degraded. Note from Figure 2.11 that elastin is degraded at the very small section of aorta, about 2 cm in length, while aneurysms shown in Figure 2.16 are 5 and 10 cm long.

2.3.4. Saccular aneurysms (axially non-symmetric)

The finite element implementation is also tested on axially non-symmetric geometry. Elastin is degraded in both axial and circumferential degradation, $Q^{\mathrm{e}}(z,\vartheta,s)=1-\left(1-e^{-K_e s}\right) f_\infty(z)\, f_\infty(\vartheta)$, as to simulate formation of a saccular aneurysm. Since saccular aneurysm is not axially symmetric, the computational model for fusiform aneurysm cannot be used for saccular aneurysm. Note, however, that Gaussian elastin degradation function is double-symmetric, allowing us to use one fourth of cylinder instead of full geometrical model. Again, the created mesh, shown in Figure 2.17, is non-uniform, similar to fusiform aneurysm – finer at the places where elastin will be degraded, coarser where the aorta will stay healthy.

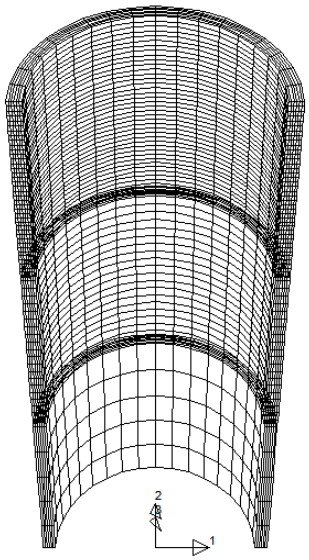

Figure 2.17: Mesh used for simulation of saccular aneurysm

Simulated geometry at the time of rupture is shown in Figure 2.18, left. Again, initial geometry is represented by gray cylinder.

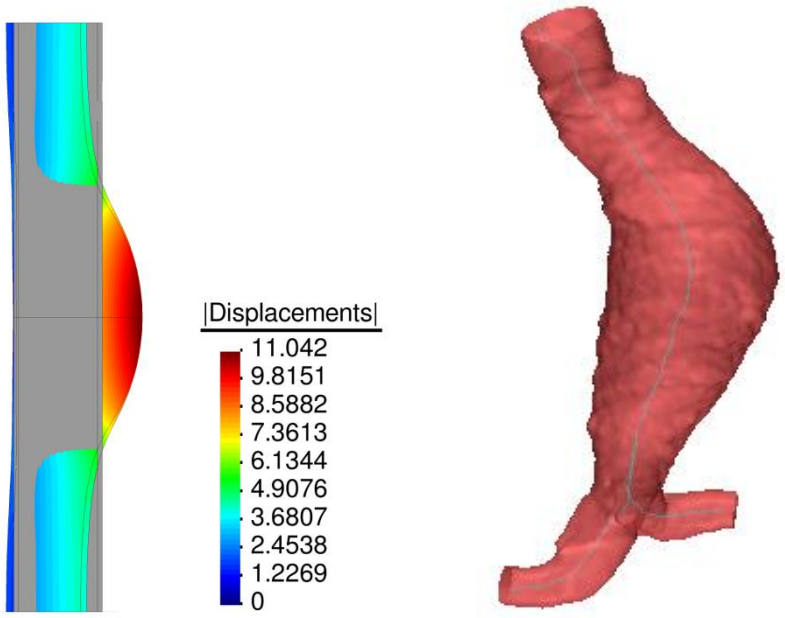

Figure 2.18: Radial displacements of saccular aneurysm (left), CT scan of real aneurysm (right). Note: gray cylinder represents initial, healthy geometry

It is very interesting to note that the aorta bent: healthy aorta (parts above and below the sac) shifted in the direction opposite the aneurysm (i.e., to the left), while part behind the sac shifted in the direction of the sac (to the right). This phenomenon, tortuosity of aneurysmal aorta, has been observed clinically (see Figure 2.18, right), and is one of the morphological parameters are associated with risk of rupture [107]. It is important to emphasize that no additional boundary conditions (e.g., by constraining aneurysm expansion by the spine) were enforced, meaning it is a consequence solely of asymmetric elastin degradation. Still, elastin degradation was modeled as a pre-defined time function. In the future analysis its degradation due to increased amount of elastase due to thrombus deposition should be considered.

3. Biochemomechanical overview of thrombus-laden aneurysm

Intraluminal thrombus (ILT) within AAAs is a complex, fibrin-rich structure that shows few signs of healing by endothelial cell coverage or replacement of the fibrin network with collagen (cf. Franck et al. [106]). Hemodynamics is likely a key factor in the development of ILT; complex vascular geometries lead to disturbed flows that can result in a shear-history induced platelet activation and endothelial dysfunction sufficient to develop thrombus [108].

3.1. Hemodynamics and ILT development

The disturbed hemodynamics that characterizes blood flow in AAAs likely plays a major role in initiating and sustaining the cascade of processes that promote ILT. Several experimental and computational studies of blood flow in idealized and patient-specific models of AAAs suggest that particular characteristics might be recurrent [5,109]. For example, vortical structures may develop during systole and then propagate and dissipate during diastole [5–7]. The outer regions of these vortices, in turn, may allow regions of high fluid shear stress that can exist away from the arterial wall. Noting that wall shear stress has been consistently reported to be lower on the aneurysmal wall compared with values typically computed on the endothelium of the healthy aorta [5,109], the hemodynamic environment in nascent AAAs thus may contain simultaneously regions favorable to platelet activation (due to high shear stresses in the lumen where platelets activate) and adhesion (due to low wall shear stresses where platelets may aggregate on a vulnerable endothelium).

Note, therefore, that early thrombus development is characterized by aggregation of activated platelets and entrapment of erythrocytes and a small number of leukocytes within an evolving fibrin mesh; this fibrin accumulates as activated thrombin cleaves fibrinogen into fibrin, which then polymerizes to form the underlying mesh. Fibrin is stabilized via crosslinking by activated factor XIII (i.e., fXIIIa). Primary thick fibrin fibers may form around the initially plentiful erythrocytes, but as the fibrin-dominated matrix grows under the activity of additional platelets recruited from the bloodstream, focal areas of higher fibrin density may arise as old erythrocytes lyse and the porous structure of the matrix becomes sufficiently small to exclude the influx of new cells from the lumen [60]. With continued loss of erythrocytes, increased secondary fibers form between the thick primary fibers, which could contribute to a stiffening of the fibrin matrix (cf. [8]). Interestingly, plasma samples from AAA patients form denser, lower porosity clots that resist fibrinolysis more than controls, with the degree of resistance correlating with aneurysm size [56]. These findings

appear to be independent of fibrinogen or changes in thrombin generation; yet, other agents such as lipoprotein (a) or activated factor XII (fXIIa) may affect clot structure independent of thrombin [56]. Notably, lipoprotein (a) is elevated in AAA plasma vs. control, and fXII activity correlates with aneurysm size. These correlates may also contribute to the increased stiffness observed during the aging of ILT [8].

The process of coagulation, the mechanical properties of fibrin, and fibrinolysis are described in detail in several reviews [57–59] and recent papers [60–62]. A number of computational models have also been proposed for thrombus development, many of which are reviewed in Xu et al. [110]. In general, two approaches have been used to model coagulation and the development of thrombus within flowing blood. Continuum models at the macro level include reaction-diffusion (differential) equations that attempt to describe changes in the concentration and activation of essential hemostatic factors. Illustrative examples of this approach include Lobanov and Starozhilova [45], who were among the first to model effects of flow on fibrin deposition to a thrombus attached to a vessel wall and the subsequent effect of the growing clot on the flow, as well as Anand et al. [46], who focused on both the biochemical and mechanical factors governing thrombus formation and lysis. Another, increasingly popular, approach includes hybrid formulations that combine discrete and continuum models. For example, since thrombin is generated on a nanoscale while blood flows at a macroscale, a hybrid formulation attempts to integrate these processes spatiotemporally and to take advantage of individual strengths of the different models. Illustrative examples include Xu et al. [48,50] who combined a discrete cellular Potts model for platelets, red blood cells, and white blood cells with the continuum Navier-Stokes equations, and Biasetti et al. [111], who investigated the relationship of flow vortices, coagulation, and thrombus deposition while including both plasma and membrane phase biochemical reactions. See, too, the works by Leiderman & Fogelson [51], Scianna & Preziosi [52], Flamm & Diamond [53], and others.

Many phenomenonological models have also been employed to identify potentially useful metrics for predicting the location and timing of thrombus development within the aneurysmal sac. For example, a particle-hemodynamics analysis by Basciano et al. [23] suggested a generally greater maximum time-averaged shear stress on simulated particles in the proximal and middle AAA as well as a potential correlation between measures of near-wall particle transit times and future thrombus deposition. These findings indirectly support computational results by Biasetti et al. [6,111], which suggest that platelets can activate within proximal regions of high fluid shear stress (e.g., flow vortices) and convect toward the

wall distally to deposit in zones of low wall shear stress. Although larger sample sizes are needed to confirm and extend these results, such studies are promising, indeed prerequisite, to modeling the development of thrombus-laden AAAs over physiologically relevant timeframes. Timing and location of thrombus deposition alone represent, however, only one aspect of understanding the role of ILT in AAA progression. Thus, the heterogeneous structure and inherent mechanical properties of the thrombus itself is described below.

3.2. ILT structure and mechanical properties

Based on gross examination, two major types of ILT have been described in AAAs: "discrete transition" and "continuous transition" [13]. In the discrete type, the thrombus appears to be layered, with sharp demarcations and weak attachments between adjacent layers. Properties, therefore, are generally distinct amongst the multiple (often three primary) layers. In contrast, in the continuous transition thrombus, there are gradual transmural changes in structure with strong radial connectivity. These differences could reflect the nature in which the thrombus was formed; that is, by temporally separated discrete deposition events resulting in various thicknesses versus a slow gradual build-up. Interestingly, the aforementioned study by Basciano et al. [23] appears to have captured a potential discrete deposition event (see Figure 3.1). Note the changes in the volumes of lumen, ILT, and AAA sac over time showing a possible discrete deposition event between June 2005 and March 2006. Furthermore, noting that multiple studies have observed both continuous and stepwise (or "staccato") expansion of AAAs [21,22], the type of thrombus deposition (i.e. continuous versus discrete) may reflect, if not contribute to, these modes of expansion.

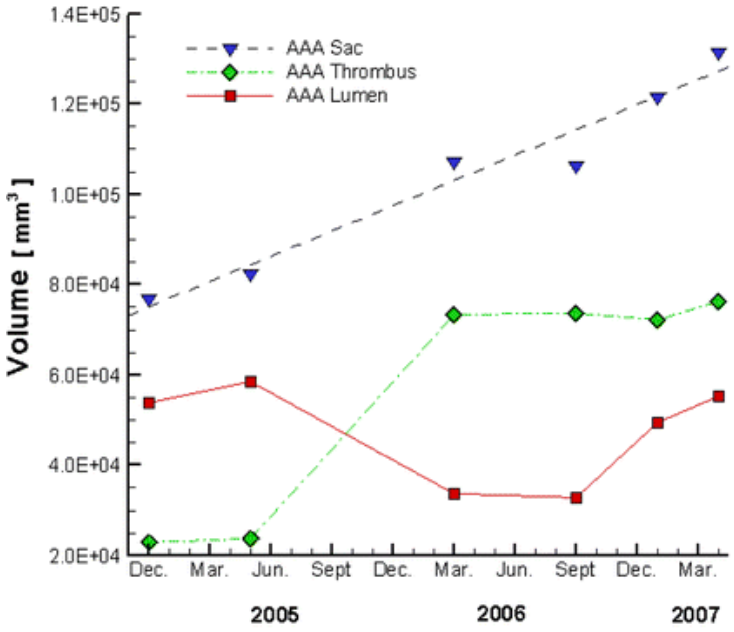

Figure 3.1: Patient's AAA volume history, from [23]

The three regions of layered ILT (Figure 3.2) are often referred to as luminal (nearest the blood), medial (or middle), and abluminal (nearest the aneurysmal wall). The luminal layer appears red due to the high content of erythrocytes, while the medial layer appears white to yellow, due in part to the lysing of erythrocytes. In contrast, in thick ILT, the deepest (abluminal) layer may appear brown [12,13]. In some cases (up to 40% of cases in one study [10]), a liquid phase is also found at the interface between the abluminal layer and the wall, suggestive of local liquefaction. It should be noted, however, that not all layered ILT contain all three layers. Thin thrombi may consist entirely of "luminal-type" thrombus, while thicker thrombi may have luminal and medial layers, luminal and abluminal layers, or all three. There is, therefore, a need to develop a more consistent and inclusive terminology to describe the type of thrombus observed in future studies. Given clear differences in biochemical and biomechanical properties of the three layers, as determined by gross morphology, histology, and mechanical tests, the terms "luminal", "medial", and "abluminal" are used in this Thesis to refer to intrinsic differences in clot type, not simply positions relative to the wall. That is, a luminal thrombus should include all thrombi with certain specific characteristics (e.g., high numbers of activated platelets and infiltrating neutrophils) even if part of it is immediately adjacent to the aortic wall. Thus, over time, a luminal thrombus may be buried by subsequent clot deposition and evolve into medial and eventually abluminal thrombi following erythrocyte lysis, leukocyte apoptosis, and various degrees of fibrinolysis.

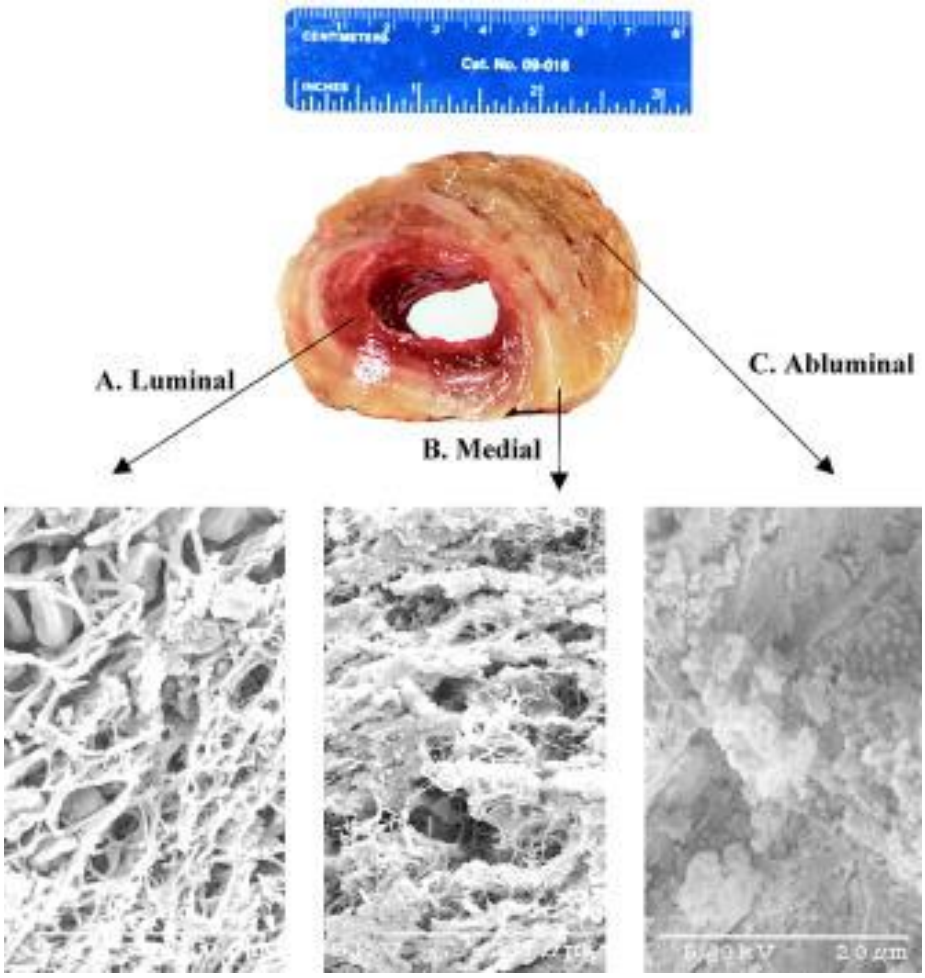

Figure 3.2: Gross and ultrastructural appearance of a layered intraluminal thrombus sample from a human AAA, from Wang et al. [12]

In terms of fibrin structure, the luminal layer is characterized by thick primary fibers of fibrin with fine interconnecting secondary fibers forming a well-organized matrix. These secondary interconnections are lost in the medial layer with evidence of progressing matrix degradation [12,13], consistent with the observation that thin fibrin fibers cleave more quickly than thick ones [112]. This finding is also consistent with the observation that small interconnected channels termed “canaliculi” found throughout the ILT appear to increase in mean area from the luminal toward the abluminal layer [9]. Within the abluminal layer, the matrix is almost completely degraded, with minimal fibrin organization [12].

Just as our understanding of structural characteristics of ILT has increased significantly over the past few decades, so too has our understanding of the mechanical properties. An early study by Di Martino et al. [113] reported uniaxial, tensile data for

circumferentially oriented surgical samples of ILT and used a simple linearly elastic Hookean model. While no distinction was made as to the layer of ILT tested, only "well-organized" thrombi were selected for testing, which likely reflects the luminal layer; reported Young's moduli were 0.05 to 0.2 MPa. To quantify potential viscous properties of ILT, both linear [13] and nonlinear [114] viscoelastic models have been proposed. These results suggest that elastic behavior dominates in multiple layers, though viscous effects may be important in attenuating pressure waves. Although linearized constitutive relations continue to be used, it has become increasingly clear that such models cannot capture all responses [115,116]. This finding should not be unexpected given that Vorp et al. [63] demonstrated many years ago that ILT may undergo large strains *in vivo*.

Wang et al. [12] conducted uniaxial tensile tests on luminal and medial layers of ILT in both circumferential and axial directions and fit the data with a nonlinear, hyperelastic constitutive relation. They reported distinct mechanical properties for two layers, with increased stiffness and strength exhibited by the luminal layer; results from circumferential and axial tests further suggested material isotropy. Vande Geest et al. [117] similarly concluded that the luminal layer was isotropic and nonlinearly hyperelastic using biaxial tests; they were only able to test the luminal layer, however, noting that medial and abluminal layers were too weak. Interestingly, they noted significant differences in the predicted mechanical behavior when comparing results from the biaxial and prior uniaxial results, highlighting the importance of appropriate protocols when formulating constitutive relations. Indeed, although tests are usually designed to explore tensile behavior, Ashton et al. [64] used unconfined compression tests to calculate a drained secant modulus at 5% strain for all three layers. Interestingly, they reported significantly higher compressive stiffness for abluminal than for medial and luminal layers, a gradient opposite that observed in most tensile tests.

Recently, biaxial tests on all three layers by Tong et al. [8] suggested the need to classify ILT even further by both position and age, due to possible evolving phases of development of the mechanical and histological properties of each of the three layers. Specifically, they observed a decreasing maximum tangent modulus and tensile stress at failure from the luminal to the abluminal layer, but suggested that the tensile modulus may increase for each layer as it evolves through four phases over time (Figure 3.3), most notably in the axial direction for the luminal layer [8]. These phases were histologically distinct (Figure 3.4): Phase I (very fresh) was characterized by an abundance of erythrocytes, Phase II (young) by loose fibrin networks entrapping the erythrocytes, Phase III (intermediate) by disrupted erythrocytes and a condensing fibrin network, and Phase IV (old) by disrupted

fibrin networks and condensed residue proteins. They also reported a subclass of generally older luminal ILT that demonstrated anisotropic behavior with increased stiffness in the axial direction. Interestingly, associated mechanical testing of the underlying aortic wall similarly revealed increased anisotropy when located directly underneath an older, anisotropic ILT. Thus, biochemomechanical models of ILT may not only require delineation of the layers of thrombus, but also their unique evolution in properties and their influence on the mechanics of the underlying wall. This consideration leads us naturally to the associated spatiotemporal biochemical activity of ILT.

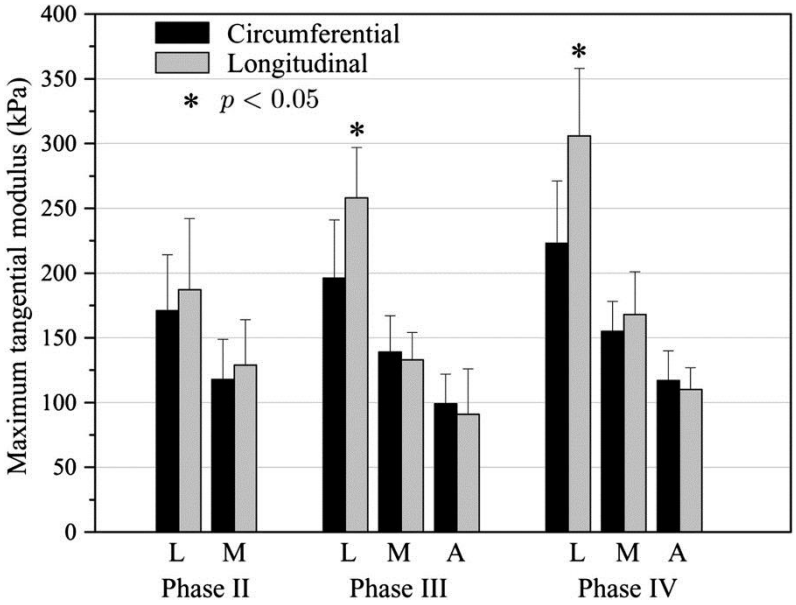

Figure 3.3: Maximum tangential moduli of ILT from human AAAs divided by luminal (L), medial (M), and adventitial (A) layers and phase type, from Tong et al. [8]

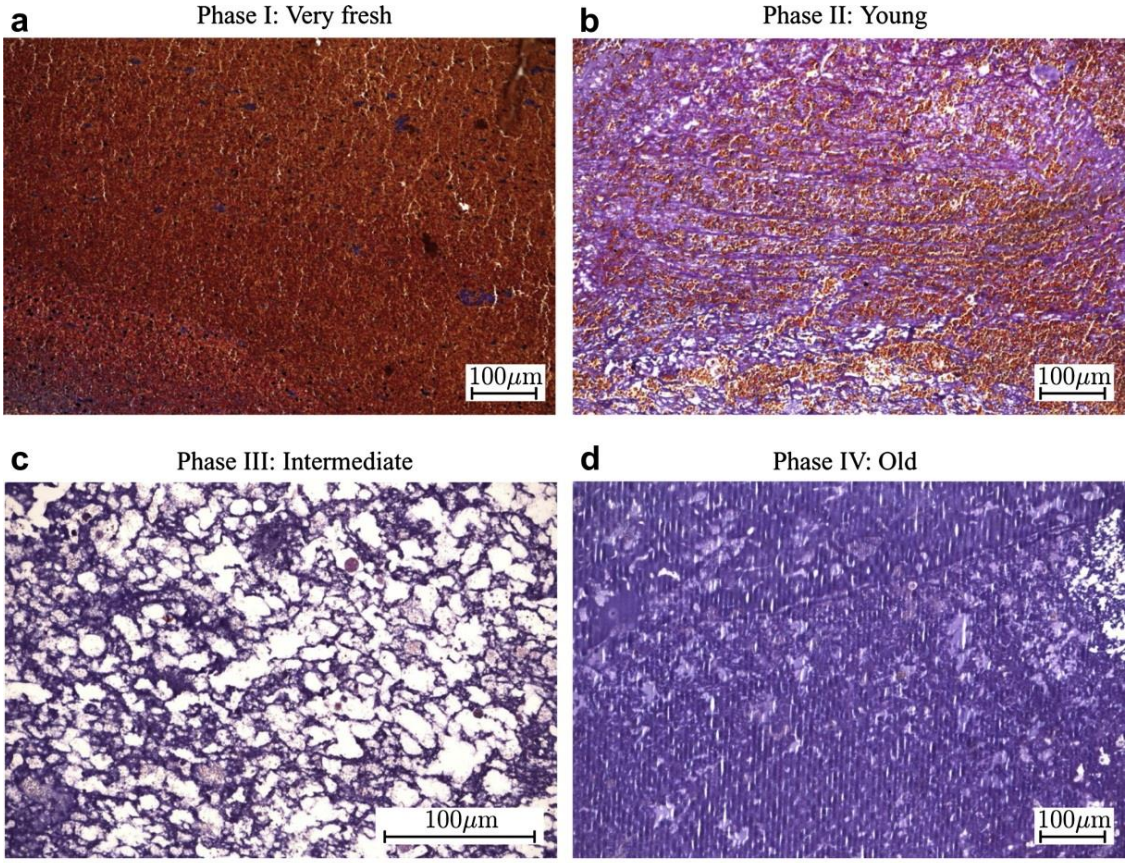

Figure 3.4: Histological phases of ILT maturation, from Tong et al. [8]

3.3. The biologically active ILT

Thrombus may occur throughout the body, including other focal areas of ILT (e.g., deep vein or coronary thrombosis), yet thrombi within AAAs are characterized by unique biochemical and biomechanical properties secondary to their persistent contact with flowing blood and their apparent inability to heal through mesenchymal cell invasion and collagen deposition [55]. As a result, ILT within AAA may contribute to the often chronic inflammation of the underlying aortic wall, with persistent renewal of cellular activity at the luminal interface via the aggregation, entrapment, and recruitment of activated platelets and inflammatory cells. Consequently, ILT can serve as a reservoir for myriad proteinases that can be released and activated during fibrinolysis. Any attempt to understand and model the effects of ILT on AAA progression thus requires insight into not only its mechanical properties and its often eccentric spatio-temporal distribution within an aneurysm [11], but also its heterogeneous synthesis, storage, and release of relevant biomolecules: mitogenic, synthetic, proteolytic, and so forth.

3.4. Prominent role of the luminal layer in ILT activity and renewal

The luminal layer is the primary site in the ILT for new thrombus deposition via activated platelets and cellular activity. Interestingly, cellular content almost exclusively remains isolated to the luminal layer, with cells (including neutrophils, macrophages, and lymphocytes) generally found only to a depth of ~1 cm, despite the aforementioned network of interconnected canaliculi that permeate the ILT [9]. Circulating leukocytes, consisting predominately of neutrophils, are actively recruited by and retained in the luminal layer, aided by the exposure of P-selectin by activated platelets and the affinity of neutrophils for binding to the co-polymer of fibrin-fibronectin in the clot [10]. Neutrophils in the luminal layer can produce interleukin-8 (IL-8) and leukotriene B4, which reinforce further neutrophil invasion [118,119]. Indeed, *in vitro* tests confirm a potent neutrophil chemotactic activity of the luminal layer that can be inhibited by antibodies to RANTES or IL-8 or by the IL-8 receptor antagonist, reparixin [118]. Ultimately, the neutrophil content of the luminal layer can be 12-fold greater than that of blood [65].

Neutrophils are highly active cells that express and release a number of proteolytic enzymes, including myeloperoxidase (MPO), leukocyte elastase (LE), matrix metalloproteinases (MMPs) 8 and 9, and urokinase plasminogen activator (uPA) [66]. Lucent halos have even been observed around neutrophils in regions of fibrin degradation [68], likely due to local activation of plasmin via urokinase plasminogen activator (uPA) or direct activity of secreted LE or cathepsin G [83]. Notably, MMP-8 is a potent collagenase for type I collagen whereas MMP-9 has specificity for partially degraded collagen [66]. Both of these MMPs, along with MMP-2, are elevated in AAAs, while the MMP inhibitors TIMP-1 and -2 are decreased [66,67]. Nevertheless, both TIMP-1, released from platelet α-granules [67], and the elastase inhibitor α1-antitypsin (α1-AT) exist in the luminal layer, potentially explaining (along with latency of the pro-form of the enzymes) some reports of high MMP-9 and elastase levels in the luminal layer but low activity [69]. Indeed, a negative gradient of latent MMP-9 but positive gradient of active MMP-9 has been reported from luminal to abluminal layers of ILT [10]. Importantly, binding of an inhibitor to its target can depend strongly on whether the protease is cell/matrix bound or freely soluble; thus, there is a need for careful control and documentation of methods of measurement. Indeed, LE, MMP-9, plasmin, and tissue plasminogen activator (tPA) can bind to fibrin [55], whereas clot retraction and fibrinolysis can release proMMP-9, elastase/ α1-AT, MMP/NGAL (neutrophil gelatinase-associated lipocalin), and RANTES [10,118].

Most proMMPs can be activated by other proteases (e.g., the serine protease plasmin) or by reactive oxygen species and nitric oxide [67]. An exception is the activation of proMMP-2, which generally utilizes a membrane-type MMP on the cell surface, such as MT1-MMP. While MMP-9 is frequently produced by inflammatory cells, the main source of MMP-2 in the aortic wall appears to be SMCs. This difference may explain the predominant role of MMP-2 in small AAAs, when SMCs are likely more abundant, compared to larger AAAs where MMP-9 activity is increased and SMCs are decreased [67]. Of note, MMP-2 has a greater ability to degrade elastin than does MMP-9 [67], though MMP-2, -7, -9, and -12 all have activity against insoluble elastin [120]. Future studies are needed to quantify spatiotemporal fluctuations of MMP levels and their respective regulation by gene expression, zymogen activation, inhibition, and inactivation [121]. In theory, temporal imbalances between proteases and inhibitors could lead to a destabilizing increase in matrix degradation (i.e., a "spike" in protease activity) that could overwhelm the currently available inhibitors. For example, delivery of fresh blood deep within an ILT due to hemorrhage into the thrombus (radiographically known as the "crescent sign"; see Figure 3.5) could release and activate numerous bound proteases from the fibrin matrix that could overwhelm inhibitors and lead to rapid degradation of the wall. Notably, in one study, the crescent sign was seen in 21% (11/52) of ruptured aneurysms but 0% (0/56) of asymptomatic non-ruptured aneurysms [122].

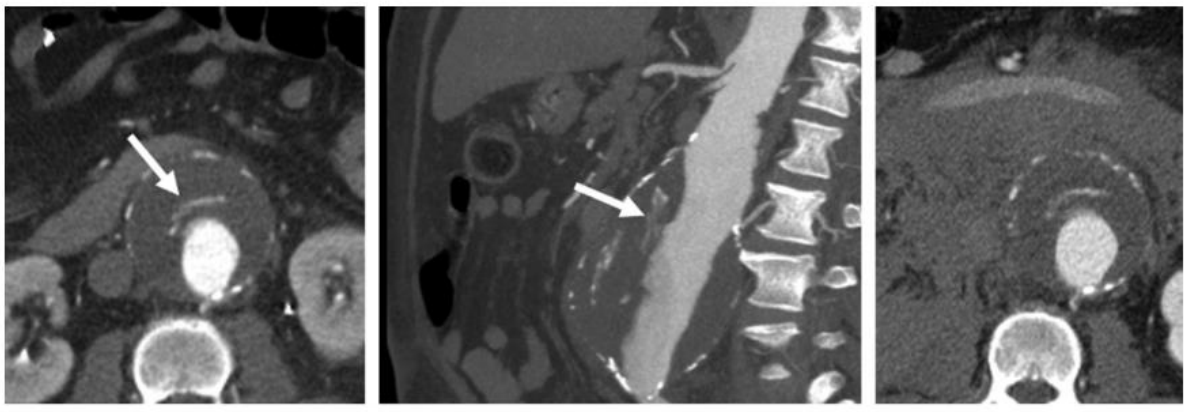

Figure 3.5: Contrast-enhanced CT scan of AAA with crescent, from [72]

While most thrombi tend to resolve over time, those in AAAs show few signs of healing by endothelial cell coverage or mesenchymal cell invasion and replacement of the fibrin network with collagen (cf. [123]). *In vitro* experiments reveal the inability of SMCs to seed the luminal layer, likely due to the high proteolytic activity. Indeed, luminal extracts induce anoikis of SMCs and stromal cells of bone marrow origin, although this effect could be

blocked by protease inhibitors, including α1-AT. Notably, LE can degrade fibronectin, a key adhesive protein for adherent cell survival, and LE has been identified in neutrophils and the matrix around dying cells in the luminal layer [55]. Neutrophils are also capable of detaching endothelial cells from their underlying extracellular matrix [55]. Ultimately, many neutrophils undergo apoptosis (common in the luminal layer), which may lead to further expression of chemotactic and pro-coagulant factors. Additionally, the luminal layer is characterized by high levels of hemagglutination as erythrocytes deteriorate and release free hemoglobin, a powerful oxidizing agent capable of forming free radicals [65].

Of the cell-derived proteases produced within the luminal layer, LE and MMP-9 are two of the most frequently studied enzymes in AAA development. Notably, a significant correlation has been observed between LE and MMP-9 when compared within the luminal, as well as abluminal, layer [69]. While MMP-9 can be inhibited by TIMP-1, neutrophils can upregulate MMP-9 activity by releasing NGAL, which binds MMP-9 and prevents its inactivation [11]. Interestingly, NGAL has been identified in ILT, interphase fluid, and even aortic media not covered by thrombus, consistent with the ability of NGAL to diffuse from thrombus to wall and/or to be produced by leukocytes invading from the *vasa vasorum*, including monocyte derived macrophages [67]. Leukocyte elastase (LE) can also increase MMP-9 activity by directly activating proMMP-9, indirectly activating it through the activation of proMMP-3 [83], or by degrading TIMP-1, thereby protecting MMP-9 from inhibition [66]. Of note, TIMP-1 not only can inhibit active MMP-9, it can also inhibit the activation of proMMPs and neoangiogenesis [67].

3.5. Luminal ILT – aortic interactions

Because the ILT is a heterogeneous structure, with its primary cellular activity in the luminal layer, those elements of the aortic wall nearest the luminal layer would be expected to be most at risk for proteolytic attack. Indeed, aneurysmal walls covered by a thin (≤ 1.0 cm) thrombus have significantly higher levels of leukocyte elastase (LE) activity, concentrations of active MMP-9 and total MMP-8, and ratios of active MMP-9/TIMP-1 than those covered by a thick (≥ 2.5 cm) thrombus [66]. MMP-9 and LE concentrations are also higher in luminal layers compared with deeper layers, and a significant negative correlation exists between the concentration and activity of LE in the abluminal layer and ILT volume, suggesting that LE may not penetrate well a thick ILT [69]. Of note, the slightly alkaline environment in the aneurysmal wall next to a thin ILT may also accelerate local degradation by elastase [66].

In addition to cell-derived proteolytic activity, the luminal layer is characterized by high levels of fibrinolytic activity, as evidenced by elevated release of plasmin-antiplasmin complexes (PAPs) and D-dimers (a measure of cross-linked fibrin degradation), greater immunostaining for plasminogen and plasminogen activators, and greater ^{99m}Tc-Aprotinin activity (a potential imaging agent that binds serine proteases like plasmin and elastase) compared with other layers [124]. Although fibrin may deposit throughout the thrombus, it decreases significantly toward the abluminal layer, consistent with activated platelets being predominately confined to the luminal layer [9]. Indeed, Touat et al. [68] demonstrated that procoagulant activity and markers of platelet activation were 3 to 5 fold higher in the luminal compared with deeper layers. Yet, because activated platelets degranulate within the clot [9], there is a potential for diffusion/convection of biomolecules through the canaliculi. Overall, these findings suggest possible continual cycles of fibrin deposition and degradation within the luminal layer, indicative of an active remodeling and renewal of the fibrin matrix [56,83]. Whether fibrin deposition within the luminal layer could eventually become dense enough to exclude further cellular infiltration (thus rendering the layer more inert) remains to be proven, although findings by Tong et al. [8] for older luminal layers having few erythrocytes supports this possibility.

In summary, the luminal layer on an ILT is a site of renewable biochemical activity via the accumulation of platelets, recruitment of proteolytically active leukocytes (notably neutrophils), formation of fibrin, erythrocyte hemagglutination, and retention of tPA and plasminogen for postponed progressive fibrinolysis [65]. With continued deposition of thrombus, either gradually or discretely, the luminal layer may eventually become buried. This process could trigger a unique evolution of properties of the ILT and underlying aortic wall.

3.6. Medial and abluminal layers

The medial layer is characterized by a transition from the active cellular luminal layer and the disorganized, degrading abluminal layer. It is generally devoid of intact erythrocytes and only rarely has infiltrating leukocytes despite a dense fibrin network. The abluminal layer is distinguished by its location adjacent to the aortic wall in thick ILTs, a brown discoloration, lack of cells, degraded fibrin network, and weak gelatinous material with high compressive stiffness [64,68]. Its interface with the aneurysmal wall may exist as a liquid interphase with high levels of soluble proteins [10]. The lack of cellular content in the deeper layers of the ILT renders the clot unable to synthesize new proteases in these regions; nevertheless,

biomolecules bound to the fibrin matrix during its formation in the luminal layer may persist and be released and/or activated. As a result, measurements of proteolytic activity in these layers may potentially vary in time and space as well as from patient to patient, depending on past and current fibronolytic activity. For example, Folkesson et al. [69] found abluminal proteases to be predominately inactive whereas Fontaine et al. [10] reported active MMP-9 at the liquid interface between the ILT and wall.

The ability of the degrading fibrin matrix to release bound proMMPs in the presence of plasmin (potentially formed by a ready supply of plasminogen activators, such as tPA, in the immediately adjacent wall [124]), may activate MMPs at the interface and cause subsequent degradation of the underlying wall. Indeed, the aneurysmal wall has shown 100-fold higher tPA activity than the ILT [125], and MMP-9 activity has been localized to the inner wall of AAA [126], as has elastase activity [66] and plasmin [74], consistent with an ILT-mediated degradation of the wall. Yet, remnant SMCs, infiltrating macrophages, and endothelial cells from the *vasa vasorum* may also produce MMP-9 [127], which may relate to the ability of these cells to migrate toward and neovascularize the injured aortic wall. For example, noting that plasmin is a key activator of proMMP-9, plasminogen$^{-/-}$ mice had reduced macrophage migration through the extracellular matrix that was rescued with administration of active MMP-9 [128]. Nevertheless, increased MMP-9 activity in the wall significantly exceeded the increase in MMP-9 expression [127], consistent with diffusion/convection from the ILT and/or increased release and activation of stored MMPs.

It remains to be shown whether deeper layers of ILT may eventually become depleted of stored pro-enzymes as they degrade. If so, their level of proteolytic activity may vary depending on the spatiotemporal availability of activators and inhibitors, leading to a potentially significant source of patient variability in proteolytic activity. Indeed, there is a large range of reported MMP-9 levels in the ILT, interface, and wall (e.g., see Figure 3.6), thus highlighting the need to develop improved patient-specific methods of determining proteolytic content and activity in thrombi. It is important to note that while averaged data on biochemical potential and activity are insightful for population-based studies, patient-specific determinations of rupture risk may require individualized spatiotemporal assessment of key enzymes and regulators, or at least localized measures of net proteolytic activity.

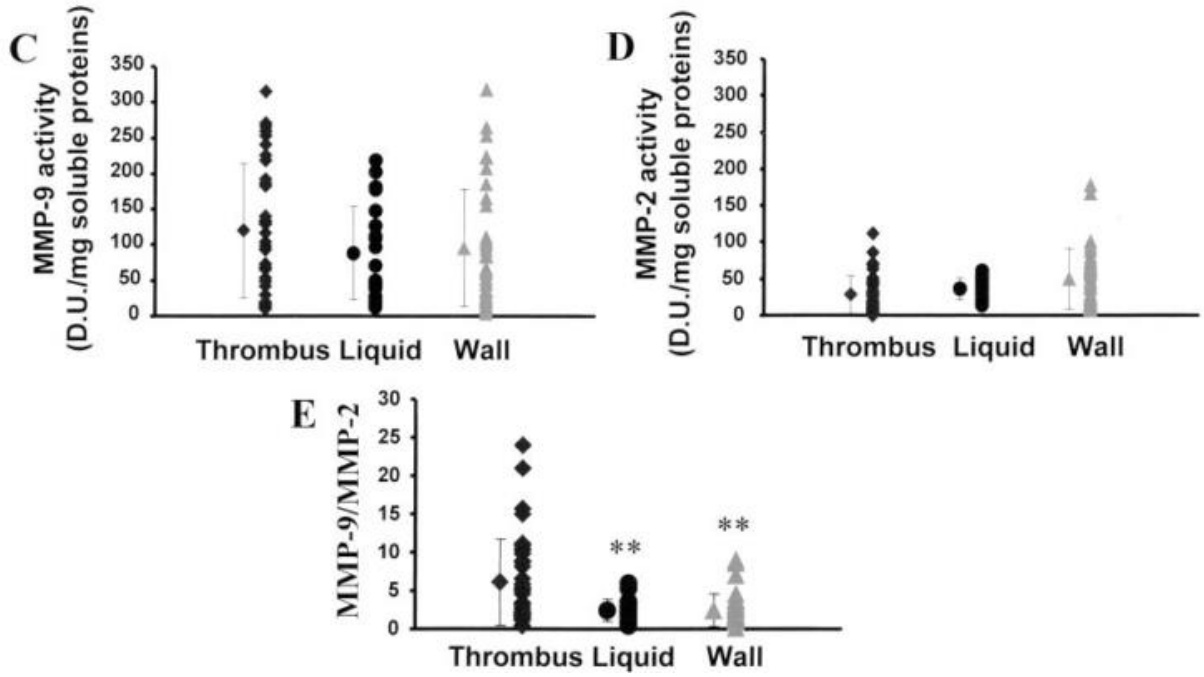

Figure 3.6: Protease activity level in AAAs, from [10]

3.7. The fibrinolytic system and AAAs

Just as LE, MMPs, and other proteases are important in AAA development and progression, the fibrinolytic system is fundamental to regulating the ILT. Plasminogen, synthesized by the liver and released into the blood, is naturally bound within the fibrin matrix during its formation and is present in large quantities in thrombus [54]. Cleavage of plasminogen, classically by uPA or tPA, to the potent serine protease plasmin results in many proteolytic consequences, including direct degradation of fibrin and extracellular matrix [83], direct or indirect activation of various proMMPs (including MMP-1, -3, -7, -9, -10, -12, and -13) [67,124], regulation of growth factors and chemokines [129,130], and proteolysis of cellular anchoring fibers, which may induce anoikis [65,131]. Plasmin also exerts a fibrin-catalyzed positive feedback to activate additional plasminogen. The major inhibitory proteins in the fibrinolytic system are plasminogen activator inhibitor 1 (PAI-1), which inhibits uPA and tPA, and α2-antiplasmin (α2-AP), which binds to and inhibits active plasmin to form PAP complexes. Interestingly, while plasmin can activate MMPs, MMPs can also affect the fibrinolytic system. For example, activation of proMMP-9 by MMP-3 can cleave plasminogen and inactivate PAI-1, α2-AP, and α1-AT [83]. Similarly, elastase can indirectly activate plasminogen through alternative pathways [69].

While some report that the luminal layer releases most of the D-dimers [124], indicating degradation of fibrin, the medial and especially abluminal layer appear to undergo greater *net*

fibrinolysis, likely due to the lack of significant new fibrin deposition within these deeper layers. Suggestive of abluminal plasminogen activation by activators in the inner wall, Fontaine et al. [10] reported that free uPA and tPA activities were only noted in the wall, while plasminogen was identified only in the ILT; however, Houard et al. [124] later reported that while tPA in the wall localizes to the inner media (and *vasa vasorum* in the adventitia), abundant tPA and uPA immunostaining are also present in the luminal ILT, potentially bound to fibrin and associated with neutrophils, respectively. Co-incubation of ILT and wall extracts in the presence of fibrin also produces plasmin *in vitro* [10]. The degree to which patient-specific and layer-specific variability in the samples of thrombi tested influence these results may require further consideration.

Notably, PAI-1 and α2-AP may not be as effective in inhibiting plasmin activity when their targets are bound to fibrin or the cell surface [83,131]. Since plasminogen, tPA, and plasmin can each bind to fibrin (as can α2-AP) [83,132] and localize to fibrin-rich areas in the luminal layer [124], they could potentially exert local activity before becoming soluble and thereby vulnerable to increased inhibition. Thus, PAPs are often present in areas of active fibrinolysis, such as the thrombus-wall interface [10], even though they are inhibitory complexes. In fact, a positive correlation exists between PAPs and D-dimers in all ILT layers [124]. In addition to decreasing inactivation, binding of plasminogen, such as to an inducible cell surface receptor, may also increase its activation and serve to direct its proteolytic activity to specific targets [129]. Clearly, therefore, it is important to report and interpret measures of fibrinolytic enzymes (and MMPs) carefully in terms of their expression (mRNA), storage/binding (stained), or release (solubilized) as well as whether the protein is latent, activated, or inhibited. For example, upregulation of a particular gene may lead to increased transcription and translation of a protease or cytokine but no immediate increase in its extracellular activity due to intracellular storage or release of only the latent form.

Synthesis of tPA and PAI-1 appear isolated to the wall, while uPA is expressed by inflammatory cells within the wall and luminal layer of the ILT [10,124]. Interestingly, SMCs can use constitutive tPA on their cell surface to locally activate plasmin and cause pericellular proteolysis of attachment molecules like fibronectin [131], a process potentially involved in activation, migration, and/or anoikis in the aortic media; tPA also localizes to the adventitia, possibly related to its release by endothelial cells of the *vasa vasorum* [124]. As for PAI-1, it was highly stained in the luminal layer of the ILT, but most readily released from the medial and abluminal layers consistent with its strong affinity for the γγ-fibrin chain, which is intact in the luminal layer but degraded in deeper layers [124]. Given the significant ability of the

fibrinolytic system both to remodel the ILT and regulate proteolysis of the extracellular matrix of the underlying wall, the spatiotemporal distribution of plasmin, its activators, and its inhibitors represent key data that could improve future patient-specific models of AAA progression and rupture risk.

3.8. A unique role for matrikines

Despite appropriate emphasis on proteolytic enzymes that directly affect the remodeling of fibrin and extracellular matrix, degradation products of matrilysis (including elastin [133], laminin [134], and fibrin [135]) are not simply removed. Rather, these products may serve as active signaling and catalytic molecules, termed matrikines [83], that help regulate inflammation, repair, angiogenesis, and other processes. Of these, the elastin degradation products (EDPs) are likely of particular significance in AAAs given their chemotaxis for monocytes, neutrophils, fibroblasts, and endothelial cells [136], stimulation of the release of elastase in the wall by neutrophils [66], augmentation of MMP-1 production by aortic SMCs, promotion of angiogenesis [136], and influence on the differentiation of Th1 cells that can upregulate interferon-γ (IFN-γ and interleukin-2 (IL-2) [48].

Interestingly, Nackman et al. [136] demonstrated that perfusion of a segment of the infrarenal aorta in a rat with an elastin peptide fragment (VGVAPG) could reproduce the extensive neovascularization of the wall that occurs in elastase-infusion, a classic rodent model of AAAs, despite the aortic diameter increasing only 26% with the peptide fragment instead of 142% with elastase. This importance of elastin breakdown products stimulating neovascularization (as opposed to just hypoxia from a thickening ILT) may explain, in part, why significant differences in neovascularization were noted between aneurysmal walls and control aorta, but not between thick versus thin thrombus covered aneurysmal walls [74] or thrombus covered versus non-covered aneurysmal walls [15]. Faisal et al. [134] similarly showed that a laminin peptide found in AAAs, due to release from the degrading ECM, can upregulate uPA and MMP-9 in macrophages. Notably, laminin is a susceptible target of plasmin degradation [137]. Finally, fibrinogen derived peptides may increase leukocyte chemotaxis and permeability of the aneurysmal wall [138].

In healthy aorta, the media has been considered an immunologically “privileged” site to which immune cells have minimal access [139,140]; yet, when the well-organized elastic lamellar units are disrupted, otherwise inaccessible antigens and degradation products may become exposed and participate in the observed shift from innate to adaptive immunity in AAAs. In addition to EDPs, these local mediators may include post-translationally modified

proteins, reactive oxygen species (ROS), and bi-products of SMC apoptosis [138]. Proteolysis of extracellular matrix can also release and activate transforming growth factor beta (TGF-β), a key biomolecule in the regulation collagen synthesis and secretion [138]. Notably, plasmin at cell surfaces is an activator of TGF-β [141], and whether via TGF-β or other factors, increase in the pro-collagen gene expression in AAAs is mediated by soluble tissue factors [142]. Indeed, even in regions beyond the infrarenal aorta, AAAs have been associated with increased aortic collagen, elevated expression of MMP-2 by SMCs, diffuse arteriomegaly, arterial elongation, and peripheral aneurysms, which suggest a widespread process [142,143]. Whether this process is causal or responsive to the aneurysm is yet unknown.

3.9. Convection/diffusion

Adding to the complexity of identifying the major proteolytic enzymes and signaling molecules that influence AAA progression, these macromolecules likely convect/diffuse through the canaliculi of the ILT toward the underlying wall. Adolph et al. [9] showed, for example, that ILT is fluid permeable, although diffusion becomes limited across very thick thrombi. Levels of LE and MMP-9, which are produced predominately in the active luminal layer, decrease through the depth of the ILT [69]. Similarly, proteases, degradation products, antigens, and other soluble biomolecules may be transported radially through the aneurysmal wall toward the adventitia, which can play a major role in arterial responses to disease, including fibroblast activation, neovascularization, immunoinflammation, and fibrosis [138]. It is also likely that the permeability increases as the endothelial lining is lost [15] and the organized structure of the healthy aortic wall is degraded [65]. Along these lines, recent attempts at modeling the thrombus and aneurysmal wall as porohyperelastic structures [144,145] may provide insight into the complex interstitial fluid flows in thrombus-laden AAAs. Thus, a complete model of the biochemical influences of various mediators may require accurate quantification of the transmural hydraulic conductance, diffusion down concentration gradients, binding affinities, and wall permeability [138].

3.10. Role of animal models

In concluding the discussion of biochemical processes in ILT, note that diverse animal models have been used to study AAAs because of the difficulty of obtaining human tissue, particularly under controlled longitudinal conditions. The two most common animal models of AAAs that can also lead to formation of thrombus are the angiotensin II (Ang-II) infusion

model [146] and the elastase intraluminal perfusion model [75]. The former involves subcutaneous implantation of an osmotic mini-pump whereas the latter involves direct perfusion of the infrarenal aorta during open surgery. Note that the Ang-II model is typically used in Apo-E deficient mice and produces dissecting aneurysms in the suprarenal aorta, as opposed to dilatory aneurysms in the infrarenal aorta as classically seen in humans. Moreover, intramural thrombi within the dissected wall in the Ang-II model can heal through cellular invasion and eventual replacement of the fibrin matrix with collagen [123]. Thus, the natural history of AAAs in the Ang-II infusion model may have distinct differences from the human pathology, particularly in terms of thrombus formation and evolution.

In contrast, although the elastase perfusion model tends not to yield ILT in mice, the same experiment in rats often does, and the aneurysms are appropriately in the infrarenal aorta. Using this model, Coutard et al. [132] demonstrated higher levels of MMP-9, elastase, uPA, plasmin, and microparticles in the ILT compared with the wall, while MMP-2 activation was similar. Interestingly, ILT correlated positively with wall levels of pro- and active MMP-2, elastase, and plasmin, whereas total wall MMP-9, MMP-2 activation, plasmin activity, and microparticle release correlated with aneurysm diameter. The potential importance of these and other factors in future modeling and therapeutic efforts is highlighted by the attenuation of aneurysm development in various experimental models of AAA by depletion of neutrophils, T-cells, macrophages, or mast cells [11,15], inhibition of platelet aggregation or activation [118], inhibition of neutrophil recruitment [132], knockout of plasminogen [128], deficiency of uPA [128], knockout of MMP-9 [67], or increases in PAI-1 [128], TIMP-1 [11], or catalase [65].

3.11. Role of ILT in AAA wall mechanics

Clinical and experimental observations

While a primary focus thus far has been on biomechanical properties of and biochemical processes within the ILT itself, numerous studies have attempted to determine effects of the ILT on the underlying wall. Compared to thrombus-free wall, the wall beneath an ILT may have increased inflammation and neovascularization as well as fewer elastic fibers and smooth muscle cells, many of which are apoptotic [70]. An increase in phenotypically synthetic SMCs, many with elongated processes suggesting ongoing migration, has also been noted [70,133]. In comparison, aneurysmal wall without ILT can have dense collagenous matrix with phenotypically contractile SMCs and increased staining for alpha-actin [70], although expression of MMP-1, -7, -9, and -12 can be higher than in the covered wall [147].

While both thrombus-covered and thrombus-free wall exhibit increased CD68+ macrophage counts and caspase-3 staining for apoptosis, the thrombus-covered wall can also have increased CD3+ T-cells, CD8+ cytotoxic T-cells, and CD20+ B-cells, along with increased TUNEL staining for DNA fragmentation in the intima and media, often in association with inflammatory cells [70]. Clearly, there are significant differences in the structure of the matrix, cellular content, and inflammatory status of the wall underneath an ILT that require further investigation to improve future modeling.

Interestingly, thrombus has been found to be thinner, on average, in ruptured versus non-ruptured aneurysms [66], though thick thrombus covered walls may have fewer remaining elastic fibers, more inflammation, and lower tensile strength compared with wall covered with thin ILT [74]. A possible reason for this apparent discrepancy is that any wall covered by thick thrombus likely was originally covered by thin thrombus (i.e. a luminal layer in direct contact with the wall); thus, changes may reflect cumulative damage from the past because intact lamellae are not regenerated in adulthood. One may hypothesize, therefore, that the most active degeneration of the wall occurs in regions of thin thrombus and that thickening of the ILT with subsequent deposition events may be somewhat protective, at least insofar as the wall is farther from the active luminal layer. In fact, if a thin thrombus presents excess proteolytic molecules to the wall, which in turn heightens wall degeneration and lesion expansion, and if expansion leads to hemodynamic changes conducive to new clot deposition, then one would naturally expect thrombus to be thick in regions of significant wall degeneration. Indeed, Swedenborg & Eriksson [11] note that loss of elastin may primarily cause a decrease in axial support, leading to an elongation and tortuosity of the aorta that may induce endothelial injury due to disturbed blood flow and abnormal wall stress. Thus, despite increased aneurysmal diameter correlating with both increased rupture risk and ILT volume in some reports [11,67], one must interpret cautiously possible causation as the expanding geometry and associated hemodynamic changes may naturally precipitate further ILT deposition. Nevertheless, the growth rate of ILT in moderately sized AAAs may be a better predictor of rupture risk than total amount of ILT or the common metric of maximum diameter of the lesion [148], which potentially explains why a simple static ratio of lesion size to ILT volume has been unrevealing when comparing ruptured and non-ruptured AAAs [11,149].

Alternatively, or perhaps complementarily, the fibrinolysis that predominates in the abluminal layer may release and activate previously bound or soluble proteases (e.g., plasmin or MMPs) that could then diffuse into the adjacent wall and directly degrade the ECM or

activate other proteases, thus contributing to the increased degradation behind thicker thrombi. Additionally, thick thrombi may also exacerbate hypoxic conditions in the wall that may contribute to neovascularization from the *vasa vasorum* or even alter collagen production [1,74], though a convection/diffusion model of oxygen transport by Sun et al. [150] suggested that thickening of the ILT beyond approximately 5 mm may not have much more effect on mural oxygen tension. Of note, formation of these neovessels not only requires proteases for endothelial cell invasion, it establishes a direct path for circulating inflammatory cells to invade the degenerating media. Indeed, inflammatory cell retention, elastin degradation, and lymphoid neogenesis all correlate with adventitial neovascularization [138].

Implications of spatial distribution – the shoulder and neck regions

Multiple studies have focused on the shoulder regions of the AAA (i.e., proximal and distal regions between the dilated and non-dilated aorta) as they may both reflect "early" stages of aneurysmal development (which are difficult to study due to the asymptomatic nature of the early disease process) and represent regions that may dictate the axial expansion of the lesion into the proximal and distal necks (i.e., the adjacent non-dilated areas) of the infrarenal aorta. Moreover, the proximal neck is particularly important clinically as the location for seating the endovascular stents that are increasingly used for AAA repair.

Assuming the thrombus approximately "space-fills" the dilated portions of the body of an AAA (see Figure 3.7), the active luminal layer of the ILT would always remain in contact with the evolving shoulder of an aneurysm. As suggested by Yoshimura [151], this situation would predict increased thrombus-derived proteases in the shoulders of the lesion. Indeed, Curci et al. [120] observed that areas of "active" elastic lamellar degradation predominated in the proximal shoulder region, while the body of the lesion consisted of mostly "amorphous" fibrocollagenous regions with few remaining elastic fibers and only scattered "inflammatory" and "active" regions. The shoulder also appears to be a site of increased MMP-9 activity, decreased medial thickness, fewer intact lamellar units, and increased pJNK, inflammation, and neovascularization [127]. Notably, JNK may be a pivotal intracellular signaling molecule in SMCs and macrophages that can be upregulated by a plethora of biomolecules frequently associated with AAAs, including MMP-2 and 9, angiotensin-II, histamine, interleukins, IFN-γ, and TNF-α [15,127]. Interestingly, expression of both TNF-α and its activating enzyme TACE are not only higher in AAAs compared to control aortas, they are also higher in the neck compared with the apex of the lesion, where they co-localize with macrophages of the media and adventitia. TNF-α can also induce other inflammatory cytokines and several

MMPs, promote apoptosis, and increase uPA, tPA, and PAI-1 levels (which are pro-angiogenic) [152]. The delivery of a TNF-α specific binding protein has even been shown to prevent AAA formation in a rat elastase perfusion model [152].

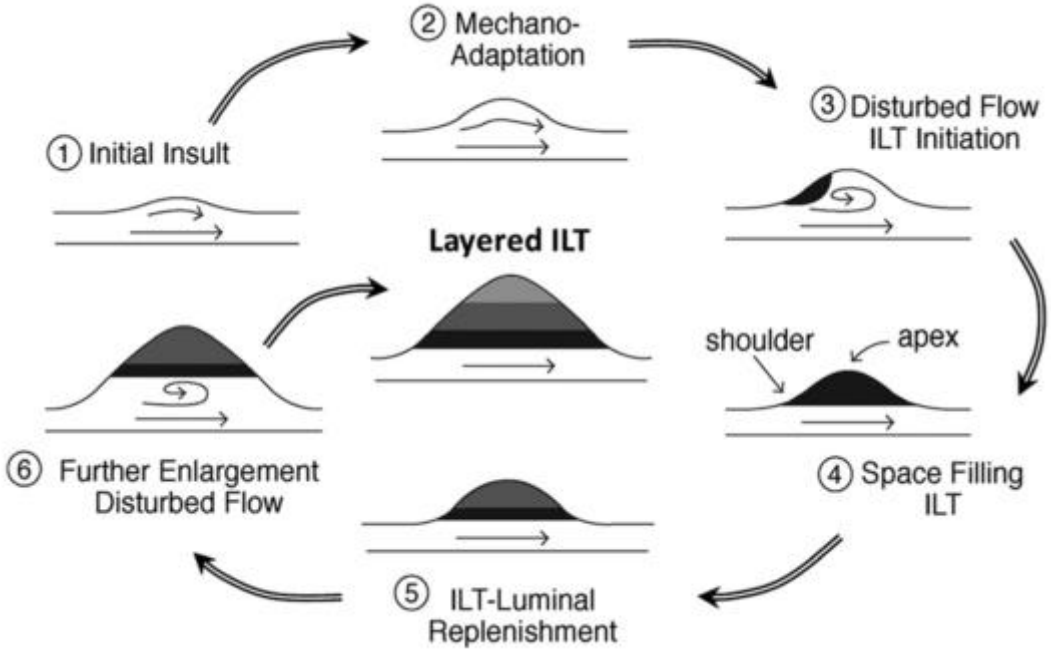

Figure 3.7: Simplified schema of the possible formation of a layered "space filling" ILT by multiple cycles of AAA sac enlargement and ILT deposition secondary to disturbed flow

Early damage to the aortic wall is not confined to the shoulder, however. Increased degeneration in the non-aneurysmal neck region has been associated with maximum AAA diameter [127], and the neck can be a site of early inflammatory cell infiltration with elevated levels of MMP-12 strongly bound to elastic fiber fragments, which may augment its elastolytic activity [120]. In comparing samples of aneurysmal necks from different patients, those with mild degeneration were characterized by damage to inner medial elastin with some mid-medial and patchy outer-medial loss of SMCs, while more heavily damaged samples showed widespread degeneration with significant loss of smooth muscle in the outer media [127]. This observation may suggest an initial process of damage to the inner wall, particularly to the elastic fibers, followed by a strong adventitial response.

Computationally, many finite element studies suggest that the highest values of wall stress occur at sites other than the maximal diameter. Li et al. [153] specifically suggested that elevated shoulder stress associates with rapidly expanding AAAs. Growth and remodeling (G&R) simulations from [43] also suggest that the shoulder represents a region where elastin

may fail mechanically as an aneurysm enlarges, thus leading to steep gradients in stress. The computational models of AAAs expanding axially against fixed ends (e.g., at the renal arteries and iliac bifurcations) also predict decreasing axial stress in the neck and shoulder regions, which suggests a potentially increased risk of tortuosity (e.g., buckling) [73]. Consistent with the proposal by Swedenborg & Eriksson [11] that elongation and tortuosity may result from elastin degradation, the computational results may potentially link changes in the neck and shoulder regions with the induction of disturbed flow and subsequent thrombus deposition. Interestingly, hemodynamic simulations also demonstrate regions of backflow in the proximal neck of the aneurysm, which may convect important biomolecules, including proteases and inflammatory mediators, from nearby thrombus to the proximal neck. Indeed, NGAL-MMP-9 complexes, which are abundant in the luminal layer, have been found in the neck [127], though they might also originate from early infiltrating leukocytes in the wall as well. In addition, thrombin and fibrin from the nearby thrombus may activate endothelial cells, which are still present in the neck and possibly shoulder regions, to increase production of tPA and uPA [46] and thus potentially affect ILT remodeling.

Particular attention should be given to the neck and shoulder regions of the AAA, including their biomechanical and biochemical properties, their role in the axial expansion of the aneurysm, and their relation to nearby thrombus. Future data regarding changes in these regions may provide important clues to understand early aneurysm formation and tortuosity that may ultimately guide new therapeutics, such as stent seating and design, and improve future G&R models which must account for the evolving non-aneurysmal aortic regions in the modeling domain.

ILT shielding, attachment, and compressibility

It has long been appreciated that mathematical models of the aneurysmal wall can provide important insight into the biomechanics, and thus structural stability, of these potentially life-threatening lesions. While the earliest models did not include ILT, their incorporation into models of AAAs has developed over the past two decades from axisymmetric [17,154] to 2-D eccentric and finally to fully 3-D patient-specific geometries [155–157]. The majority of these computational studies, as well as an *in vitro* experimental study using a synthetic AAA model with thrombus [18], support the initial work by Inzoli et al. [17] that an ILT may provide a mechanically protective effect (i.e. a “cushioning” or “shielding”) by reducing the stress on the aneurysmal wall; yet, others question the ability of the porous thrombus to reduce wall

stress consistently, as assessed computationally [20] or by direct intraoperative pressure measurements *in vivo* [19]. Clearly, controversy remains.

Two important factors in determining the presence or extent of this potential stress shielding are the attachment of the thrombus to the underlying wall and the degrees of porosity and compressibility of the ILT. Adhesion of platelets to collagen has been investigated extensively, but connection of fibrin to the aneurysmal wall has not. As noted earlier, several papers report a "liquid phase" at the interface between the ILT and wall [10,11], suggesting that thrombus may not be attached to the wall, at least in some instances. The type of thrombus layer in contact with the wall may also affect the degree of attachment; that is, an actively remodeling thin luminal layer in direct contact with an aneurysmal wall could be attached differently than a degenerated abluminal layer as observed in many thick ILT. Most finite element analyses that include ILT have assumed its perfect attachment to the wall. While a potential reduction of intraluminal pressurization of the wall by the ILT could reduce wall stress, Meyer et al. [20] showed that the thrombus can still have a stress-reducing role even if it does not directly reduce pressurization on the wall as long as the ILT is fully attached. With only partial attachment, however, a porous thrombus capable of transmitting pressure also has the potential to generate stress concentrations and increase wall stress. Clearly, there is a pressing need for greater experimental insight to resolve this question since any estimation of stress distributions, and thus rupture risk, will depend on the mechanical tethering of the ILT and wall.

The compressibility of the ILT will also directly affect its mechanical behavior and its ability to shield the aneurysmal wall. Using non-invasive ultrasound, Vorp et al. [63] suggested that ILT is incompressible, and the vast majority of computational works to date have invoked incompressibility when modeling ILT. Yet, some question this assumption. *In vitro* experiments on fibrin gels demonstrated a dramatic decrease in clot volume due to water expulsion (and thus manifold increase in protein content) with negative compressibility upon stretching [158]. This volume change may be associated with the exposure of hydrophobic groups upon protein unfolding and bundling of stretched fibrin fibers. Of note, the compressibility of the fibrin gels was limited to strains of ~0.5, as further stretching did not alter volume. Provocatively, an *in vivo* study by Truijers et al. [159] that quantified volumes of lumen, intraluminal thrombus, and whole AAA through the cardiac cycle in 17 patients using dynamic electrocardiographically-gated CT angiography showed wide patient-specific variability (0.4% to 43.6% compressibility by volume between diastole and peak systole). No correlation was found between compressibility of thrombus and aneurysm size, thrombus

volume, or pulse pressure. Since this study analyzed the volume of thrombus within the entire aneurysm, no distinction can be made between the compressibility of the heterogeneous layers of ILT that may possess different inherent mechanical properties and times of deposition; nevertheless, this study strongly suggests that not all ILT are incompressible. Furthermore, since thrombus is constantly evolving, the compressibility of a given ILT may change over time. The potentially evolving compressibility of ILT may not only affect its stress-shielding of the wall (and require a reformulation of the constitutive relations used for its mechanical modeling), it may also significantly affect the transport of key biomolecules produced by the ILT. Clearly, studies are needed to determine the compressibility, attachment, and stress buffering capability of ILT in a patient-specific manner, as some ILT may provide significant shielding effects while others may not.

Strength and failure of the ILT and wall

Aneurysms rupture when local wall stress exceeds wall strength [71]. Hence, including the potential ability of ILT to alter spatiotemporally both the mechanical stress and the inherent strength of the underlying aneurysmal wall may improve our ability to predict patient-specific rupture risk. Indeed, Vande Geest et al. [160] already proposed ILT thickness as a key parameter in formulating a statistical estimate of wall strength, and Tong et al. [8] showed that aneurysmal wall underneath older thrombus was generally weaker in the high loading domain during biaxial testing compared with that under young thrombus.

Gasser et al. [161] tested the hypothesis that mechanical failure of ILT itself could lead to subsequent AAA rupture. They subjected specimens of luminal, medial, and abluminal ILT to uniaxial fatigue and strength tests and concluded that ILT fails before the wall. Indeed, CT evidence suggests that focal hemorrhage into the ILT, described radiographically as a "crescent sign" (Figure 3.8), associates with an increased risk of rupture or impending rupture [83]. Such a failure could not only expose the wall to increased stress (if the assumption of stress-shielding by the ILT is true), the fresh hemorrhage into the ILT could also weaken the underlying wall structurally via the delivery and release of active proteases (as discussed earlier), both of which may increase rupture risk.

In addition to revealing the crescent sign, medical imaging may provide further insights into the mechanics and interactions of the ILT and aortic wall that could significantly advance the assessment of rupture risk by revealing patient-specific properties of the thrombus and wall non-invasively. For example, Nchimi et al. [162] reported a correlation of phagocytic leukocytes and changes in magnetic resonance signal via the use of superparamagnetic iron

oxide (SPIO) at the luminal interface of the thrombus, thus suggesting a potential means of determining activity of the luminal layer. Later, Richards et al. [163] showed that distinct mural uptake of ultrasmall SPIO (or USPIO) in the aneurysmal wall associated with a three-fold higher expansion rate than no or non-specific USPIO uptake despite similar maximum diameters. This finding is consistent with the idea that active areas of inflammation augment the degradation and remodeling of the extracellular matrix and hence influence expansion. Moreover, MRI may help differentiate distinct layers of ILT within some aneurysms *in vivo* (e.g., see Figure 3.8). Whether these layers correspond to the biochemically and/or biomechanically distinct layers discussed herein requires future investigation. Nevertheless, the potential for medical imaging to inform the next generation of patient-specific G&R models of AAAs holds significant promise.

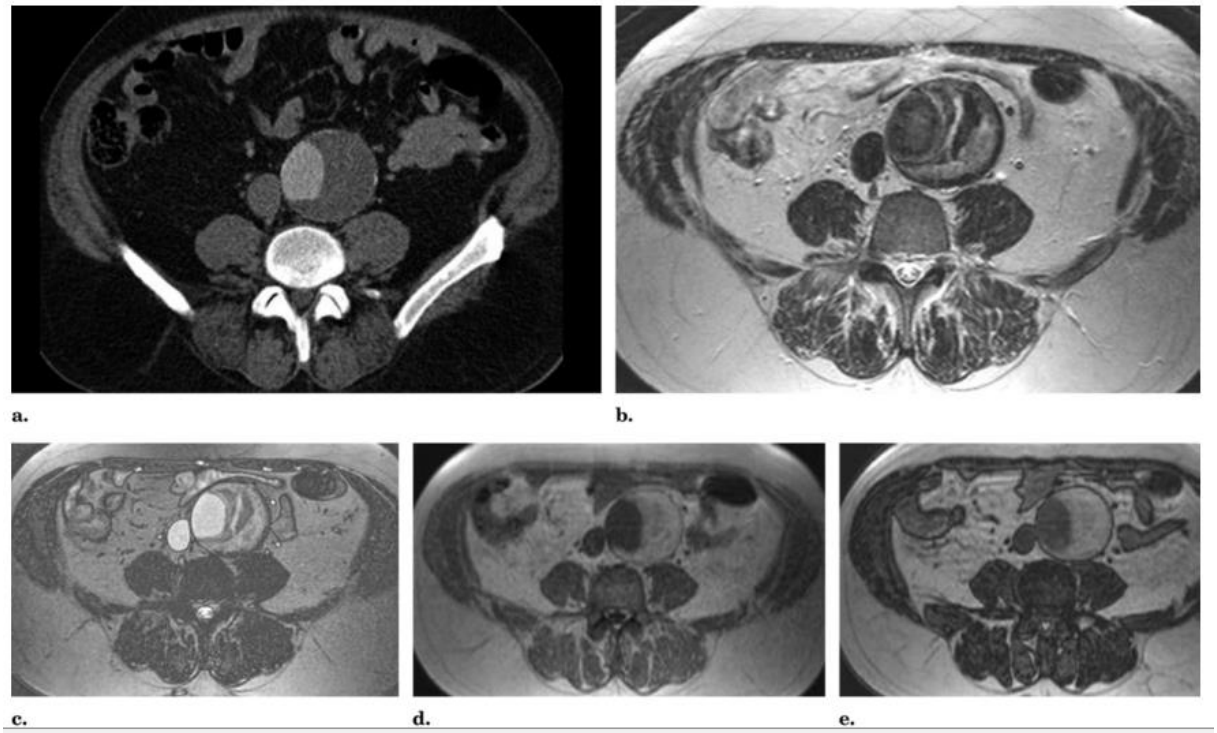

Figure 3.8: Clearly visible layers of ILT, from [72]

4. Growth and remodeling of thrombus-laden aneurysm

4.1. Methodology

The present model for the formation and maturation of ILT was motivated by prior review of the literature [84] and expectation that the aortic wall in closest proximity to the luminal layer of ILT (i.e., underneath thin thrombus) could experience augmented G&R and potential weakening secondary due to thrombus-derived proteases [55,118]. Note that the thickness of the luminal layer is limited by the depth (~2 mm) [117] to which blood components can penetrate the evolving fibrin mesh. The medial and abluminal layers in thicker ILTs are largely acellular and consist of a variably degraded fibrin mesh. Apoptosis and degradation of fibrin can create fluid-filled voids that form transmural canaliculi of increasing cross-sectional area from the lumen to the wall [9]. Such canaliculi could allow transport of blood borne cells and proteins deeper within the ILT, but this possibility has not been confirmed experimentally and was not considered herein. Rather, from the above considerations, fibrin, fibrin degradation products (FDPs), RBCs, and voids were assumed to be the most significant space-occupying constituents of a layered ILT. Although contributions of inflammatory cells and proteases to overall clot volume were neglected, the leukocytes and associated proteolysis (which are critical to the biological activity of the thrombus) were nevertheless included within the luminal layer.

As noted above, a constant overall luminal diameter as the AAA evolved was assumed; that is, once a thrombus initiated, it continuously filled the available space within the aneurysm to maintain a constant luminal diameter as seen on many medical images of large AAAs. This of course is not always true, but it seems like a reasonable assumption supported by some clinical observations. For example, see figure 9 from (Zambrano et al., 2015) showing changes in cross-sectional area of four different patients over time. Three of them (patients P-6, P-8 and P-9) show the increase of the cross-sectional AAA outer area while the lumen area remained nearly constant. Thus, pre-existing thrombus was effectively pushed deeper into the model ILT as the AAA dilated and new thrombus formed luminally. A new layer of thrombus layer deposited on any previous ILT, at each time step to maintain a constant luminal diameter, is hereinafter labeled as layer *i*. Naturally, this suggests that deposited thrombus transitions from initially luminal to medial and eventually abluminal. Thus, medial and abluminal layers were not prescribed a priori, they emerged as a result of AAA progression. In this way, mathematical model of an ILT within an AAA presented

herein could describe evolving biomechanical and biochemical behaviors of the thrombus and its constituents (e.g., fibrin, FDPs, RBCs, and voids) as a function of time and position.

Fibrin

Fibrin accumulates when activated thrombin cleaves fibrinogen into fibrin, which then polymerizes to form an interconnected cross-linked mesh. Formation of fibrin has been modeled in several ways [46,50], typically based on *in vitro* studies that do not necessarily represent *in vivo* behavior. Such models necessarily describe clots that develop in minutes and dissolve in hours, highly atypical for ILT in aneurysms. Clearly, there is a need for more understanding of the *in vivo* mechanisms and mechanics.

Similar to G&R models for arterial adaptations and disease progression, a sufficient supply of fibrinogen at the luminal surface of an ILT was assumed, such that the rate of production of fibrin ($\dot{m}_i^f$) in layer i does not depend on the concentration of hemodynamically supplied fibrinogen. Rather, the production of new fibrin decreased with increasing fibrin density ϕ_i^f or increased with an increased number of platelets M_i^{plt},

$$\dot{m}_i^f(\tau) = K_{plt,\phi}^f M_i^{plt}(\tau)\left(1-\phi_i^f(\tau)\right), \tag{23}$$

where $K_{plt,\phi}^f$ is a simple correlation parameter. In contrast, degradation of fibrin depends on the concentration of plasmin, which is derived from the conversion of plasminogen in the blood. Interestingly, fibrinolysis appears to be inversely proportional to the density of the fibrin mesh and mechanical stretch [56]. Thus, a rate-type parameter for the removal of fibrin was considered to be

$$K_q^f(\tau) = k_q^f + w_q^f \frac{M_i^{pls}(\tau)\left(1-\phi_i^f(\tau)\right)}{\lambda_i(\tau)}, \tag{24}$$

where k_q^f is a homeostatic value independent of plasmin, stretch, and mesh density. M_i^{pls} is the mass of plasmin, λ_i is the fibrin stretch, and w_q^f is a weighting function. Hence, similar to constituents in the wall, the mass of fibrin was computed as:

$$M_i^f(s) = M_i^f(0)Q_i^f(s) + \int_0^s \dot{m}_i^f(\tau)\, q_i^f(s-\tau)\,\mathrm{d}\tau, \tag{25}$$

where $M_i^f(0)$ is the initial mass of fibrin in a newly deposited luminal layer, and $Q_i^f(s) = q_i^f(s-0) = \exp(-\int_0^s K_q^f(\tilde{\tau})\,\mathrm{d}\tilde{\tau})$.

Cells/Platelets

The majority of blood-derived cells within an ILT reside in the luminal layer [9,118]. It has been proposed that the proximity of the luminal layer to flowing blood allows these cells to be replenished; as new layers are deposited, however, cells can generally not penetrate into or survive within the deeper medial and abluminal layers. Hence, a first order decay process for cells previously in a luminal layer that became buried during new deposition of ILT as the lesion enlarged (with a half-life of 7-11 days for platelets and 120 days for erythrocytes) was assumed.

The boundary of the luminal layer was defined by either: (a) a critical fibrin mesh density $\phi_{crit}^{f,RBC}$ that was reached when RBCs were excluded or (b) a critical radius r_{crit} that was attained beyond which cells could not be replenished. This critical radius was defined as a function of a critical mass of fibrin M_{crit}^{f}, such that

$$\int_{r_i}^{r_{crit}} M_i^f(r)\,\mathrm{d}r = M_{crit}^f . \tag{26}$$

Therefore, the quantity of platelets (or other blood-borne cells) in the luminal layer depended on the quantity in the luminal blood, M_l^{plt}, which could potentially vary in time (e.g., in a flow field having evolving vortical structures [111]). In the deeper layers, these platelets were presumed to degrade according to a first-order process, with the rate-type parameter inversely related to the half-life $\tau_{1/2}^{plt}$:

$$K_q^{plt} = \frac{\ln 2}{\tau_{1/2}^{plt}} . \tag{27}$$

In this way, consistent with histological findings [8], new fibrin was predominately deposited in the luminal layer where the mass of platelets was necessarily highest.

In summary, the mass of platelets was calculated as

$$M_i^{plt}(\tau) = \begin{cases} M_l^{plt}(\tau) & r_i(\tau) < r_{crit}(\tau) \quad \text{and} \quad \phi_j^f < \phi_{crit}^{f,plt}, \ \forall j \geq i \\ M_l^{plt}(\tau_{crit}^{i,1}) \cdot e^{-K_q^{plt}(\tau - \tau_{crit}^{i,1})} & r_i(\tau) \geq r_{crit}(\tau) \\ M_l^{plt}(\tau_{crit}^{i,2}) \cdot e^{-K_q^{plt}(\tau - \tau_{crit}^{i,2})} & \phi_j^f(\tau) \geq \phi_{crit}^{f,plt}, \ \forall j \geq i \end{cases} , \tag{28}$$

where $\tau_{crit}^{i,1}$ is the time at which a critical mass of fibrin (and r_{crit}) was achieved, thus transitioning the initial luminal layer to medial with a low platelet count. Similarly, the time

$\tau_{crit}^{i,2}$ represents when the limit of the luminal layer was achieved by reaching the critical mass fraction of fibrin.

The distribution of RBCs within the ILT was defined similarly, with the exception of using a mass fraction instead of the mass. Note that $\phi_i^{RBC}(\tau) = 1 - \phi_i^f(\tau)$ in the luminal layer because the sum of the mass fractions over all constituents must equal one, $\phi_i^f + \phi_i^{RBC} + \phi_i^v + \phi_i^{FDP} = 1$, and voids and fibrin degradation products are generally absent in the luminal layer. Thus,

$$\phi_i^{RBC}(\tau) = \begin{cases} 1 - \phi_i^f(\tau) & r_i(\tau) < r_{crit}(\tau) \quad \text{and} \quad \phi_j^f < \phi_{crit}^{f,RBC} \\ \min\left((1 - \phi_i^f(\tau_{crit}^{i,1})) \cdot e^{-K_q^{RBC}(\tau - \tau_{crit}^{i,1})}, 1 - \phi_i^f(\tau) \right) & r_i(\tau) \geq r_{crit}(\tau) \\ \min\left((1 - \phi_i^f(\tau_{crit}^{i,2})) \cdot e^{-K_q^{RBC}(\tau - \tau_{crit}^{i,2})}, 1 - \phi_i^f(\tau) \right) & \phi_j^f(\tau) \geq \phi_{crit}^{f,RBC} \end{cases} . \quad (29)$$

Like the platelets, the leukocytes were assumed to not contribute significantly to the volume of the ILT; hence, they were excluded from the mass fraction summation. Their presence was important nonetheless for the production of proteases such as plasmin, MMPs, and macrophage or neutrophil elastases. Thus, the quantity of leukocytes (primarily neutrophils) M_i^N was modeled similar to the mass of platelets, with defined concentrations in the luminal layer and a first-order decay within the deeper layers.

Plasmin, EDPs, and neovascularization

Plasminogen is converted to plasmin by different enzymes, most importantly tissue plasminogen activator (tPA) and urokinase plasminogen activator (uPA). The tPA is found on endothelial cells, while the uPA comes mainly from the blood stream via mesenchymal and inflammatory cells. For this simplified model, two primary sources of active plasmin were considered: the leukocyte-rich luminal layer of the ILT and the aortic wall itself. The latter may be due to an influx of inflammatory cells into the aneurysmal wall from multiple sources, including an increased *vasa vasorum* [15]. Regardless of the source, an increased production of plasmin within an evolving wall consistent with immunohistological reports [10] was assumed. The overall increase in activated plasmin (while excluding the kinetics associated with changing concentrations of plasminogen, tPA, uPA, and the inhibitors PAI-1 and alpha-2 antiplasmin) was sought to be captured phenomenologically, future studies should seek to quantify and incorporate these complexities spatially and temporally. For now, however, the assumption that the mass of activated plasmin M_i^{pls} that degrades fibrin was used, such that

$$M_i^{pls}(\tau) = K_N^{pls} M_i^N(\tau) + \underbrace{M_{wall}^{pls}(\tau) - \sum_{j=1}^{i} K_f^{pls} M_j^f(\tau)}_{\geq 0}, \tag{30}$$

where K_N^{pls} is a correlation factor between plasmin and neutrophils in the thrombus, K_f^{pls} is the amount of plasmin consumed per unit of fibrin, and $M_{wall}^{pls}(\tau)$ is the mass of plasmin in the wall calculated by

$$M_{wall}^{pls}(\tau) = K_{EDP}^{pls} M_{tot}^{EDP}(\tau) + K_{VV}^{pls} A_{tot}^{VV}(\tau). \tag{31}$$

Plasmin generated within the wall is considered to depend largely on the total mass of elastin degradation products M_{tot}^{EDP}, which are chemoattractants for inflammatory cells and stimulate neovascularization of the wall (i.e., increase the amount/area of *vasa vasorum* A_{tot}^{VV} that allows increased migration of inflammatory cells into the remodeling wall [136]). Correlations between plasmin and EDPs/*vasa vasorum* were accounted for by K_{EDP}^{pls} and K_{VV}^{pls}, respectively.

The production rate of EDPs, $\dot{m}_i^{EDP}$, was prescribed by the amount of elastin degraded over the previous time step, that is,

$$\dot{m}_i^{EDP}(\tau) = -\frac{\mathrm{d}M_i^e}{\mathrm{d}\tau} = \frac{M_i^e(\tau - \Delta\tau) - M_i^e(\tau)}{\Delta\tau}, \tag{32}$$

while the EDPs degraded with rate-type parameter K_q^{EDP}:

$$q_i^{EDP}(s-\tau) = \exp\left(-\int_{\tau}^{s} K_q^{EDP} \, \mathrm{d}\tilde{\tau} \right). \tag{33}$$

Thus the total mass of EDPs in each layer i was

$$M_i^{EDP}(s) = \int_0^s \dot{m}_i^{EDP}(\tau) q_i^{EDP}(\mathrm{s}-\tau) \, \mathrm{d}\tau, \tag{34}$$

and the total mass of EDPs, M_{tot}^{EDP} for the aortic wall was

$$M_{tot}^{EDP}(s) = \sum_i M_i^{EDP}(s). \tag{35}$$

Development of *vasa vasorum* has been thought to be connected with increased hypoxia due to thick ILTs [74]. Yet, Mäyränpää et al. [15] reported that the expression of genes associated with intramural neovascularization is the same or only slightly increased in thrombus-covered versus thrombus-free walls in AAAs. Interestingly, EDPs also appear to affect neovascularization [136]. For example, both intraluminal infusion of the rat aorta with elastase (to create AAAs) and direct delivery of EDPs to the wall cause comparable

neovascularization [136]. The development of *vasa vasorum* was modeled as a function of the mass of EDPs, but neglected the influence of hypoxia. Thus,

$$A_{tot}^{VV}(s) = A_0^{VV} + \int_0^s K_{EDP}^{VV} M_{tot}^{EDP} \, \mathrm{d}\tau, \tag{36}$$

where A_0^{VV} denotes a homeostatic area of *vasa vasorum* in healthy aorta and K_{EDP}^{VV} is a correlation factor that relates *vasa vasorum* growth per unit of EDPs per unit time.

Voids and fibrin degradation products

The fibrin mesh in the luminal layer is characterized by thick primary fibers and fine interconnecting secondary fibers. Since thinner fibers cleave more quickly than thicker ones [112], these secondary interconnections are lost in the medial layer, thus leaving small interconnected channels ("voids" or "canaliculi") throughout much of the ILT [9]. Degraded fibrin was assumed to turn partly into fibrin degradation products (FDPs) and to be partly removed by macrophages, which leaves voids. Overall, the mean void area increased from the luminal toward the abluminal layer.

Biochemomechanical interaction of ILT and the wall

To model biochemomechanical interactions between the aortic wall and ILT, two models must be interconnected. Stress in the ILT was modeled similar to that in the wall. The stored energy of fibrin-rich ILT was assumed to be [8],

$$\hat{W}^f = \mu^f (I_1 - 3) + \frac{k_1}{k_2}\left[\exp\left(k_2(1-\rho^{aniso})(I_1-3)^2 + \rho^{aniso}(I_4-1)^2\right) - 1\right], \tag{37}$$

where μ and k_1 have units of stress, k_2 is dimensionless, $I_1 = \mathrm{tr}(\mathbf{C}_{n(\tau)}^f)$, and $I_4 = \mathbf{m}(\tau)\cdot\mathbf{C}_{n(\tau)}^f\cdot\mathbf{m}^T(\tau)$. Similar to that for intramural matrix, $\mathbf{C}_{n(\tau)}^f$ is the right Cauchy-Green tensor, $\mathbf{m}$ represents the orientation of the fibers, and $\rho^{aniso} \in [0,1]$ is a measure of mechanical anisotropy. Since anisotropy of the luminal layer may increase with aging [8], ρ was modeled as a function of the time that the layer was in contact with the flowing blood and associated wall shear stress, that is

$$\rho^{aniso}(\tau,\tau_w) = f(\tau)g(\tau_w) = K_{\max}^{aniso}\left(1-\exp\left(-K_t^{aniso}(\tau-\tau_{i,0})\right)\right)\exp\left(K_{\tau_w}^{aniso}\left(\frac{\tau_w}{\tau_{w,h}}-1\right)\right), \tag{38}$$

where $K_{\max}^{aniso}$, K_{t}^{aniso} and $K_{\tau_w}^{aniso}$ are correlation factors and $\tau_{i,0}$ is the time at which the current luminal layer was formed. In cases of isotropic ILT, $\rho^{aniso}=0$, and Eq. (37) reduces to:

$$\hat{W}^{f}=\mu^{f}(I_1-3)+\frac{k_1}{k_2}\left[\exp\left(k_2(I_1-3)^2\right)-1\right]. \tag{39}$$

Similar to elastin, a neo-Hookean strain energy function was used to model the mechanics of the fibrin degradation products:

$$\hat{W}^{\mathrm{FDP}}=\mu^{FDP}\,\mathrm{tr}\left(\mathbf{C}_{n(\tau)}^{\mathrm{FDP}}-\mathbf{1}\right). \tag{40}$$

Erythrocytes (RBCs) and voids only affected the compressive properties.

Biochemical effects of the proteolytically active luminal layer were incorporated via additional terms in the degradation functions for collagen and elastin. In general, the survival function of all structurally important constituents was modeled by a first order decay, similar to Eq. (2):

$$q_i^k(s-\tau)=\exp\left(-\int_{\tau}^{s}K_q^k(\tilde{\tau})\,\mathrm{d}\tilde{\tau}\right). \tag{41}$$

The K_q^k in Eq. (41) need not be constant as were K^k in Eq. (41). For example, whereas K^e for elastin in a normal aging aorta depends primarily on its natural half-life ($\tau_{1/2}^e$) of ~40 years, namely $K^e=k_q^e=\dfrac{\ln(2)}{\tau_{1/2}^e}$, the increased degradation of elastin in an aneurysm due to inflammation was modeled as

$$K_q^e(t)=k_q^e+w_{q,elas}^e M^{elas}(r,t), \tag{42}$$

where, k_q^e is the constant degradation rate associated its normal half-life and the second term represents further degradation due to an increased concentration of inflammatory cell released elastases, M^{elas}, with weighting factor $w_{q,elas}^e$.

For collagen, the model from [34] was extended to be

$$K_q^c(\tau)=\frac{\left\|\partial W^c/\partial\mathbf{F}_{n(\tau)}^c\right\|}{\left\|\partial W^c/\partial\mathbf{F}_{n(0)}^c\right\|}k_q^c+w_{q,MMP}^c M^{MMP}(r,\tau), \tag{43}$$

where K_q^c depends on the ratio of the current ($\dfrac{\partial W^c}{\partial\mathbf{F}_{n(\tau)}^c}$) to the homeostatic ($\dfrac{\partial W^c}{\partial\mathbf{F}_{n(0)}^c}$) value of fiber tension, and k_q^c is the homeostatic half-life; the additional terms account for the presence

of MMPs (i.e., collagenases) that were activated by ILT-related plasmin as well as other mechanisms.

Similar to plasmin and oxygen, the distribution of MMPs may depend on two cell sources: those from the luminal layer in the ILT and those coming from the *vasa vasorum* within the aortic wall. Each of these sources may evolve as the lesion expands. This situation implies diffusion with two sources and a line sink. Ideally, to calculate distribution of MMPs, amount of different types separately, activation of MMPs by plasmin, half-life of MMPs and many other factors should be all taken into account. Convection also requires modelling of flow through the ILT. However, there is a lack of experimental data about all of these problems, and therefore, MMP distribution was captured phenomenologically based on available data. Therefore, as a first approximation, considering only a quasi-static solution

$$\frac{\partial M^{elas}}{\partial \tau} = \nabla \cdot \left[D \nabla M^{elas} \right] \tag{44}$$

was solved using available experimental data on the radial distribution of proteases [55,118], where D is the diffusion coefficient. The luminal boundary condition was defined as the elastase/MMPs available from the luminal layer, $K_N^{elas} M_{tot}^N$ (or $K_N^{MMP} M_{tot}^N$ for MMPs), where $K_N^{elas/MMP}$ describes how much elastase/MMP was produced per unit of leukocytes per time step. The location of the source of the proteases was prescribed at radius r_L by:

$$r_L(s) = \frac{1}{M_{tot}^N(s)} \sum_i M_i^N(s) r_i(s), \tag{45}$$

similar to a center of gravity calculation for each layer *i*. The concentration of elastase/MMPs at the outer radius depended on the area of *vasa vasorum* and quantity of inflammatory cells: $K_{WBC}^{elas} M_{tot}^{WBC}(s) + K_{VV}^{elas} A_{tot}^{VV}(s)$. Thus, the overall distribution of proteases was:

$$M^k(r,s) = \frac{K_N^k M_{tot}^N(s) - K_{WBC}^k M_{tot}^{WBC}(s) - K_{VV}^k A_{tot}^{VV}(s)}{\ln(r_L(s)/r_o)} \ln\left(\frac{r(s)}{r_o}\right) + K_N^k M_{tot}^N(s), \tag{46}$$

where k can indicate elastases or collagenases (indeed any MMP). The mass of inflammatory cells in the wall, M_{tot}^{WBC}, was modelled similar to Eq. (1), with degradation depending on cellular half-life and production $\dot{m}_{tot}^{WBC}$ increasing with increases in mass of EPDs and *vasa vasorum*, such that

$$\dot{m}_{tot}^{WBC}(\tau) = K_{EDP,VV}^{WBC} \left(\frac{A_{tot}^{VV}(\tau)}{A_0^{VV}} \right)^{\alpha} M_{tot}^{EDP}(\tau), \tag{47}$$

where $K_{EDP,VV}^{WBC}$ is a correlation factor that relates the proliferation of white blood cells with EDPs and neovascularization, and α is power parameter.

With the above survival functions, the mass of collagen can be calculated by Eq. (1); because there is no production of elastin, its evolving mass can be calculated by the reduced expression:

$$M^e(s) = M^e(0)Q^e(s)\,. \tag{48}$$

The half-life of SMCs was also prescribed by a first order decay rate [34], but its degradation was additionally linked to the degradation of elastin to model anoikis (a type of apoptosis caused by loss of attachment to the surrounding matrix). AAA initiation when there is a local loss of elastin was assumed, which in turn results in a local loss of smooth muscle via anoikis. The elastin degradation function was prescribed similar to that used by Valentín et al. [96], namely

$$q_i^{SMC}(s-\tau) = \exp\left(-\int_{\tau}^{s} K_q^{SMC}(\tilde{\tau})\,\mathrm{d}\tilde{\tau}\right) Q^e(s)\,. \tag{49}$$

Yet, smooth muscle cells can also become more synthetic, so maximal active stress T_m decreased as [96]

$$T_m(s) = T_m(0)\cdot\left(\beta_m + (1-\beta_m)Q_e(s)\right), \tag{50}$$

where β_m is a scaling parameter that controlled the degree of proportionality between elastin content and vasoactivity.

To summarize, Figure 1.4 outlines interactions among the primary contributors that affect the G&R of a thrombus-laden AAA. The left side of the schema highlights the most important reactions in the thrombus: fibrin is produced by thrombin and degraded by plasmin. The right side refers to processes within the aortic wall: MMPs degrade structurally significant constituents, thus releasing elastin degradation products and increasing neovascularization. Arrows connecting the two boxes delineate the impact of thrombus on the wall and the influence of intramural cells on the maturation of thrombus. Of particular note, plasmin produced in the ILT by leukocytes can diffuse into the wall and help activate proMMPs. Conversely, inflammatory cells within the wall can impact the conversion of plasminogen to plasmin by degrading the fibrin to which it was bound. Clearly, there are complex biochemical interactions between the ILT and wall of the AAA.

4.2. Parameter values

Similar to growth and remodeling parameters for the aortic wall (Table 1) the constitutive relations and parameters were classified by level of consensus and function (Table 4). Again, easily measured parameters (such as thrombus stiffness [8]) were classified as "observed".

Table 4: Parameter values used for G&R of ILT.

Class	Role	Parameter value	Eq. #	Refs.
Observed	Homeostatic kinetics	$\tau_{1/2}^{RBC} = 15$ days $\tau_{1/2}^{PLT} = 5$ days, $\tau_{1/2}^{WBC} = 20$ days, $\tau_{1/2}^{EDP} = 40$ years, $\tau_{1/2}^{f} = 4$ years	e.g., (27)	[87,98, 99]
	Passive elasticity	$\mu^f = 0.0082$ MPa, $k_1 = 0.0123$ MPa, $k_2 = 0.6$	(37)	[8,97]
Bounded	Pre-stretches	$G^{\mathrm{f}} = 1.08$	See Figure 2.1	[96]
	Luminal layer definition	$M_{\mathrm{crit}} = 0.9 \cdot 10^{-4}$ kg mm^{-1}, $\phi_{\mathrm{crit}}^{\mathrm{RBC}} = 0.9$, $\phi_{\mathrm{crit}}^{\mathrm{PLT}} = 0.9$, $\phi_{\mathrm{crit}}^{\mathrm{N}} = 0.9$	(28) (29)	[8]
	Vasa vasorum	$A_0^{VV} = 5 \cdot 10^{-4}$ mm^2	(36)	[9]
	Masses of cells	$M_l^{plt} = 0.15$ g mm^{-1}, $M_l^{N} = 0.2$ g mm^{-1}	(28)	[117]
Empirical	Correlation factors	$K_{EDP,VV}^{WBC} = 150$ mm$_{VV}^2$ (kg$_{EDP}$ · day)$^{-1}$, $K_N^{pls} = 0.01$ g$_{pls}$ (g$_N$ · day)$^{-1}$, $K_{plt}^{f} = 0.25$ g$_f$ (g$_{plt}$ · day)$^{-1}$, $K_N^{MMP} = 5.5$ g$_{MMP}$ g$_N^{-1}$, $K_{WBC}^{MMP} = 0.01$ g$_{MMP}$ g$_{WBC}^{-1}$ $K_{VV}^{MMP} = 0.00015$ g$_{MMP}$ mm$_{VV}^{-2}$, $K_N^{elas} = 0.12$ g$_{elas}$ g$_N^{-1}$, $K_{WBC}^{elas} = 0.002$ g$_{elas}$ g$_{WBC}^{-1}$, $K_{VV}^{elas} = 0.00035$ g$_{elas}$ mm$_{VV}^{-2}$	(31) (30) (46)	
	Weighting	$w_q^f = 125$ (g$_{pls}$ · day)$^{-1}$,	(24) (42)	

	factors	$w^{e}_{q,elas} = 500\ (\mathrm{g}_{elas} \cdot \mathrm{day})^{-1}$, $w^{c}_{q,MMP} = 750\ (\mathrm{g}_{MMP} \cdot \mathrm{day})^{-1}$	(43)	

In contrast to the wall, "bounded" parameters were not defined by parametric studies from the literature, but were estimated from indirect experimental observations, as, for example, on the extent of the *vasa vasorum* [74] or the critical mass of a luminal layer of thickness 2 mm [117]. Additionally, "empirical" parameters have not been quantified directly, but were chosen to model findings reported in the literature (e.g., spatial distribution of MMPs and elastases [55]).

4.3. Biochemical influence of thrombus on aortic wall

In order to account for mechanical effects of intraluminal thrombus in finite element analysis, one must first implement model into finite element code. However, note that contrary to finite elements describing aortic wall whose number remains the same throughout analysis, but their mass changes, finite elements describing ILT would have constant mass while their number would increase rapidly in each time step, starting from zero in healthy aorta. Thus, for the first approximation of the model only biochemical influence was modeled, whereas mechanical effects ware neglected. This was achieved by using *Matfeap. Matfeap* is an interface between *Matlab* and the finite element analysis program *FEAP* that allows communication and exchange of variables through a common block between these two programs (Figure 4.1).

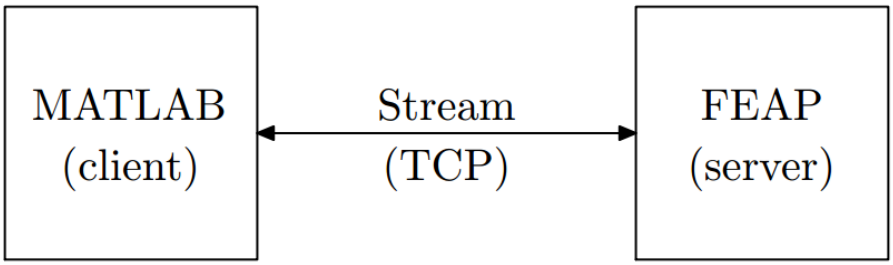

Figure 4.1: Communication between *Matlab* and *FEAP*

Three basic *Matfeap* functions are as follows:

- *feapcmd*: this routine is used to invoke FEAP macro routines, i.e. to assign commands from *Matlab* to *FEAP*

- *feapgetm*: the routine that either reads a common block variable from the standard input or writes a common block variable to the standard output
- *feapsetm*: similar to *feapgetm*, except that it receives data from the client using *feaprecvint* and *feaprecvdbl* where *feapgetm* sends data.

Therefore, *Matfeap* enables one part of code to be calculated in *FEAP*, and the other part in *Matlab*. In this case, the spatial distribution of proteases through ILT and aortic wall is calculated in *Matlab* in each time step. This information is then sent back to *FEAP* in order to calculate masses of elastin and collagen, stresses and displacements.

As a test example for verification of communication between two programs, aging of healthy aorta was simulated. During aging elastin is uniformly degraded with half-life $\tau_{1/2}^{e}$ of 40 years. Since elastin is not produced during maturity, its mass is calculated by Eq. (1) simplified to form $M^e(s) = M^e(0)Q^e$, where survival function is $Q^e = q^e(s-0) = \exp\left(-\int_0^s \frac{\ln(2)}{\tau_{1/2}^e} \mathrm{d}\tilde{\tau}\right)$. *Matlab* received current time s from FEAP, calculated Q^e and returned it back to *FEAP*. Note that during aging geometry of the vessel remains cylindrical, meaning the results obtained by *Matfeap* can be compared with semi-analytical solution. The comparison of results is shown in Figure 4.2. Clearly, the results match perfectly. Simulations also agree with clinical observation that due to loss of elastin aorta slowly dilates with age, with average expansion rate of 0.07 mm/year [94].

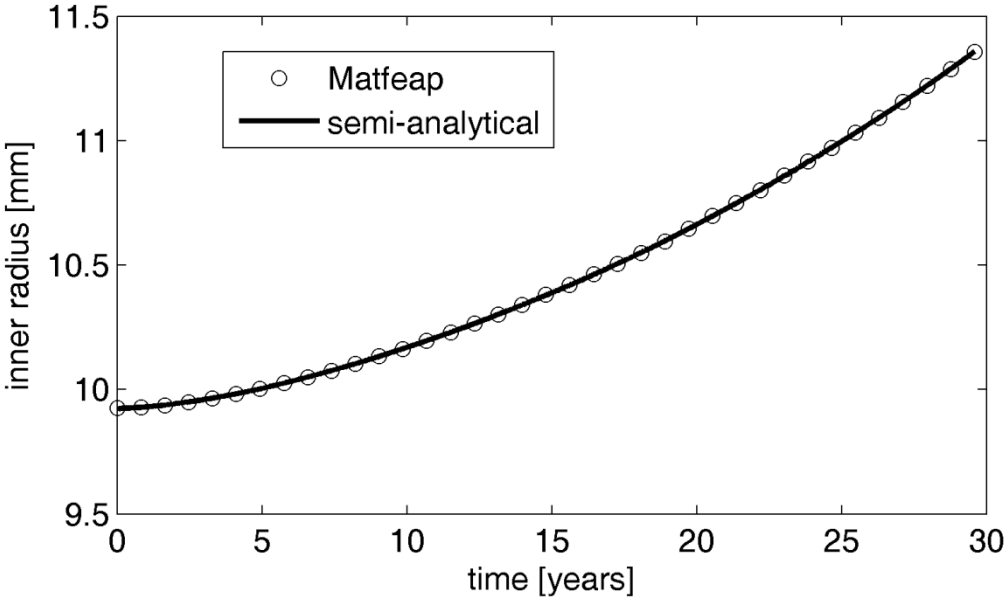

Figure 4.2: Evolution of inner radius during aging obtained by *Matfeap* and *Matlab*

In order to model biochemical effects of thrombus on aneurysm expansion, in every time step *Matlab* needs to calculate distribution of elastase and collagenase (Eq. (46)). Therefore, part of the code in *Matlab* should calculate and write in common block four constants – two for each protease – at each axial position, which will enable FEAP to calculate masses of constituents, stresses and strains. On the other hand, it needs to receive information about geometry of thrombus (i.e., inner radius of the wall) for calculation of r_L, and radial degradation of elastin at each axial location. Mass of degraded elastin is necessary as it is directly connected to elastin degradation products, and thus growth of *vasa vasorum* and number of leukocytes in the wall.

To minimize size of the common block, cylindrical aneurysm was modeled. Unlike aneurysm without thrombus, where elastin was degraded uniformly in radial direction as a function of time (or additionally, axial and circumferential location, for fusiform and saccular aneurysms), this is not the case for thrombus-laden aneurysm. Figure 4.3 shows evolution of elastin mass fractions at different radial locations. Since luminal layer of ILT is the most proteolytically active, intimal elastin was degraded more rapidly than adventitial elastin (Figure 4.3). Thus, after 7 years elastin was almost completely degraded in the inner parts of the wall adjacent to the ILT, whereas some elastin still remained in the outer parts of the wall.

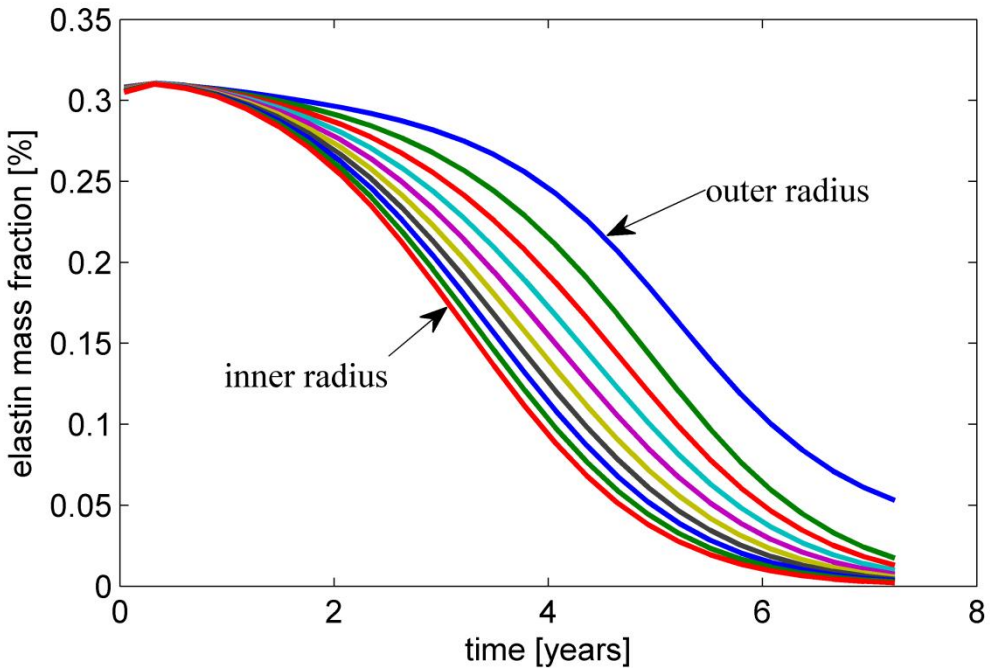

Figure 4.3: Evolution of mass fraction of elastin at different radial locations

Corresponding evolutions of maximum diameter and expansion rates are shown in Figure 4.4 and Figure 4.5. It is interesting to note that expansion rate is not monotonic curve, as it was the case for aneurysm growth simulations presented both above and in the literature (e.g., [73]). These periods of more rapid and slower periods of growth seem to be more realistic, as was suggested by clinical observations (e.g., [21]).

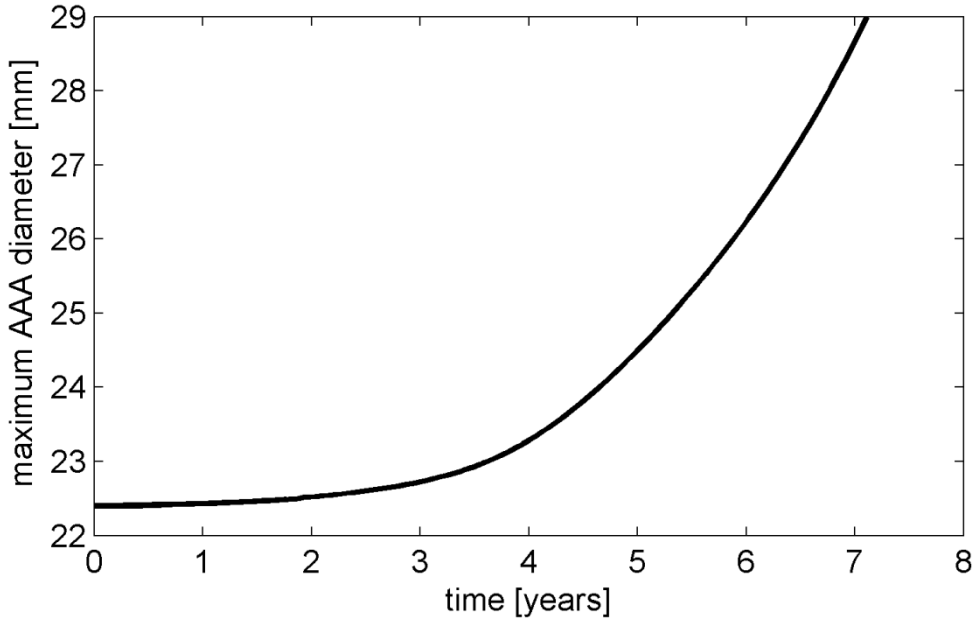

Figure 4.4: Evolution on maximum diameter of thrombus-laden aneurysm

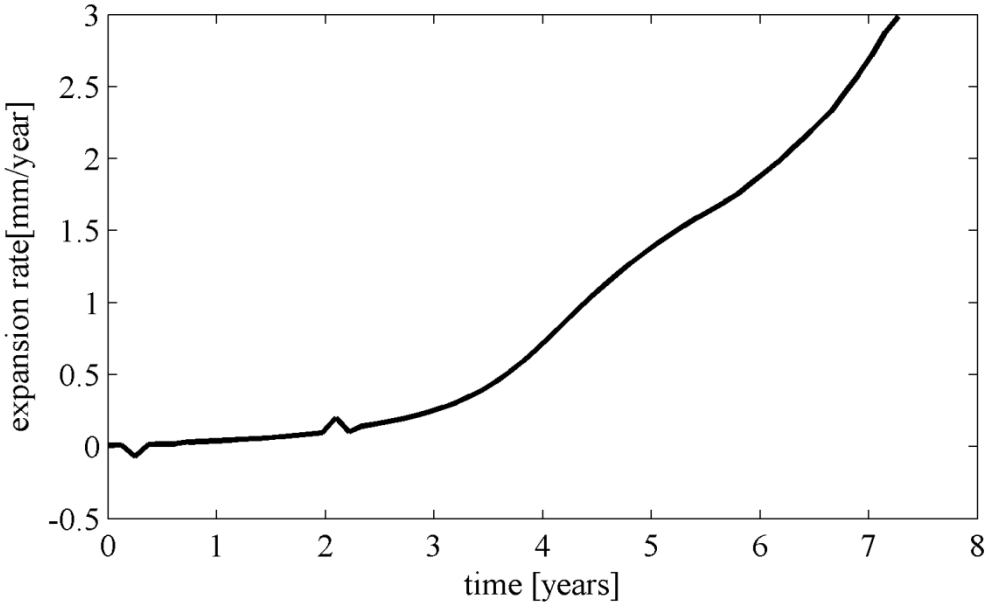

Figure 4.5: Dilatation rate of thrombus-laden aneurysm

However, exchange of data between two programs significantly increases computational time. Even for simulation of aging, where only one variable in common block (i.e., current time) was needed, computational time increased several times. Note that simulations of thrombus-laden fusiform and saccular aneurysms would require much larger number of common variables – intimal radius and amount of degraded elastin in each of several thousand elements, which would slow down the process remarkably. Besides being time consuming, it is also important to remember that mechanical effects cannot be taken into account using *Matfeap*. Additionally, there is a lack of experimental data about molecular distributions and heterogeneities in mechanical properties in the axial and circumferential direction in the literature, which will make the translation of some of the modelling assumptions to 3D quite a complex problem. For all these reasons, the first approximation of the model was performed on cylindrical geometry using semi-analytical solution, and used to study whether intraluminal thrombus influences expansion of aneurysm at all. If thrombus did not affect the outcome of AAA growth, it would not be necessary to use the more complex model (i.e., the G&R model of the aortic wall alone is sufficient). Additionally, it was used to investigate which bounded parameters influence AAA growth the most, either positively or negatively, and to recognize the key features of the thrombus-laden model. This parametric study will be most helpful when implementing the model into finite elements for analysis of 2D and 3D geometries. While these geometries will be much more realistic, they will also introduce further assumptions, as almost all experimental (especially histological) data considers only distance from the lumen, and not axial or circumferential heterogeneities. Moreover, the analysis of key parameters will be computationally much more expensive on realistic geometries, and these simplified 1D analyses give important insight into the main model features. The model was also verified by modeling potential effects of commonly proposed rupture and stabilization factors and comparing the results with clinical observations. It can also provide insight into possible roles of risk factors on the natural history of AAAs.

4.4. Biochemomechanical influence of thrombus on 1-D aneurysm expansion

The simulated development of an AAA was initiated by prescribing a uniform 5% loss of elastin in an initially healthy, but aged aorta (defined by the original material parameters). This insult led to acute changes in stress, and stress-mediated G&R, and an early dilatation. Assuming a space-filling deposition of thrombus (Figure 3.7 and Figure 4.6), and its

associated biochemical effects (e.g., further degradation of the aortic wall via increased quantity of MMPs), allowed the potential effects of thrombus to be modeled for the first time. As can be seen in Figure 4.6 initially three-layered healthy aorta expands, and, under assumption of constant luminal area, thrombus deposits concentrically. The assumption that luminal layer remains constant is not necessarily a bad assumption – clinical observations in [164] have shown that for the most patients it is correct (see Figure 4.7 on the right), yet thrombus is commonly depositing eccentrically (Figure 4.7 in the middle). Unfortunately, this cannot be modeled using semi-analytical solution.

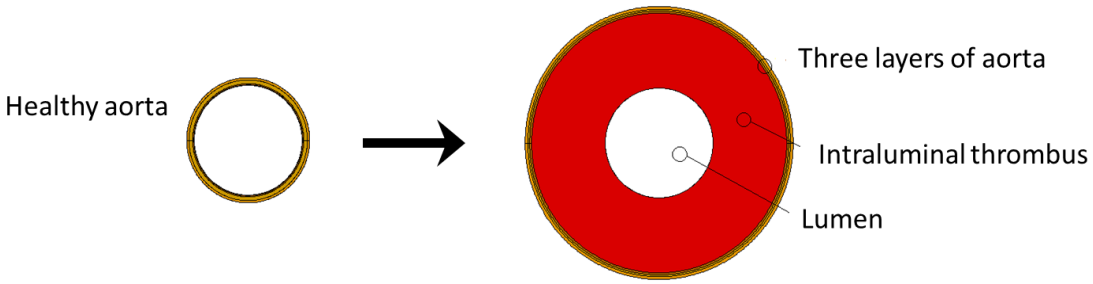

Figure 4.6: Space-filling deposition of thrombus during AAA evolution

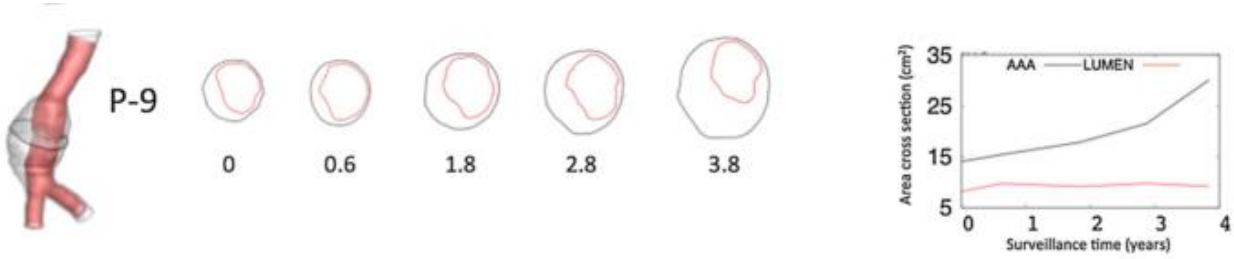

Figure 4.7: Lumen and AAA's outer cross-sectional areas at the region of maximum diameter for patient P-9 after 4 follow-ups, from [164]

4.4.1. Geometric changes

The progression of a representative AAA for the aforementioned model parameters (cf. Table 4) is shown in Figure 4.8. The dot-dashed line at 9.925 mm denotes the constant luminal radius, which enforces a space-filling thrombus. The lower-most gray line denotes the extent of the luminal layer of ILT, typically about 2 mm thick. The solid black line denotes the interface between the abluminal layer of the ILT and the intima, the dashed gray (barely visible) line denotes that between the intima and media, the dashed black line denotes that between the media and adventitia, and the upper-most gray line denotes the outer radius of the aneurysmal wall. For the first 2.5 years (i.e., until the inner radius dilated by 2 mm, the

maximum thickness of a luminal layer), the lesion continued to expand significantly as the proteolytically active luminal layer remained in contact with the aortic wall. In particular, the intimal-medial thickness decreased due to the loss of elastin (proteolytically) and smooth muscle (via anoikis). As the lesion enlarged, intermediate and abluminal layers of ILT formed and acted as a barrier to the diffusion of biomolecules from the luminal layer, effectively diminishing the direct biochemical influence of the ILT. Thus the adventitia thickened, and the concavity of the growth curve switched from positive to negative (i.e., the lesion slowed its growth, perhaps moving towards stabilization). In this idealized geometry, the thrombus had a minimal biochemical effect on progression of the lesion as soon as sufficiently thick intermediate layers of ILT formed; in actual fusiform AAAs, however, the lesion geometry is often complex and the thrombus is often eccentric, hence unique locations of thin thrombus (e.g., the shoulder of the lesion) could exist throughout development wherein clot-related enzymatic activity could remain important to the overall G&R of the wall.

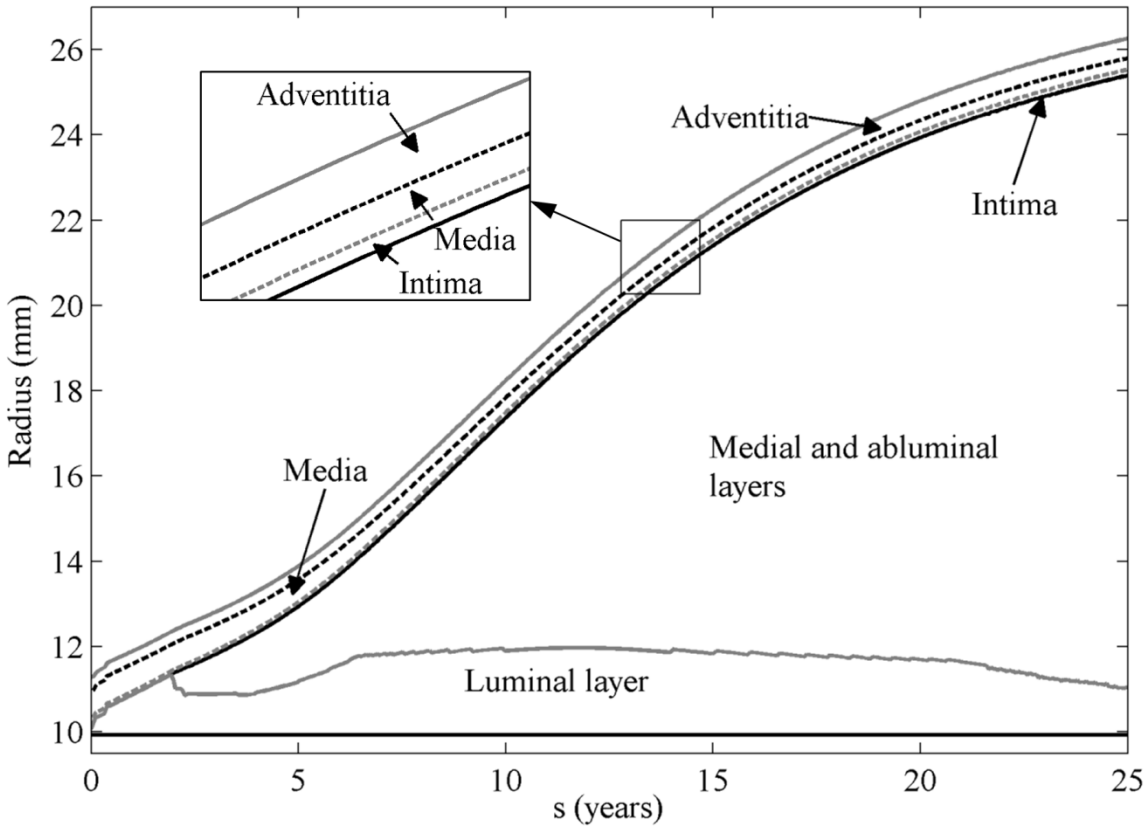

Figure 4.8: Simulated evolution of the central region of an idealized axisymmetric AAA harboring a space-filling thrombus

4.4.2. Elastases/collagenases distribution.

Figure 4.9(a) highlights the evolution of proteolytic activity in the aortic wall normalized to the value at G&R time s = 0 (e.g., from MMPs) in the wall due to the evolving thickness of the ILT. The MMPs within the neighboring wall initially increased as the thickness of the luminal layer of the ILT increased, but fell sharply as the less proteolytically active intermediate layer formed. After 25 years, the final MMP concentration was reduced ~3 fold relative to the peak value, but was yet higher than the initial value due to an increased cross-sectional area of *vasa vasorum* (and thus intramural inflammation) secondary to the production of EDPs (see Eq. (36), Figure 4.9(b)). Cross sectional area of *vasa vasorum* and mass of EDPs are both normalized by their initial, homeostatic value.

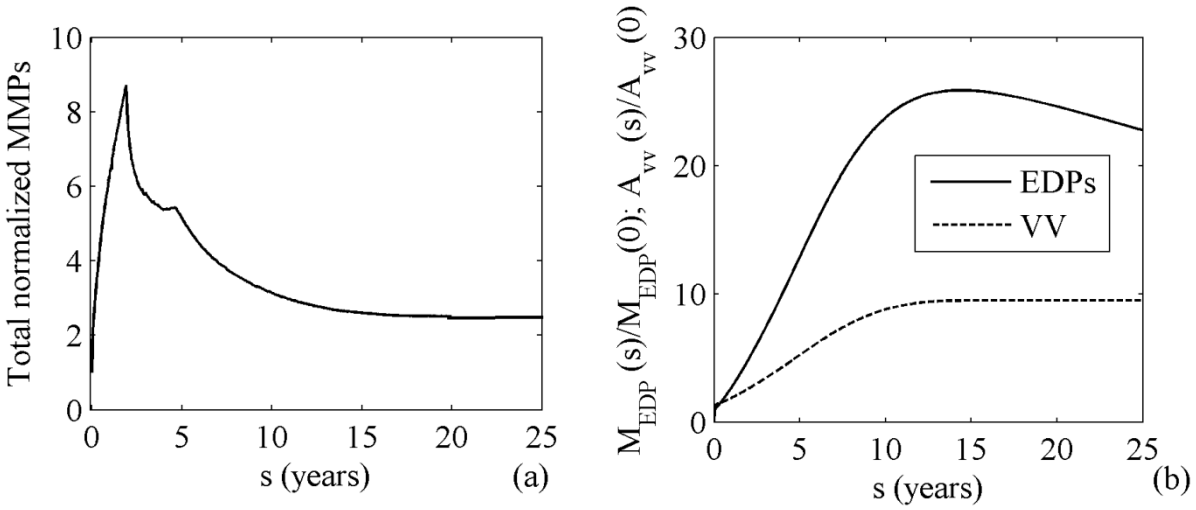

Figure 4.9: Evolution of the normalized net concentration of matrix metalloproteinases (MMPs) (a); growth of *vasa vasorum* and the mass of elastin degradation (b)

4.4.3. Composition of the aortic wall and ILT

The evolution of elastase in the wall was analogous to that of the general MMPs, leading to an initially rapid degradation of elastin that diminished as the thrombus thickened (Figure 4.10). The solid line represents elastin, the dashed line smooth muscle cells (SMC), and the dotted line collagen, all in the case of stiffening due to increased collagen accumulation.

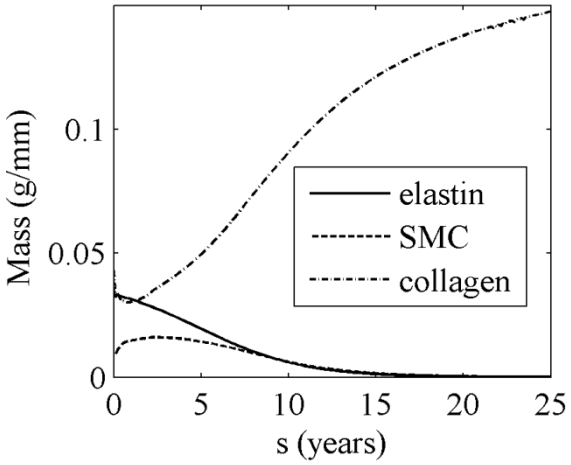

Figure 4.10: Evolution of total masses of the primary structural constituents of the wall, normalized per unit axial length

Likewise, the collagen decreased rapidly as the luminal layer formed, yet thickening of the thrombus and increased stress-mediated deposition yielded a net increase in collagen over time. Smooth muscle increased briefly as stress increased, but then declined as elastin was lost and anoikis occurred.

Distributions of constituents within the ILT at the end of simulation are shown in Figure 4.11. The solid black line represents fibrin, the dashed black line red blood cells (RBC), the gray solid line voids (canaliculi), and the gray dashed line fibrin degradation products (FDP). Note that luminal layer is easily distinguished, unlike the medial and abluminal layers (see Wilson et al.[84] for details on identifying different layers within ILT). Fresh thrombus at the luminal interface (i.e., near a radius of 9.925 mm) was characterized by low amounts of fibrin and large numbers of RBCs (recall that the volume fraction of platelets was neglected). In the deeper, more mature parts of the luminal layer, fibrin was increased and RBCs diminished. The border between the luminal and intermediate layer was evident by the steep decrease in RBCs as they could not penetrate farther into the thrombus. Similarly, platelets were unable to reach deeper parts of the ILT, wherein new fibrin production was impaired. As a result, the mass fraction of this fibrin decreased as its degradation exceeded production. The distinction between intermediate and abluminal layers was less evident; both were devoid of platelets and characterized by increasing fibrin degradation products (FDPs) and voids as the fibrin degraded. It is possible that development of an abluminal layer may be influenced by (a) a large deposition of initial thrombus with deeper regions that were not luminal long enough for the fibrin mesh to mature fully, (b) degradation of the clot from activated plasmin generated at

the ILT/wall interface, and/or (c) structural disruption of the thrombus that allows fresh blood into deeper layers – none of which were considered in this initial model. Nevertheless, these results correspond qualitatively to the reported distribution of constituents in four phases of an aging, layered ILT [8]: phase I (fresh thrombus, new luminal layer) was characterized by 90% RBCs and 10% thin fibrin bundles; phase II (older luminal layer) had less than 10% RBCs, some condensed proteins (FDPs), and increasing thin and thick fibrin fibers; phases III and IV (i.e., older thrombus) had few RBCs and condensed proteins dominated as fibrin degraded.

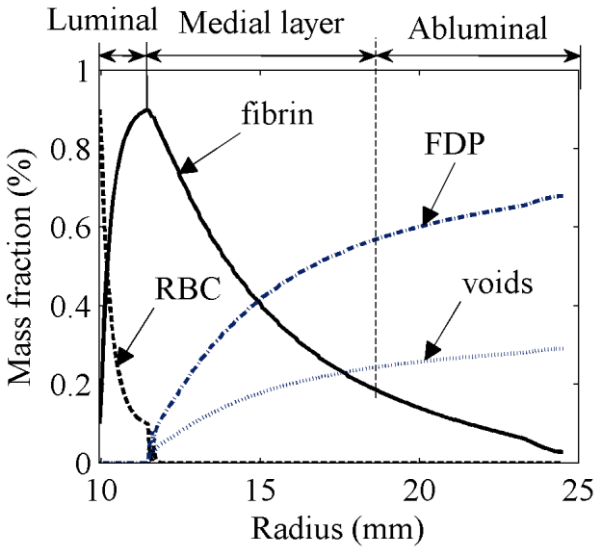

Figure 4.11 : Radial distribution of mass fractions of structurally important constituents at the time $s = 25$ years

4.4.4. Stress distribution.

To examine the mechanical influence of the ILT, radial stress and pressure (calculated as $-1/3\,\mathrm{tr}(\mathbf{t})$) were plotted versus depth through the thrombus and wall for one (long-term) instant during the evolution of the lesion and clot (Figure 4.12(a) and (b)). Note that the luminal and outer adventitial layers satisfy the prescribed traction boundary conditions. A prior clinical study [165] reported that the ratio of pressure (at end systole) within the thrombus to that within the flowing blood was 0.90±0.09, 0.86±0.10, and 0.81±0.09 at depths of 1, 2, and 3 cm, respectively. Figure 4.12 reveals that predicted reductions in pressure at depths of 1 and 1.5 cm (maximum thrombus depth in this simulation) were comparable, 0.94 and 0.93, respectively.

To evaluate the mechanical predictions of the model further, numerical equibiaxial tension tests of the aneurysmal wall underlying fresh and old thrombus were compared with experimental finding [8] (Figure 4.12(c)). Setup for experimental biaxial tension test can be seen in Figure 4.13. Abbreviations in the figure denote as follows: exp – experimental, sim – model simulation, circ – stresses in circumferential direction. It was found that the model and data shared two major features. First, the wall under fresh thrombus was more compliant when compared with that under older thrombus. Second, anisotropy of the wall increased with maturation of thrombus.

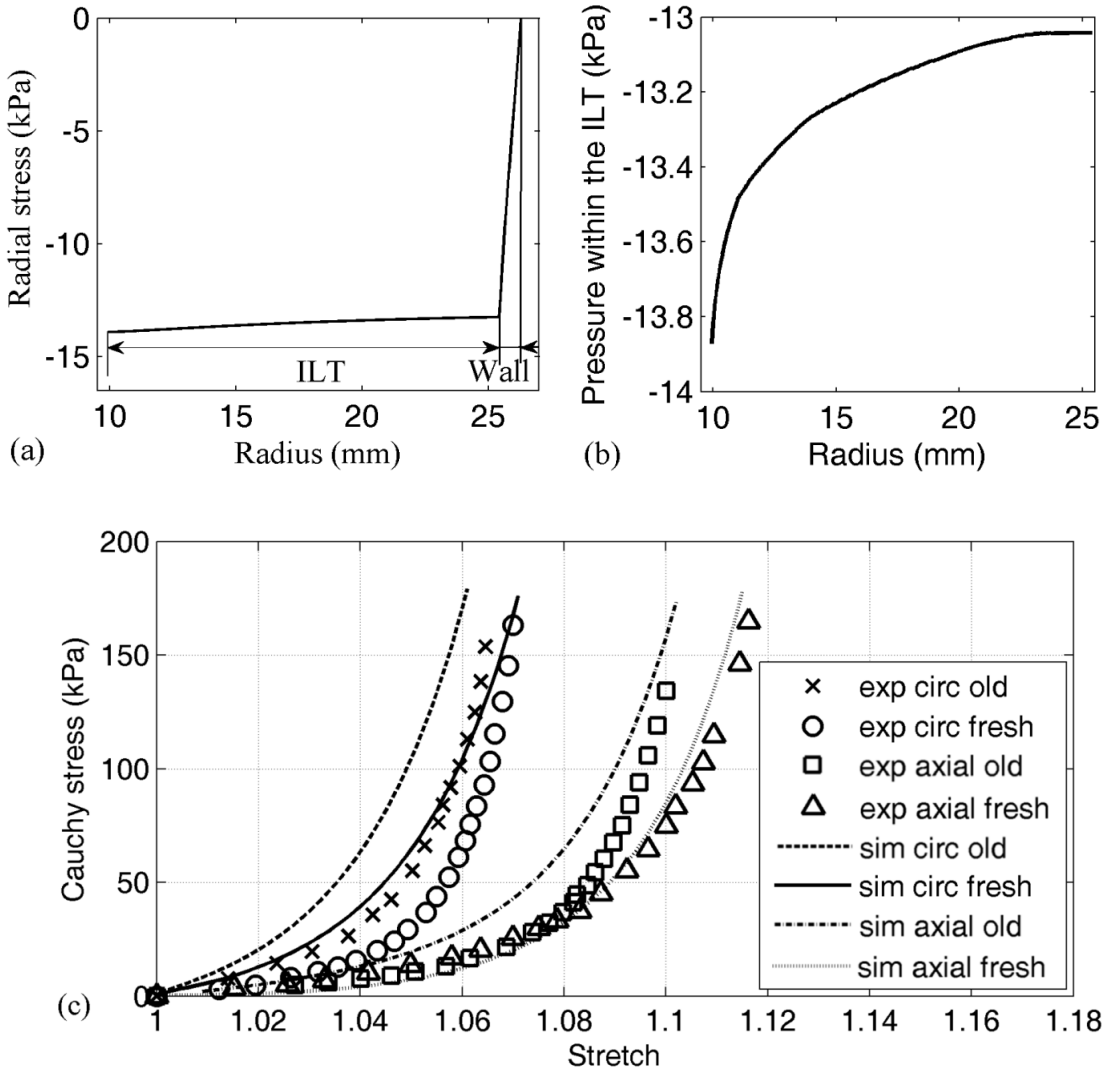

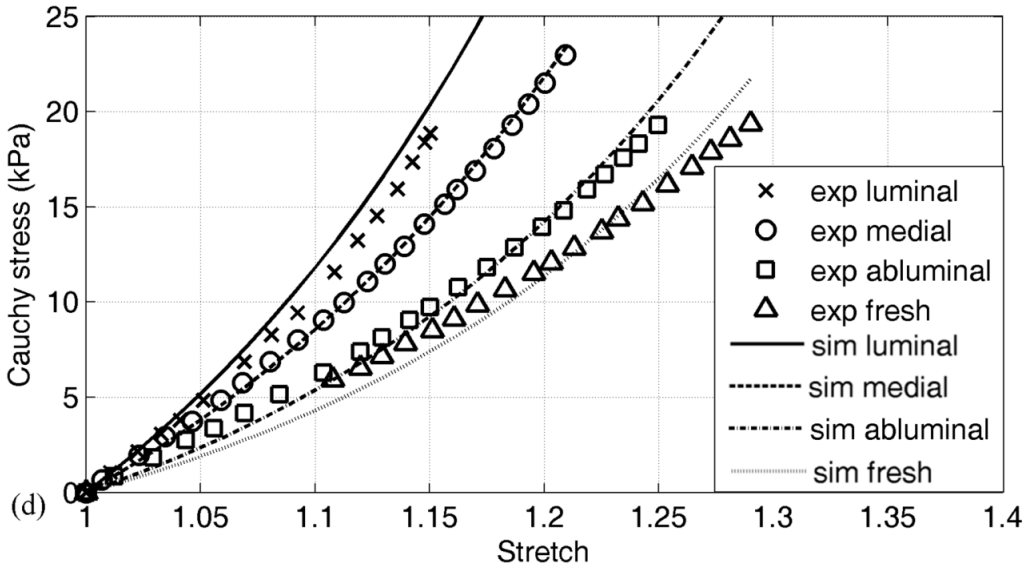

Figure 4.12: (a) Simulated transmural distribution of radial stress; (b) pressure throughout the intraluminal thrombus; (c) comparison of emergent equibiaxial tension results for the aortic wall; (d) equibiaxial tension tests on different layers of ILT

Note, therefore, that a numerical biaxial test of the initially non-aneurysmal aorta revealed an almost isotropic behavior due to the homeostatic definition: four families of collagen fibers oriented axially, circumferentially, and helically at ±45°, intact, isotropic elastin, and circumferentially oriented smooth muscle that was highly compliant.

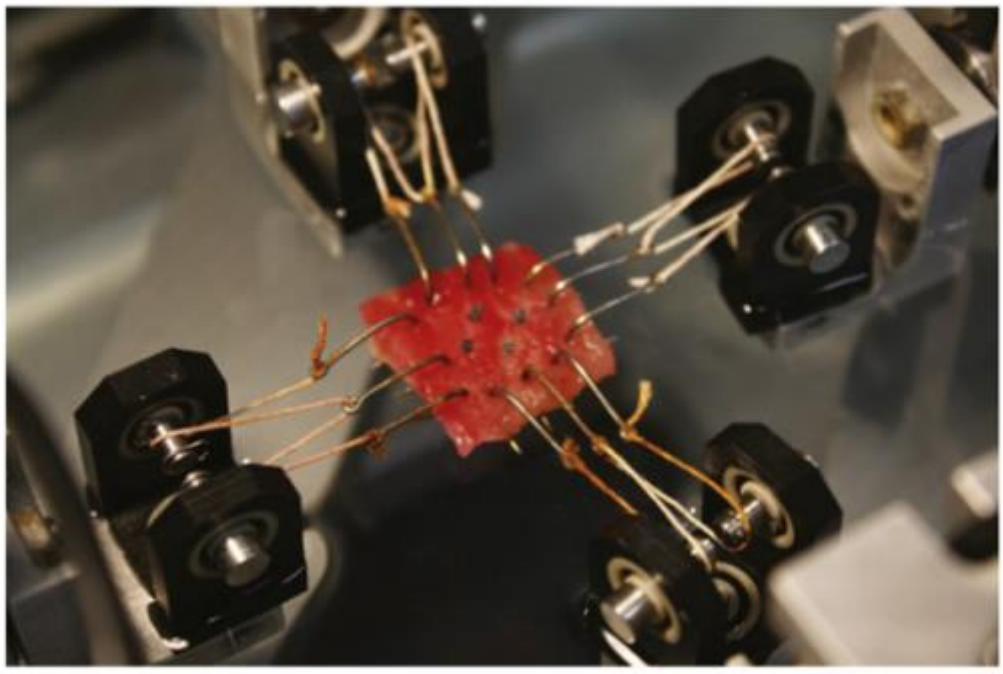

Figure 4.13: Specimen mounted in a biaxial tensile testing device, taken from [8]

Wall stiffening thus occurred due to the progressive loss of elastin and stiffening of collagen over time while anisotropy increased due to an active re-orientation of collagen fibers towards the circumferential direction. Although the experimental values represented average findings, not those obtained by following changes in one aneurysm over time as in this model, the overall agreement was nonetheless encouraging.

Comparison of numerical and experimental equibiaxial tension tests of fresh, luminal, medial, and abluminal thrombi (Figure 4.12(d)) also shows good agreement. The luminal layer is the stiffest and possesses the highest amount of the primary load-bearing material (fibrin); the mass fraction of fibrin (Figure 4.11), and thus stiffness, decreases in other layers.

4.4.5. Possible clinical outcomes

In prior G&R simulations of AAAs without thrombus, the effects of key aspects of collagen turnover on AAA progression were explored parametrically, including rates of production and values for the half-life, deposition stretch, and stiffness [73]. Similarly, three cases for collagen stiffness in AAAs herein were considered: loss of stiffness, constant stiffness, or increased stiffness. For simplicity, changes in stiffness relative to the homeostatic value and the ratio of the current to the initial stretch were modeled: $c_3^c(s) = c_3^c(0)\dfrac{\lambda^c(s)}{\lambda^c(0)}$ for stiffening, the inverse of this ratio for softening, and $\lambda^c(s) = \lambda^c(0)$ for maintenance in the healthy aorta (i.e., constant stiffness in maintenance). This model confirmed the prior results that a sufficiently high production can stabilize AAA enlargement in the absence of thrombus (results not shown). To consider the effect of increased ILT stiffness on lesion expansion, four cases were modeled with different fibrin properties (Figure 4.14). The black lines denote lesions with stiffer collagen and the gray lines baseline collagen properties. Moreover, the solid lines show results for stiffer ILT relative to the dashed lines which show results for more compliant ILT. Stiffer ILT was modeled using the upper limit of model parameters for the isotropic luminal layer determined in Tong et al. [8] ($\mu = 0.0099$ MPa, $k_1 = 0.016$ MPa, $k_2 = 0.9$); compliant ILT was modeled with the lower limit ($\mu = 0.0065$ MPa, $k_1 = 0.0086$ MPa, $k_2 = 0.3$). Each case was modeled with and without stiffening of collagen in the aortic wall.

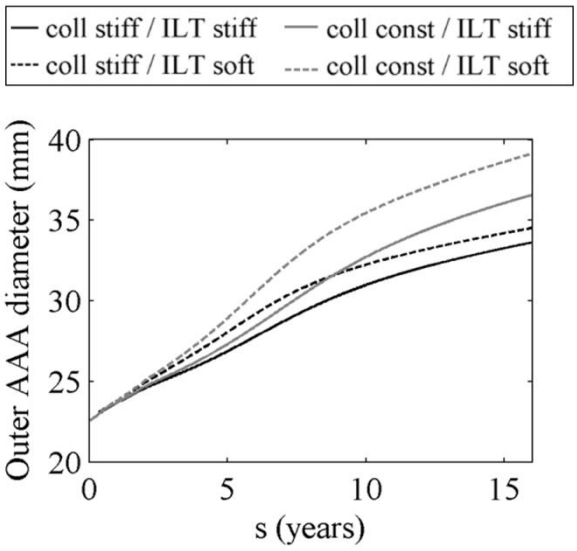

Figure 4.14: Simulated dilatation of AAAs having different mechanical properties of ILT

Results indicated that stiffening either the fibrin in the thrombus or the collagen in the aneurysmal wall reduced the diameter at which the AAA slowed its growth, with possible stabilization. That is, stiffening of collagen alone may not be necessary for ultimately arresting enlargement in thrombus-laden AAAs (at least for the range of parameters tested). Further simulations using more realistic geometries may prove useful to better explore the mechanical contribution of fibrin.

5. Modeling roles of rupture risk factors

One goal of computationally modelling aneurysmal G&R is to help clinicians predict rupture risk. Although multiple risk factors have been suggested for AAA rupture [166], a few key factors were considered within the limitations of the model. Herein, rupture was assumed to be possible when any normal component of wall stress reached 460 kPa [167]. It is worth noting that strength is heterogeneously distributed just like mechanical properties, and constitutive laws for the evolution of strength also need to be developed. These laws will also likely depend on a variety of parameters, e.g. age, sex, family history of rupture risk factors, etc. It is also worth noticing that computational models should be part of clinical procedure, yet clinicians should look for family history and all other parameters.

However, the point of this paper however is not to model strength or even to predict exact rupture times, but to investigate whether certain factors increase, decrease or not influence at all the likelihood of rupture. This is a qualitative study to determine how ILT influences growth of AAA and what makes rupture more or less likely. We do not claim certain aneurysm will rupture exactly at certain size. For illustrative purposes a simple metric has been chosen to predict possible higher risk of rupture. More sophisticated assessment of rupture potential should be used for patient-specific cases.

5.1. Smoking

Smoking has been linked to multiple vascular diseases. Among other effects, smoking elevates oxidative stress, compromises the arterial endothelium, and promotes atherogenesis [168]. It also promotes monocyte migration into the subintimal space, which promotes localized inflammation of the wall [169], and it increases the concentration of plasma fibrinogen and alters the activity of platelets, which together promote thrombosis on the dysfunctional endothelium [169]. Finally, smoking correlates strongly with increased aortic blood pressure, heart rate, and arterial stiffness [77], with smoking-induced stiffening appearing to be isotropic, as reflected by a consistent increase in an elastin-associated parameter and a marked increase in the collagen-associated parameters [170].

Many studies associate smoking with larger AAAs [79,171] and enlargement rates [172]. Some studies suggest that cessation of smoking may inhibit aneurysmal enlargement, even though two years of cessation does not reduce arterial stiffness [173]; indeed, it can take up to a decade to reduce stiffness to the level of never-smokers [78]. Similarly, five years of abstinence can reduce fibrinogen concentrations to the range of never-smokers [174].

Motivated by these studies, the natural histories of aneurysms in simulated smokers, ex-smokers, and those who had never smoked were investigated. Smoking was modelled by an increased elastin stiffness, collagen stiffness, inflammation, and platelet activity. Parameter values that differ between simulations are shown in Table 5. Endothelial and smooth muscle cell dysfunction are characteristic of aneurysms independent of smoking and were implicitly included in the model for both smokers and non-smokers.

Simulated AAA diameter was greater at 20 years for smokers (4,96 cm) than non-smokers (4.09 cm), with an associated mean dilatation rate 0.043 cm/year greater than that for non-smokers. Figure 5.1 shows evolution of a non-smoker (solid black line), increased elastin stiffness (dashed line), both increased elastin stiffness and inflammation (dash-dotted line), an increased elastin and collagen stiffness plus elevated inflammation (dotted line), and an increased stiffness, higher inflammation, and increased platelet activity (solid grey line) – that is, full effects of smoking. These results are consistent with clinical observations. Bhak et al. [79] reported that smoking associated with a 0.05±0.01 cm/year increase in linear enlargement rate. These results suggest further that increased stiffness is a key factor that leads to large aneurysms in smokers (Figure 5.1).

Table 5: Parameters for non-smokers and smokers: c_1^e, c_2^c and c_3^c are parameters in the stored energy functions for elastic and collagenous fibers (cf. [170]).

	c_1^e [kPa]	c_2^c [kPa]	c_3^c [-]	$w_{q,\mathrm{MMP}}^c$ [g^{-1} day^{-1}]	$w_{q,elas}^e$ [g^{-1} day^{-1}]	M_l^{plt} [g mm^{-1}]
Non-smokers	74.6	498.2	22	10	60	0.15
Smokers	148.7	861.3	44	20	120	0.2

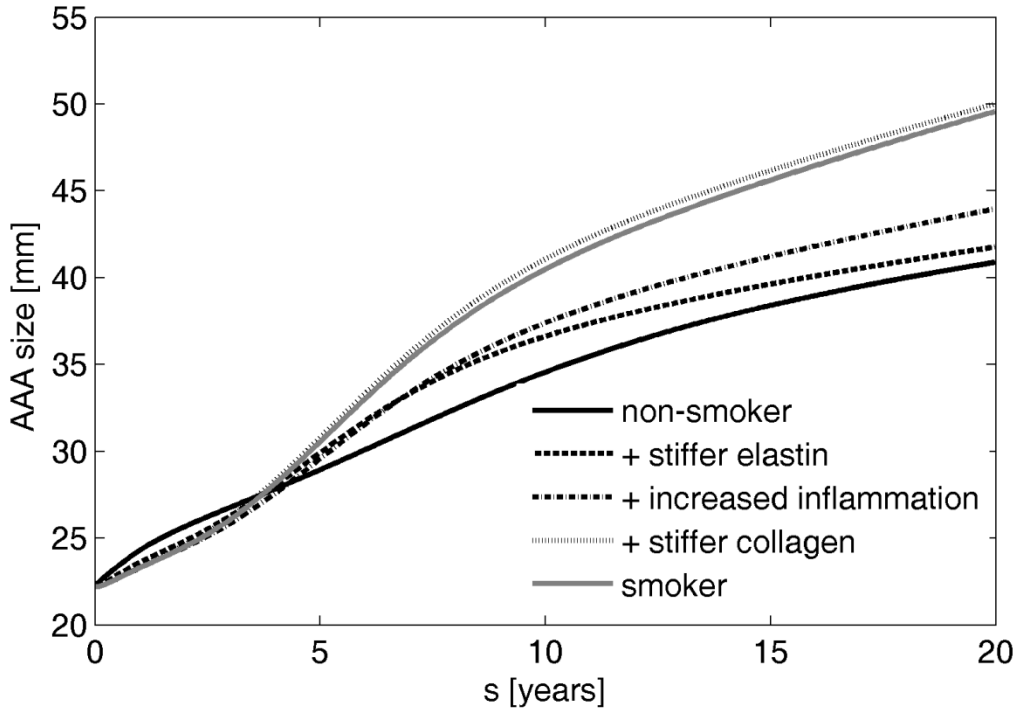

Figure 5.1: Simulated evolution of AAAs in a non-smoker, cases of different effects of smoking on the aortic wall, and full effects of smoking

There was only a slight decrease in AAA size due to increased production of fibrin through a higher platelet activity, which resulted in a slightly stiffer but thinner luminal layer. Note that this finding does not mean that increased platelet activity could potentially stabilize AAAs since platelets are chemotactic for neutrophils and monocytes [175] and can cause higher inflammation and enlargement rates.

Changes in rates of dilatation after smoking cessation have not been studied well. As it has been shown that stiffness is reduced only after 10 years [78], an immediate decrease in enlargement rate would not be expected. Rather, the competing effects to evolve after several years would be expected: a reduced growth due to attenuated rates of elastin degradation but increased enlargement due to a decrease in collagen stiffness. Thus, consistent with general public health guidelines, immediate cessation of smoking is recommended, preferably before AAA development.

5.2. Aneurysm stabilization factors

Numerous studies have proposed the use of anti-inflammatory drugs for reducing or arresting the enlargement of AAAs, some of which act directly on MMPs [176,177] while

others reduce inflammation indirectly (e.g., via platelet inhibitors [178] or immunosuppressive agents [179]). For example, one study in mice showed that preserving medial elastin can attenuate aneurysmal dilatation [176] while another study in mice showed that non-specific inhibition of collagenases can led to lesion stabilization [177]. Nevertheless, non-specific MMP inhibition has not reduced aneurysmal progression in human patients [180]. Clearly, there is a need for increased understanding of the biochemical mechanisms of aneurysm formation and evolution.

Figure 5.2 shows that the thrombus-laden aneurysm model supports results from [176], whereby inhibition of elastase activity (i.e., decreasing the degradation of elastin, $w^e_{q,elas} = 10$ 1/(g day) vs. $w^e_{q,elas} = 30$ 1/(g day)) helped to decrease the likelihood of rupture and to some extent led towards stabilization, independent of collagen stiffness. In the figure simulated evolution of rapid elastin degradation are presented with solid lines versus dashed lines for normal elastin degradation. Note that the aneurysm was initiated by degrading 5% of elastin (Figure 5.2(b)). Maximum wall stresses $\|\mathbf{t}\|_{\max}$ (black lines) and decrease of elastin stress $\left\|\mathbf{t}^e\right\|_{\max}$ (grey lines) due to elastin damage after a stretch of 2.2 can be seen in Figure 5.2(c).

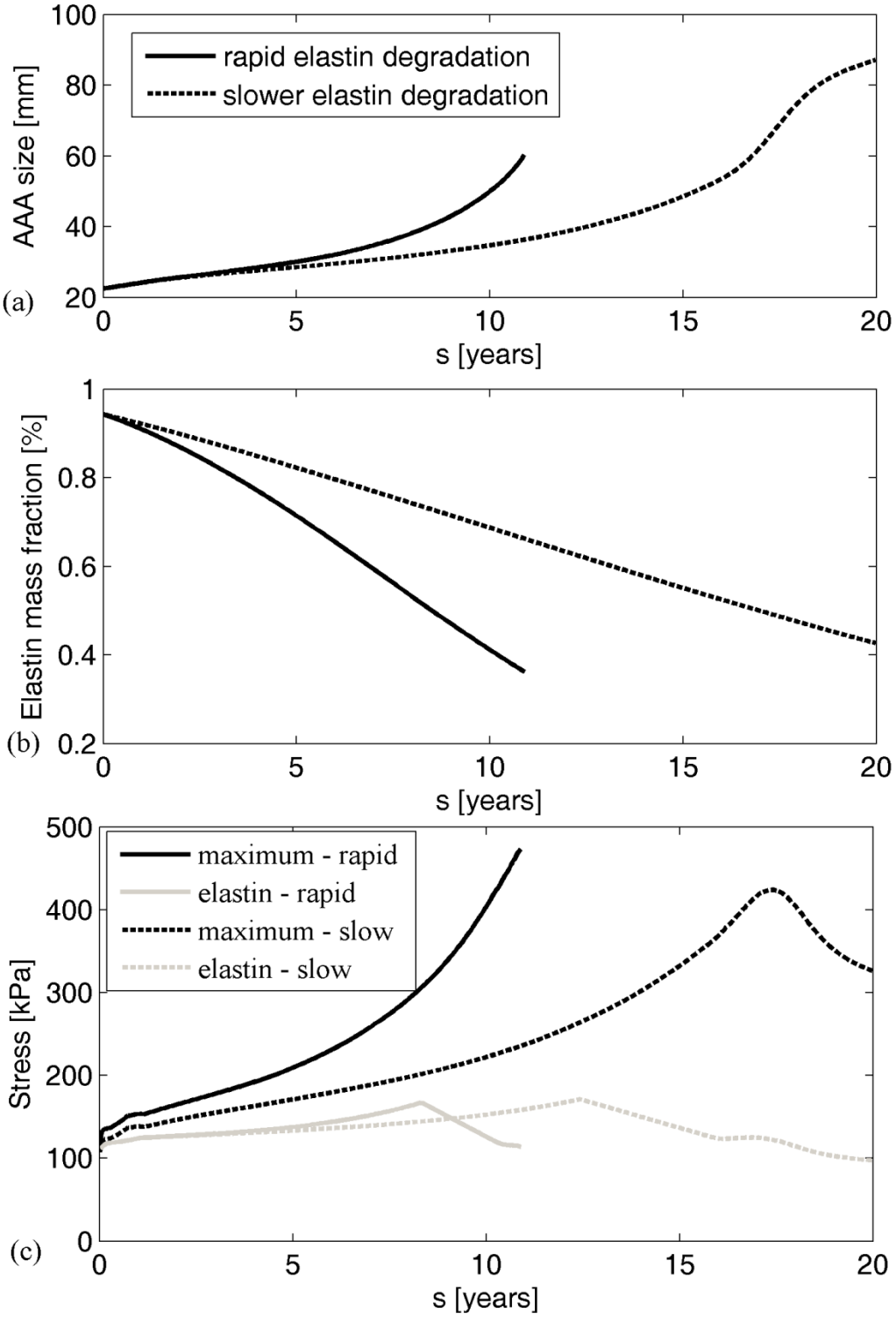

Figure 5.2: Simulated AAA evolution (a), corresponding degradation of elastin (b) and evolution of maximum wall stresses and elastin stresses (c) in cases of rapid and normal elastin degradation

The current model similarly suggests that high rates of collagen degradation ($w^c_{q,\mathrm{MMP}} = 20\ \mathrm{g}^{-1}\ \mathrm{day}^{-1}$) could lead to progressive enlargement (solid line in Figure 5.3) while reduced inflammation ($w^c_{q,\mathrm{MMP}} = 10\ \mathrm{g}^{-1}\ \mathrm{day}^{-1}$) could prevent rupture despite continued enlargement (dashed line in Figure 5.3). Thus, the current results suggest that rates of degradation of structural constituents (e.g., concentrations of proteases, controlled by parameters $w^e_{q,elas}$ and $w^c_{q,MMP}$ in Eq. (42) and (43)) should indeed affect aneurysmal progression. Note that stiffening was modelled in these simulations by changing the exponential parameter for collagen in the stored energy function relative to the homeostatic value and the ratio of the current to the initial stretch (i.e., $c^c_3(s) = c^c_3(0)\,\lambda^c(s)/\lambda^c(0)$).

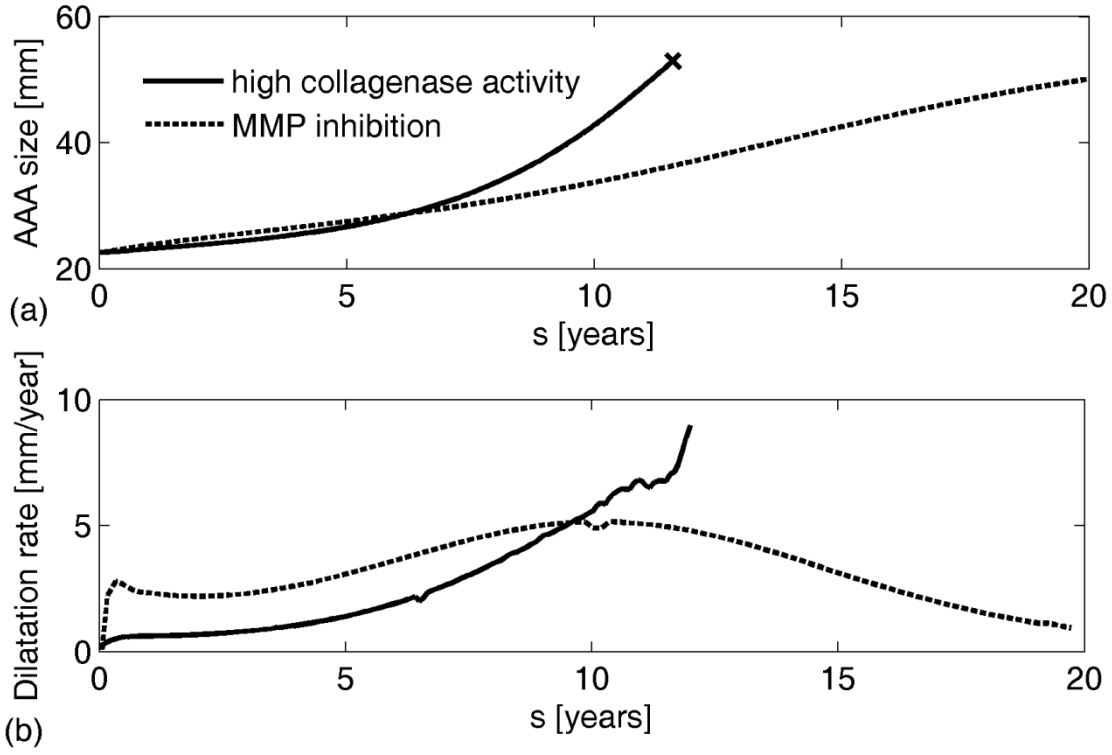

Figure 5.3: Simulated AAA evolution (a), with associated dilatation rates (b), for different rates of collagen degradation in the case of collagen stiffening. "x" denotes expected rupture

5.3. Effects of sex and age

Sex differences have been identified in cardiovascular aging and in the evolution, management, and response to treatment of many cardiovascular diseases, including AAAs [181]. For example, females have stiffer large arteries pre-puberty, but more compliant ones post-puberty [182]. Additionally, age-associated endothelial function declines in men years

before women [183]. These findings, among many others, could contribute to the increased prevalence of AAAs in men compared to women [184]. Yet, males have a 3-4 times lower risk of rupture than females [181], possibly due to higher strength of the AAA wall [4]. Similarly, noting that males have stiffer arteries on average [185], previous G&R models suggested that increased material stiffness and turnover of collagen decreases the likelihood of rupture, [73].

Beyond the effects of sex, age may also play a role in AAA progression. Wilson et al. [43] demonstrated in a G&R model that aortic properties at the age of lesion initiation may strongly influence AAA progression. Such properties likely depend on a patient's biological age (e.g., genetics, smoking status, comorbidities, and exercise) as opposed to simply a chronological age. For example, the observation that females who undergo open surgical repair for AAA are significantly older compared to males [185] may be reflective of their "younger" biological status as suggested by their later decline of endothelial function. Thus, differences in AAA enlargement in males and females were explored by prescribing different values of collagen stiffness (increasing collagen stiffness in males, but consistent stiffness in females) and different initial aortic microstructures. Initiation of an aneurysm at a younger age, typically in men, was taken into account by higher amounts of elastin and a thinner intima. Additionally, assuming equivalent elastin material properties, elastin in younger patients is less pre-stretched compared to the remaining elastin in older patients due to the slow increase in diameter with age and the lack of elastin turnover. Values of parameters that differ among simulations are presented in Table 6.

Table 6: Parameters for younger and older patients: ϕ_{int} and ϕ_{med} are volume fractions of intima and media, respectively; G_e is the initial pre-stretch of elastin; ϕ_e is the initial volume fraction of elastin in aortic wall.

	ϕ_{int} [%]	ϕ_{med} [%]	G_e [-]	c_1^{e} [kPa]	ϕ_e [%]
Young	4	80	1.3	87.8	33.6
Old	16	52	1.4	74.6	27.4

Inducing aneurysms in an initially stiffer aortic wall led to lower enlargement rates, with less likelihood of rupture (Figure 5.4). Expected rupture was denoted with "x" marker. With regards to age, a younger aortic wall was more compliant and experienced greater dilatation

(whether ruptured or unruptured). It also had greater amounts of elastin, the preservation of which may help prevent rupture (see section 5.2). Therefore, the biological age at which an aneurysm develops likely has an important impact on AAA evolution, and might be an additional factor contributing to the high rupture risk in females.

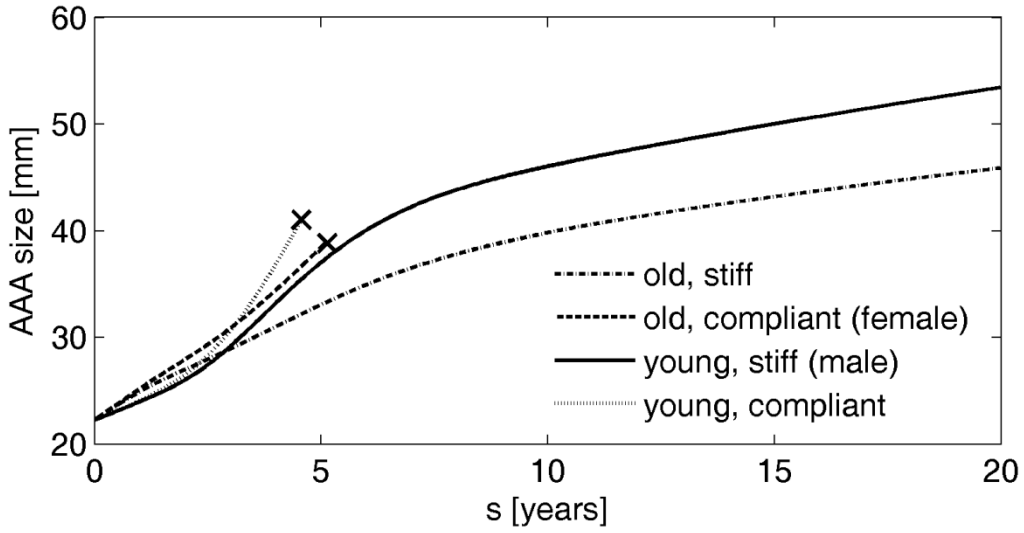

Figure 5.4: Simulated evolution of AAAs for males and females of varying age.

5.4. Hypertension

Hypertension is thought to be a key factor in AAA enlargement [79] and rupture-risk, particularly in aneurysms smaller than 5.5 cm [186]. Hypertension leads to progressive changes in vascular structure, function, and material properties that often manifest grossly as increased wall thickness, radial dilatation, and axial lengthening [5], all of which are G&R responses. To evaluate possible effects of hypertension on AAA progression, two cases are considered: patients who were hypertensive before developing an AAA and patients who developed hypertension during the progression of the lesion. In the former, firstly the G&R of a hypertensive (but non-aneurysmal) aorta was simulated and used as the initial state in which the aneurysm developed. Results suggested that aneurysms originating from a hypertensive wall tend either to rupture or to stabilize at smaller sizes (Figure 5.5(a)), depending on the properties of collagen. In the figure solid lines represent enlargement for constant collagen material properties; dashed lines represent enlargement during collagen stiffening; dash-dotted lines represent enlargement of normotensive aneurysm with constant collagen properties; dotted lines represent enlargement of normotensive aneurysm with collagen

stiffening. 'x' denotes expected rupture. Furthermore, the results suggested that lack of treatment of hypertension before aneurysmal development might increase the likelihood of rupture, since the aneurysms modelled as normotensive but with otherwise the same G&R parameters showed a tendency towards stabilization, not rupture.

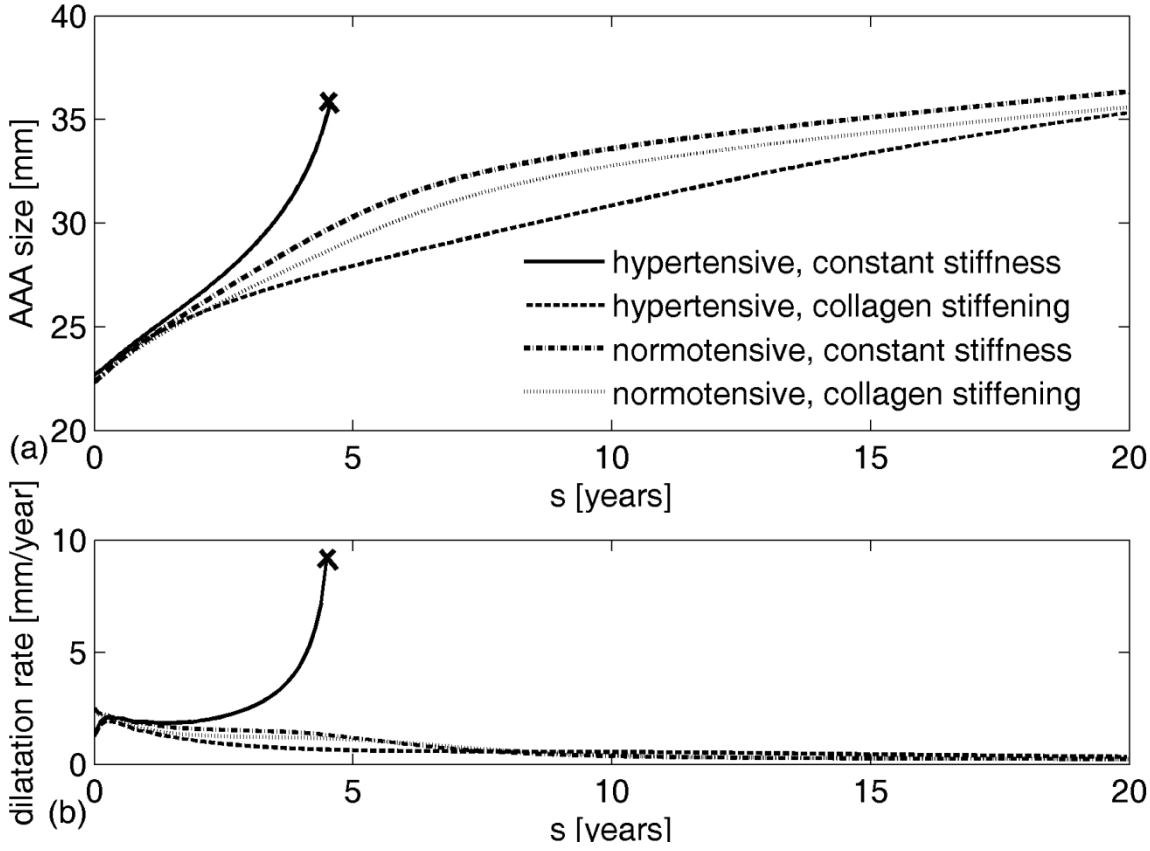

Figure 5.5: Evolution of AAA diameter (a) and enlargement rate (b) from an initially hypertensive aorta

When hypertension developed during aneurysmal progression, the increased luminal load increased the inner radius further which changed the wall stresses that drive much of the G&R. Three degrees of hypertension [187] defined as increases in mean arterial pressure of 40% (36 mmHg), 60% (54 mmHg), and 80% (72 mmHg) as Cases 1, 2, and 3, respectively, are considered. As expected, a greater increase in blood pressure resulted in a larger evolving diameter. Figure 5.6 shows evolution of AAAs arising from a heathy aorta after either retaining normal blood pressure (solid) or spontaneously developing increased blood pressure to different degrees: stage 1 (dashed), 2 (dash-dotted), or 3 (dotted). The average increase in enlargement rate of a hypertensive aneurysm over 15 years was 0.235, 0.228 and 0.221 mm/year per 10 mmHg increase (i.e., stages 1, 2 and 3, respectively). These values are in

good agreement with clinical observations of 0.02 ±0.01 cm/year per 10 mmHg [79]. Interestingly, the present computational results also suggested that a later development of hypertension is more likely to lead to rupture even though earlier hypertension may lead to larger AAAs Figure 5.7(a)). This finding highlights the importance of G&R compensation for it is not strictly the diameter that determines rupture, but rather the failure of the cells to adequately respond to a perturbation (i.e., dilatation need not imply an improper response). In this case, a relatively healthier wall (i.e., earlier in AAA development) was better able to compensate for a higher blood pressure than was a wall exposed to the same pressure after being more extensively damaged via the AAA progression, as seen from evolution of stresses (Figure 5.7(b)).

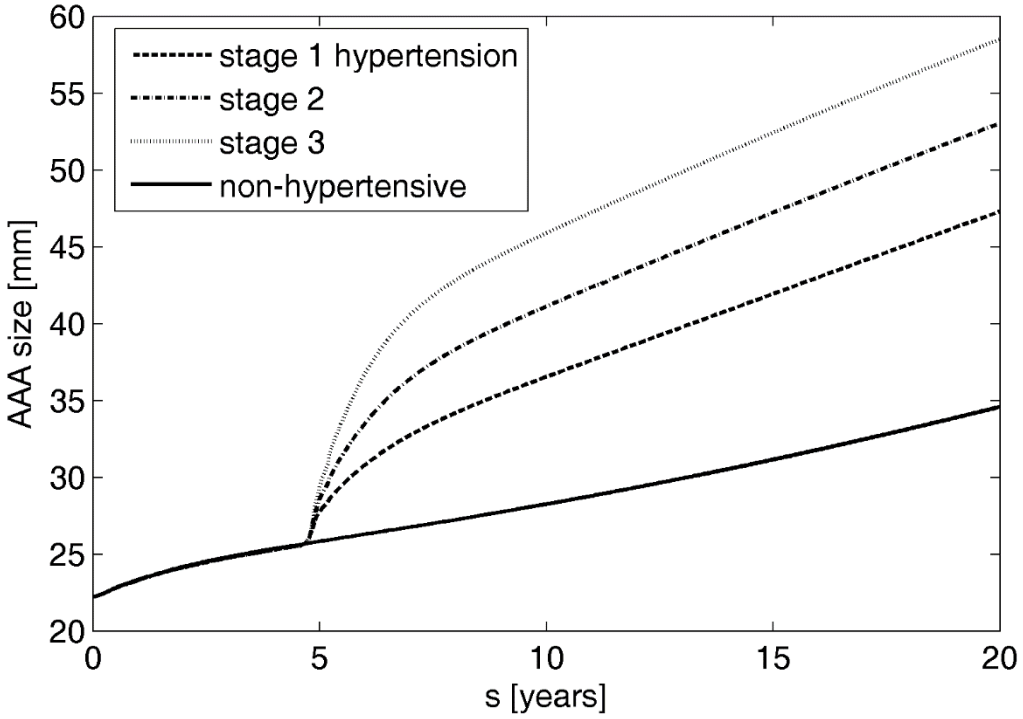

Figure 5.6: Evolution of AAAs arising from a heathy aorta after either retaining normal blood pressure or spontaneously developing different stages of hypertension

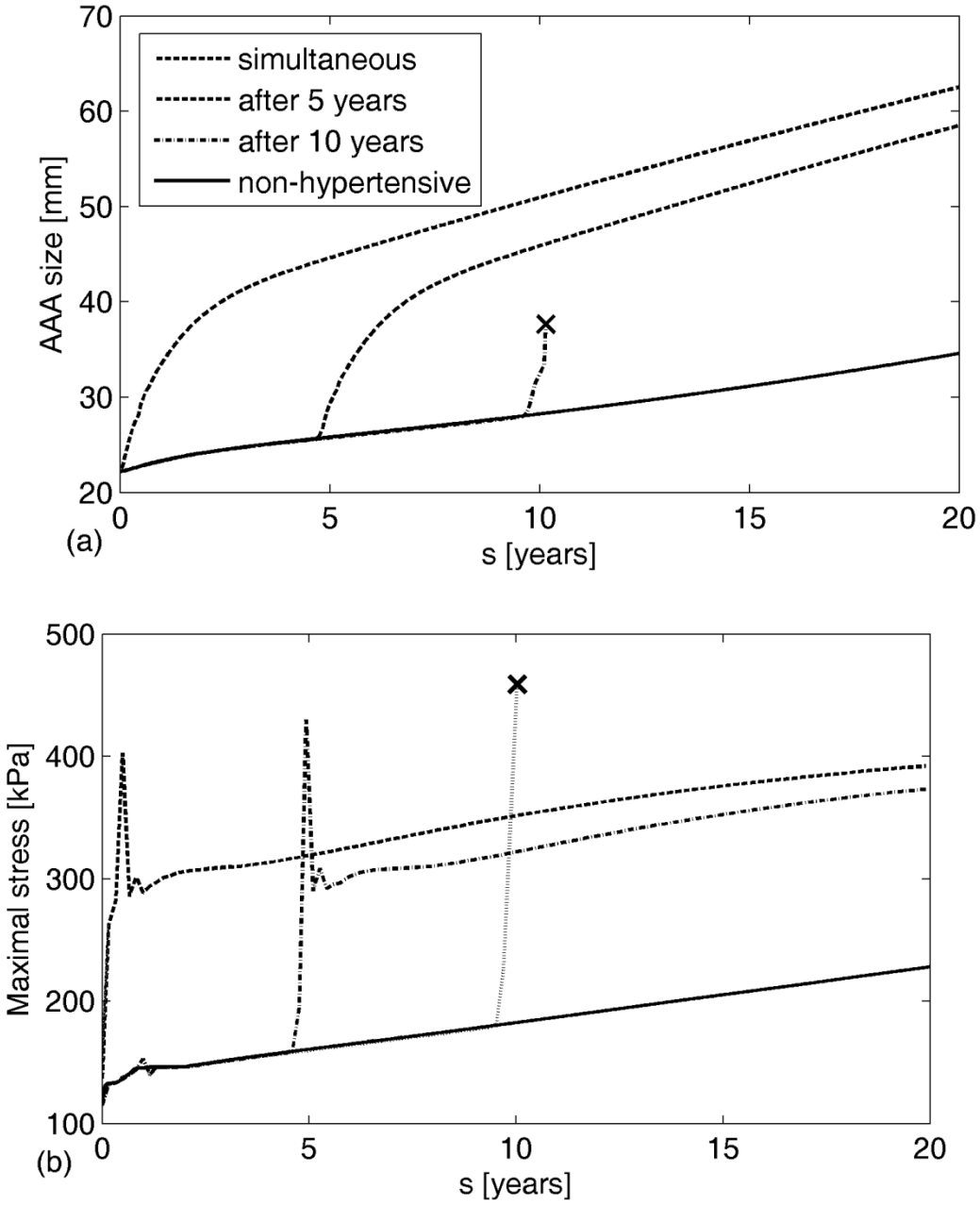

Figure 5.7: Evolution of AAAs from an initially normotensive aorta following the development of stage 3 hypertension at different times during AAA progression (a), and evolution of corresponding maximal stresses (b). "x" denotes expected rupture

5.5. Thickness of intraluminal thrombus

Another potential risk factor that has garnered increased attention is the size of the ILT. Different measures of ILT size, including thickness [74], volume [188], and relative cross-sectional area [171], have been correlated with rapid enlargement or rupture. Yet other studies suggest that ILT volume is the same in ruptured and intact AAAs [189], and case reports of unruptured giant thrombus-laden aneurysms (e.g., 25 cm in [190]) have been described.

Because of the cylindrical geometry and concentric thrombus used herein, ILT thickness, area, and volume are all a direct function of AAA diameter, and therefore, differential effects of these metrics of ILT size could not be evaluated. Nevertheless, it should be noted that the distribution of proteases (M^{elas} for elastase and M^{MMP} for collagenases) in this 1D model depends on both the available proteases from each source (luminal layer of the ILT and *vasa vasorum* in the aortic wall) and the distance between the two sources; hence, it is proportional to ILT thickness.

The amount of available proteases in the luminal layer varies significantly among patients, from virtually non-existent to very high (e.g., see measured MMP-9 activity in both thrombus and wall specimens from 35 patients in Figure 3 in [10]). Thus, the possible evolution of an AAA for different degrees of protease activity in the ILT (by increasing $K_N^k M_{tot}^N(s)$ in Eq. (46)) is investigated. Figure 5.8 shows differences in predicted AAA enlargement in cases wherein the ILT and *vasa vasorum* have equal proteolytic activity ((a)-(d)) ($K_N^{MMP} = 10\ \mathrm{g}_{MMP}\ \mathrm{g}_N^{-1}$) or the ILT is much more proteolytically active ((e)-(h)) ($K_N^{MMP} = 1000\ \mathrm{g}_{MMP}\ \mathrm{g}_N^{-1}$). In the latter case, the proteolytic activity in the wall increased sharply as long as the luminal layer was directly attached to the aneurysmal wall (i.e., while the solid and dashed lines in Figure 5.8(a) coincide), thus resulting in rapid enlargement of the aneurysm. Note that peak of expansion rate of 5 mm/year (Figure 5.8(g)) lasts very shortly, and is calculated for every time step; if aneurysms was followed every 6-12 month, average dilatation rate would have been much lower, around 3 mm/year. Although *on average* this might still be too rapid expansion, the parameters are not set to simulate average aneurysm, but one with very high proteolytic activity. As study in [191] showed in Tables II and III, 12% of aneurysms 3-3.4 cm in diameter expand to 4 cm in less than two years, meaning their expansion rate is at least 3mm/year (growing at least 0.6 cm in less than 2 years). Even more interestingly, 3% grew to from 3-3.4 cm to 5 cm in less than 2 years, having expansion rate more than 0.8 cm/year! Therefore, it can be concluded that simulated 3-5 mm/year expansion is indeed above average, but by no means unphysical.

As less proteolytically active deeper layers formed and acted as a barrier to protease diffusion, proteolytic activity decreased abruptly and the enlargement rate declined (Figure 5.8(c) and (g)). Note that elevated activity in the luminal layer led to a reduction in enlargement rate once the luminal layer was displaced from the wall, even causing a near cessation of enlargement temporarily (Figure 5.8(e)).

Several studies (e.g., [21]) report that the majority of AAAs dilate discontinuously, with periods of enlargement alternating with periods of quiescence. Though the precise causes of this phenomenon have not been determined, the current results suggest that ILT, specifically altering the proximity of the biologically active luminal layer to the wall, may directly influence enlargement rates and thus play a role in determining clinical outcomes. Although only one cycle of enlargement and arrest is allowed in this axisymmetric cylindrical geometry, extending this model to 3D patient-specific geometries will allow further testing of the relationship of ILT, discontinuous enlargement, and patient-specific outcomes by exploring more complex enlargement patterns due to eccentric deposition of thrombus (i.e., where one portion of the ILT remains thinner than the other), non-continuous deposition of thrombus, local bulging, and multiple regions where the wall is adjacent to thin thrombus throughout AAA development.

For both levels of activity within the luminal layer, a second peak of MMP activity and enlargement rate was observed due to the increase in proteases from a developing *vasa vasorum*, driven (in this model) by elastin degradation products. Interestingly, this second MMP peak is greater in the model with a lower luminal activity even though the enlargement rate is lower, perhaps due to the more consistent release of EDPs from the slower elastin degradation occurring in the case of lower luminal activity.

As expected, note from Figure 5.8(a) and (e) that the simulated AAA was larger after 20 years in the case of high proteolytic activity (5.5 cm vs. 4.5 cm in outer diameter). Yet, there is little indication that thrombus thickness increases the likelihood of AAA rupture, as seen from simulations in previous sections where expected ruptures occurred in both small and large aneurysms while some large simulated aneurysms (9 cm) remained stable. Further finite element analyses are warranted for confirmation, but it should not be expected that ILT thickness or other simple measures of ILT size to enable rupture predictions directly.

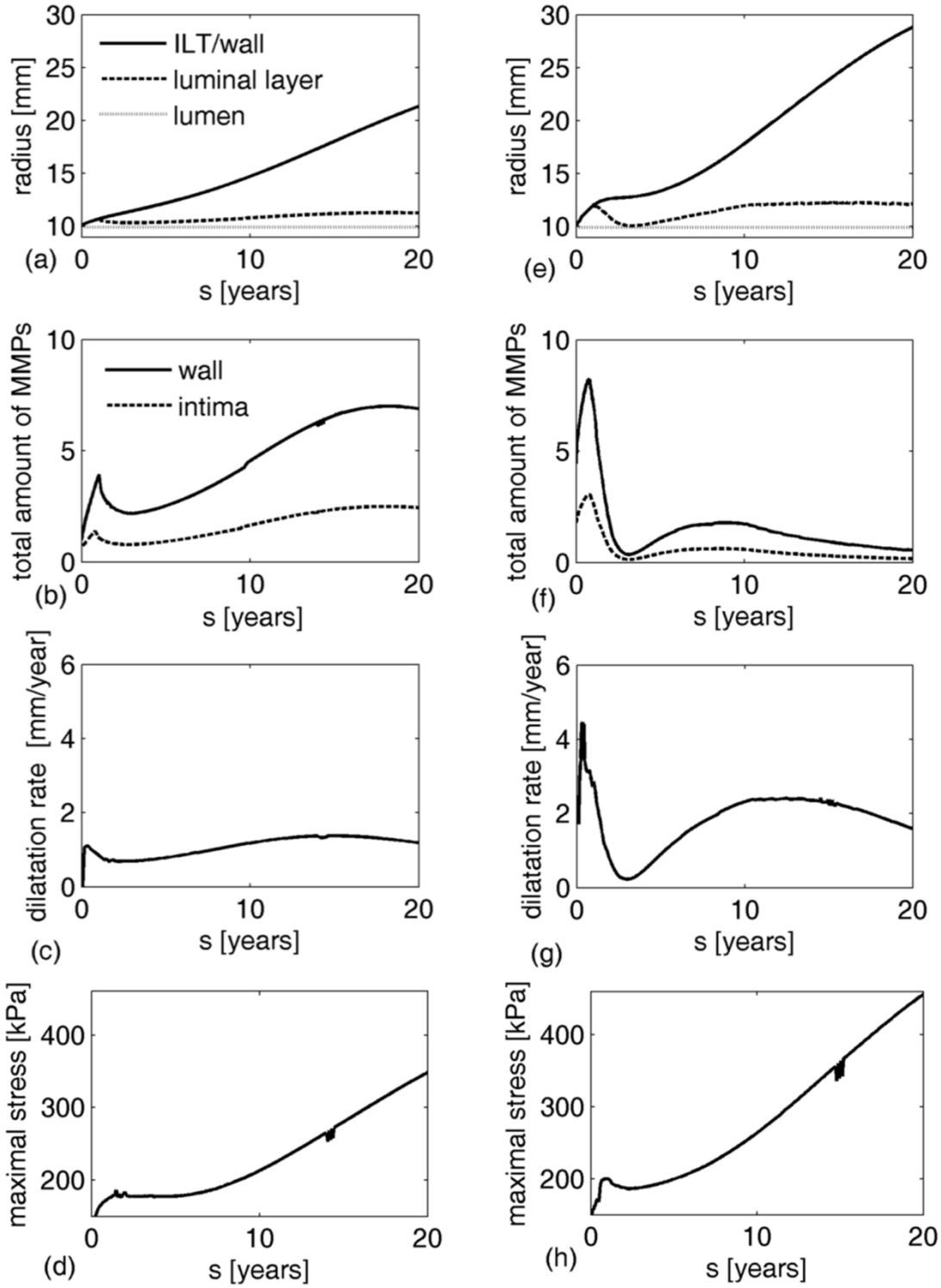

Figure 5.8: Evolution of radius, MMPs, and enlargement rate for AAAs with low proteolytic activity in the luminal layer of ILT (a-d) versus high proteolytic activity (e-h). (a,e) Evolution of radius at the ILT/wall interface (solid line), lumen/luminal layer interface (dotted line) and luminal layer/wall (for thin ILTs) or luminal/medial layer interface (when medial layer of thrombus is developed) (dashed line). (b,f) Evolution of the normalized total amount of

MMPs in the wall (solid line) and intima (dashed line). (c,g) Evolution of AAA enlargement rate. (d,h) Evolution of maximal stresses in aortic wall

5.6. Limitations and proposed experiments

The current model was developed using a cylindrical geometry to focus on the importance of different constitutive assumptions and ranges of parameter values before introducing complex geometric effects that arise with local, eccentric aneurysmal dilatation. Although patient-specific models must be considered in future studies, including fluid-solid-growth (FSG) simulations, the current simple geometric model yet yielded general insights into both the important roles that ILT may play during the evolution of AAAs and the potential roles of diverse risk and stabilization factors. Given this new insight, attention should now focus on the collection of data that will render complex simulations meaningful. For example, most prior experimental findings focus solely on the radial direction for both the thrombus and AAA wall; thus, molecular distributions and heterogeneities in mechanical properties are virtually unknown in axial and circumferential directions. Full 4-D information (radial, circumferential, and axial distributions of structural constituents and biomolecules at multiple times during lesion evolution) will thus be needed to create realistic patient-specific models including the biochemomechanics associated with ILT.

Another potential limitation of the current model is the assumption that luminal area remains constant and concentric throughout the G&R process. Some clinical observations support this assumption of constant luminal diameter in thrombus-laden aneurysms (e.g., [164]), but this is not universal, especially in smaller lesions. Non-uniform thrombus deposition is undoubtedly related to the complex evolving hemodynamics [23,164], which can vary depending on the location, size, and shape of the lesion. Future studies should explore the added complexities of incorporating a hemodynamically driven evolution of thrombus deposition within a FSG model. With such a 4D model, the G&R effects of eccentric thrombus deposition and potential internal dissection of thrombus could be explored.

Additional simplifications of our model include neglect of convection-mediated transport of biomolecules through both the thrombus and wall, which could affect the morphology of the thrombus [68]. There is similarly a need to refine the constitutive relations for the production of these biomolecules. For example, the activation of plasmin or MMPs (e.g., by tPA and uPA or plasmin, respectively) was not modeled explicitly, and neither was their inhibition (e.g., PAI or TIMP). For MMPs, this modelling is even more complex for the different sub-types (e.g., MMP1 vs. MMP2, and so forth) should be derived separately. In

order to avoid a number of additional assumptions and associated parameters, and due to the lack of spatiotemporal experimental data, plasmin and MMP distributions were modeled phenomenologically.

Notwithstanding the use of phenomenological relations to reduce the complexity of the modelling, this introduces numerous parameters, some of which are difficult to determine directly from experiments. Fortunately, however, the vast majority of the requisite parameters could be estimated indirectly from experimental observations: parameters describing growth of *vasa vasorum* (Eq. (36)) were based on data in [15] that showed an approximately 7-10 fold increase in the neovascularized proportion of the aortic wall from healthy to large aneurysmal (Fig. 2C); the initial area of neovascularization was inferred from [74] (around 0.2% of initial area). Vorp et al. showed similar results for increases in the percent area of inflammatory cells [74]. Parameter K_{EDP}^{VV} in Eq. (36) was calibrated to fit the given bound. In the absence of human data, weighing factors in equations (42) and (43) were based on animal models. Experiments on elastase-induced aneurysms in rats showed that elastolytic activity was significantly elevated within the aortic wall of animals perfused with thioglycollate plus plasmin 9 days after perfusion (207.6± 54.8 μg elastin-rhodamine lysed/18 hr; control rats, 25.43±11.13) [75]. Similarly, an approximately 50-fold increase in type 1 collagen degradation products has been observed in aneurysms compared to controls [76], assumingly over 20-30 years. The calculated values of weighting factors for elastase and collagenase were similar, as they should be, considering their physical meaning is the amount of protein degraded per unit of protease per time. Several studies ([136,192–194]) provided insight into realistic ranges of increased inflammation, and helped us bound the parameters defining increases in inflammation (i.e., production of leukocytes). Many of the remaining equations are well-known and frequently used as G&R constitutive relations. Because some of the parameters have been shown to vary significantly among patients (e.g., proteolytic activity in the luminal layer [10]), the stated range was explored parametrically. A full parameter sensitivity study would also be useful, but was beyond the present scope given our focus on the first examination of potential effects of common risk factors.

In summary, further refinement of the model in terms of both identifying relevant pathophysiological ranges of parameters and the means to assess more exact values for patient-specific models can and should proceed as the necessary experimental and clinical data become available. As outlined in the review [84], there is a pressing need for better quantification of:

- Biomolecular kinetics – identify cellular sources of relevant biomolecules (e.g., plasmin, MMPs, and inflammatory chemokines and cytokines), including rates of production/degradation, activation / inhibition, and convection / diffusion, as well as their evolving circumferential and axial distributions.
- Stress-strain relations motivated by microstructure – quantify the nonlinear heterogeneously distributed mechanical properties of the multi-layered ILT and aneurysmal wall, ideally with direct correlations to histological constituents and properties (e.g., collagen-content, elastic fragmentation, fibrin density, etc.).
- Failure/rupture – quantify regionally, and propose constitutive relations for, the evolution of the strength of the ILT and aneurysmal wall, including models of failure that consider the propagation of dissections or frank rupture.

Out of many possible experiments, some of the possibilities that could improve this thrombus-laden aneurysm model, assist with the calibration of the model parameters, as well as increase the understanding of the pathophysiology of the disease are:

1. In humans, during the open surgical repairs, samples of ILT and wall could be harvested, and locations of high MMP activity or neutrophil content in the luminal ILT or wall could be defined. One could study whether these locations could be correlated with the areas of local high dilatation rate defined from prior imaging (e.g., from CT scans obtained during follow-ups).
2. In murine models with ILT (rat elastase model, for example), one could try to eliminate functional neutrophils and/or MMPs (in genetic mutants or with drugs). The experimental results could be compared with predictions of the presented model.
3. In murine models, one could try to induce AAAs in older vs younger rats to test the prediction that older rats with stiffer aortas may have less AAA expansion than young rats, as predicted here.

6. Conclusion

Computational biomechanics is increasingly used to investigate complex processes in vascular health and disease. Prior G&R models of aortic aneurysms (cf. [43,44]) have provided considerable insight that complement histopathological studies and clinical observations, but have heretofore failed to include the biochemomechanical effects of intraluminal thrombus on the aneurysmal wall. These effects are considered to be fundamental to the evolution of this disease and therefore for predicting clinical outcomes related to AAA enlargement and rupture.

Notwithstanding advantages of this first generation model, it was necessarily limited by the assumed cylindrical geometry, which did not admit local dilatations of the aneurysmal wall and thus axial or circumferential variations in thrombus properties (e.g., shoulder regions of an aneurysm with continued thin thrombus). This was necessary due to limitation of *Matfeap* simulations – they are computationally and time consuming, require a large size of common block, incapable of taking into account mechanical effects of ILT, and there is also a lack of experimental data about molecular distributions and heterogeneities in mechanical properties in the axial and circumferential direction in the literature. Yet, this limitation does not diminish the capability of the model to study whether intraluminal thrombus influences expansion of aneurysm and to investigate which bounded parameters influence AAA growth the most.

Similarly, the assumption of a space-filling thrombus did not allow a hemodynamically-driven progression of the ILT, which likely occurs *in vivo*. To continue to gain increased insight, subsequent finite element based G&R models should probably consider, in order of increasing complexity, axisymmetric, non-axisymmetric, and finally patient-specific geometries [195]. Fortunately, computational models of lesions having complex geometries have already been achieved [42,95], though not with an evolving thrombus. The final goal, of course, is a comprehensive fluid-solid-growth model that integrates the diverse biochemomechanical factors that govern the hemodynamics, endothelial (dys)function (e.g., shear stress induced paracrine signaling), thrombus formation and progression (e.g., platelet activation and turnover of fibrin), inflammation, intramural cellular proliferation and apoptosis (e.g., phenotypic switching and anoikis of smooth muscle cells), and chemomechanical-dependent turnover of extracellular matrix. The focus herein on a geometrically simple model was prudent for exploring and verifying the new constitutive frameworks and assumptions for the roles of ILT on the evolution of the aneurysmal wall.

Prior G&R studies showed that the stiffness of collagen plays a dominant role in predicting clinical endpoints (e.g., arrest, progressive expansion, or rupture) in AAAs that do not harbor an ILT [73]. The model confirmed these prior results, but suggested further that factors in addition to collagen may also be important in thrombus-laden lesions. In particular, simulations herein with identical properties of the aneurysmal wall were capable of differential clinical outcomes depending on properties of the ILT. These results follow directly from the ability of the thrombus to not only bear load, but also to affect the turnover of extracellular matrix in the underlying wall via proteolysis. Of course, there is a need for novel experiments to better determine the many related G&R parameters in Table 4, ultimately in a patient-specific manner. For example, although experimental determination of concentrations of MMPs and elastases in different layers of the ILT and AAA wall has revealed insight into the biological activity of heterogeneous thrombi, there is a need for data on continuous distributions from the lumen to the outer wall of the aneurysm. Experimentally motivated studies of the mechanical influence of ILT on the wall have similarly been provocative, yet this issue remains controversial. Even though most of the studies support a "cushioning" effect on the wall, some suggest that whether the thrombus will decrease or increase the peak wall stress depends on its porosity and attachment to the wall. Apart from data on the existence of a "liquid interphase" in some large ILTs with a completely disrupted abluminal layer [10], which may suggest that attachment weakens with age, there are no data on this issue. Likewise, there is still a need for further data on regional variations in the composition, structure, and mechanics of the aneurysmal wall (e.g., better information on the reorientation of collagen fibers and, crucially, changes in the stiffness of collagen due to altered pre-stretches or cross-linking). Such data promise to improve current models.

Nevertheless, this initial study suggested new insights into both the important roles that ILT may play during the evolution of an aneurysm and the potential roles of diverse risk factors and therapeutic strategies. That is, basic results were largely consistent with clinical observations, intuition, and previous computational G&R models having more complex geometries but without thrombus. Simulations yielded, for example, average rates of enlargement of ~2 mm/year, while rapid enlargement (10 mm/year and more) led to rupture. Smoking increased enlargement rates by ~0.43 mm/year, and hypertension increased enlargement by ~0.22 cm/year per 10 mmHg, both of which are consistent with clinical observations [79]. The model was also consistent with observations that female sex, smoking, and hypertension increase likelihood of rupture-risk. It also introduces a hypothesis that mechanical state of aneurysm (e.g., the amount of elastin remaining or the pre-stretch of the

deposited collagen) significantly influences ability of AAA adapt to changes and damages. While stiffening the collagen fibers could help to stabilize an enlarging aneurysm (as shown previously in models without thrombus [73]), this might not be sufficient in cases of high proteolytic activity of thrombus (see Figure 5.8(e)-(h); stress after 20 years is at approximately 455 kPa, and rupture is expected within a year) or an abrupt change in blood pressure (e.g., see Figure 5.6 and Figure 5.7). Limiting proteolytic activity also appears to be important because a biologically active luminal layer of thrombus could otherwise increase enlargement rates and rupture risk when in close proximity to a remodeling wall (e.g., in a thin thrombus or in posterio-lateral or shoulder regions where the ILT contacts the wall). Indeed, an evolving ILT may contribute in this way to clinically observed discontinuous patterns of enlargement (see Figure 5.8(d) and (h)). In conclusion, therefore, that ILT should not be neglected in future experimental and computational models.

As noted above, due to lack of experimental data about molecular distributions and heterogeneities in mechanical properties in the axial and circumferential direction, the translation of some of the modelling assumptions to 3D will not be straight forward. Therefore, experimentation that will provide the requisite data for developing and validating the growth and remodeling model, which ultimate aim is to enhance the ability to understand and predict the complex, biochemomechanical processes occurring during AAA progression, and thus improve patient-specific risk stratification and clinical outcome is highly encouraged.

In conclusion, a careful, integrated consideration of the evolving mechanical, chemical, and biological properties of biologically active, multi-layered intraluminal thrombus on the natural history of AAAs will be needed to maximize the potential of computational models to help identify and ameliorate rupture-risk factors (or, equally important, promoting stabilization factors), provide patient-specific diagnostics and interventional planning, and ultimately improve clinical outcomes.

6.1. Original scientific contribution

1. Development of the numerical model that describes:
   a) formation of abdominal aortic aneurysm considering radial structural changes in the aortic wall,
   b) formation and radial changes in structure of intraluminal thrombus,

2. Implementation of growth and remodeling model into finite elements, and modeling biochemical influence of thrombus on aneurysmal wall (while mechanical effects are neglected).
3. Modeling of the interaction between thrombus and wall will allow us to investigate influence of thrombus on AAA expansion and rupture risk,
4. Support or rejection, within model assumptions, of hitherto proposed rupture risk or stabilization factors.

Biography

Date of birth 13/12/1987

Education

Since 2011	Ph.D. student, Faculty of Mechanical Engineering and Naval Architecture (FAMENA), University of Zagreb.
2011,	Master of Engineering, FAMENA, University of Zagreb.
2010,	Bachelor of Engineering, FAMENA, University of Zagreb.

Employment

Since 2011,	Research Assistant, FAMENA, University of Zagreb.

Trainings

2016,	Tongji University, Shanghai, China, August 2016.
2016,	7th Summer School on Biomechanics: Trends in Modeling and Simulation, Graz, Austria.
2014,	6th Summer School on Biomechanics: Trends in Modeling and Simulation, Graz, Austria.
2013,	International Centre for Mechanical Sciences CISM, Nonlinear Mechanics of Soft Fibrous Materials course, Udine, Italy.
2012,	Yale University, March-April 2012.
2010,	Summer School at Copenhagen University College of Engineering 2010, International Engineering Project course.

Associations

Croatian Society of Mechanics
European Society of Biomechanics

Awards

2016,	Annual award of Society of University teachers and Other Scientists of Zagreb for young researchers and artists.
2011,	Graduated summa cum laude.
2011,	Medal of the Faculty of Mechanical Engineering and Naval Architecture for the best students.
2010,	"Davorin Bazjanac" as the best student of the 4th year of study.
2009,	INETEC (Institute for nuclear technology) award for prospective students.
2009,	"Davorin Bazjanac" as the best student of the 3rd year of study.
2007,	"Davorin Bazjanac" as the best student of the 1st year of study.

Invited Lectures

2016,	Tongji University, Shanghai, China.
2015,	ESMC 2015 Conference, Madrid, Spain.
2014,	Technical University Graz, Austria.
2011,	Croatian Society of Mechanics, Slavonski Brod, Croatia.

List of publications: http://bib.irb.hr/lista-radova?autor=332692

Životopis

Datum rođenja 13.12.1987.

Obrazovanje

od 2011.	Doktorand, Fakultet strojarstva i brodogradnje (FSB), Sveučilište u Zagrebu.
2011.	Magistra strojarstva, FSB, Sveučilište u Zagrebu.
2010.	Prvostupnica strojarstva, FSB, Sveučilište u Zagrebu.

Zaposlenje

Od 2011.	Znanstveni novak, FSB, Sveučilište u Zagrebu.

Usavršavanja

2016.	Sveučilište Tongji, Shanghai, China, kolovoz 2016.
2016.	7th Summer School on Biomechanics: Trends in Modeling and Simulation, Graz, Austria.
2014.	6th Summer School on Biomechanics: Trends in Modeling and Simulation, Graz, Austria.
2013.	International Centre for Mechanical Sciences CISM, Nonlinear Mechanics of Soft Fibrous Materials course, Udine, Italy.
2012.	Sveučilište Yale, ožujak – travanj 2012.
2010.	Summer School at Copenhagen University College of Engineering 2010, International Engineering Project course.

Članstva

Hrvatsko društvo za mehaniku
European Society of Biomechanics

Nagrade

2016.	Godišnja nagrada Društva sveučilišnih nastavnika i drugih znanstvenika Sveučilišta u Zagrebu za mladog znanstvenika ili umjetnika.
2011.	Magistrirala summa cum laude.
2011.	Medalja Fakulteta strojarstva i brodogradnje za najbolje studente.
2010.	Nagrada “Davorin Bazjanac” za najboljeg studenta četvrte godine studija.
2009.	INETEC (Institute for nuclear technology) nagrada za perspektivne studente.
2009.	Nagrada “Davorin Bazjanac” za najboljeg studenta treće godine studija.
2007.	Nagrada “Davorin Bazjanac” za najboljeg studenta prve godine studija.

Pozvana predavanja

2016.	Sveučilište Tongji, Šangaj, Kina.
2015.	Konferencija ESMC 2015, Madrid, Spain.
2014.	Tehničko sveučilište Graz, Austria.
2011.	Hrvatsko društvo za mehaniku, podružnica Slavonski Brod, Croatia.

Popis publikacija: http://bib.irb.hr/lista-radova?autor=332692

Bibliography

1. Vorp DA, Vande Geest JP. Biomechanical determinants of abdominal aortic aneurysm rupture. *Arterioscler Thromb Vasc Biol*. 2005;**25**(8):1558–66. doi: 10.1161/01.ATV.0000174129.77391.55.

2. Darling RC, Messina CR, Brewster DC, Ottinger LW. Autopsy study of unoperated abdominal aortic aneurysms. The case for early resection. *Circulation*. 1977;**56**(3 Suppl):II161-4.

3. Simão da Silva E, Rodrigues AJ, Magalhães Castro de Tolosa E, Rodrigues CJ, Villas Boas do Prado G, Nakamoto JC. Morphology and diameter of infrarenal aortic aneurysms: a prospective autopsy study. *Cardiovasc Surg*. 2000;**8**(7):526–32.

4. Vande Geest JP, Sacks MS, Vorp DA. The effects of aneurysm on the biaxial mechanical behavior of human abdominal aorta. *J Biomech*. 2006;**39**(7):1324–34. doi: 10.1016/j.jbiomech.2005.03.003.

5. O'Rourke MJ, McCullough JP, Kelly S. An Investigation of the relationship between hemodynamics and thrombus deposition within patient-specific models of abdominal aortic aneurysm. *Proc Inst Mech Eng Part H J Eng Med*. 2012;**226**(7):548–564. doi: 10.1177/0954411912444080.

6. Biasetti J, Hussain F, Gasser TC. Blood flow and coherent vortices in the normal and aneurysmatic aortas: a fluid dynamical approach to intra-luminal thrombus formation. *J R Soc Interface*. 2011;**8**(63):1449–61. doi: 10.1098/rsif.2011.0041.

7. Arzani A, Shadden SC. Characterization of the transport topology in patient-specific abdominal aortic aneurysm models. *Phys Fluids*. 2012;**24**(8):81901. doi: 10.1063/1.4744984.

8. Tong J, Cohnert T, Regitnig P, Holzapfel GA. Effects of age on the elastic properties of the intraluminal thrombus and the thrombus-covered wall in abdominal aortic aneurysms: biaxial extension behaviour and material modelling. *Eur J Vasc Endovasc Surg*. 2011;**42**(2):207–19. doi: 10.1016/j.ejvs.2011.02.017.

9. Adolph R, Vorp DA, Steed DL, Webster MW, Kameneva M V, Watkins SC. Cellular content and permeability of intraluminal thrombus in abdominal aortic aneurysm. *J Vasc Surg*. 1997;**25**(5):916–26.

10. Fontaine V, Jacob M-P, Houard X, *et al.* Involvement of the mural thrombus as a site of protease release and activation in human aortic aneurysms. *Am J Pathol*. 2002;**161**(5):1701–10. doi: 10.1016/S0002-9440(10)64447-1.

11. Swedenborg J, Eriksson P. The intraluminal thrombus as a source of proteolytic activity. *Ann N Y Acad Sci*. 2006;**1085**:133–8. doi: 10.1196/annals.1383.044.

12. Wang DHJ, Makaroun M, Webster MW, Vorp DA. Mechanical Properties and Microstructure of Intraluminal Thrombus From Abdominal Aortic Aneurysm. *J Biomech Eng*. 2001;**123**(6):536. doi: 10.1115/1.1411971.

13. van Dam EA, Dams SD, Peters GWM, *et al.* Determination of linear viscoelastic behavior of abdominal aortic aneurysm thrombus. *Biorheology*. 2006;**43**(6):695–707.

14. Holmes DR, Liao S, Parks WC, Thompson RW. Medial neovascularization in abdominal aortic aneurysms: a histopathologic marker of aneurysmal degeneration with pathophysiologic implications. *J Vasc Surg*. 1995;**21**(5):761–72.

15. Mäyränpää MI, Trosien JA, Fontaine V, *et al.* Mast cells associate with neovessels in the media and adventitia of abdominal aortic aneurysms. *J Vasc Surg*. 2009;**50**(2):388–96. doi:

10.1016/j.jvs.2009.03.055.

16. Ferry JD, Morrison PR. Chemical, clinical, and immunological studies on the products of human plasma fractionation. XVI fibrin clots, fibrin films, and fibrinogen plastics. *J Clin Invest*. 1944;**23**:566–572.

17. Inzoli F, Boschetti F, Zappa M, Longo T, Fumero R. Biomechanical factors in abdominal aortic aneurysm rupture. *Eur J Vasc Surg*. 1993;**7**(6):667–74.

18. Ene F, Gachon C, Delassus P, *et al.* In vitro evaluation of the effects of intraluminal thrombus on abdominal aortic aneurysm wall dynamics. *Med Eng Phys*. 2011;**33**(8):957–66. doi: 10.1016/j.medengphy.2011.03.005.

19. Schurink GWH, Baalen JM Van, Visser MJT. Thrombus within an aortic aneurysm does not reduce pressure on the aneurysmal wall. *J Vasc Surg*. 2000;**31**:501–6. doi: 10.1067/mva.2000.103693.

20. Meyer CA, Guivier-Curien C, Moore JE. Trans-thrombus blood pressure effects in abdominal aortic aneurysms. *J Biomech Eng*. 2010;**132**(7):71005. doi: 10.1115/1.4001253.

21. Kurvers H, Veith FJ, Lipsitz EC, *et al.* Discontinuous, staccato growth of abdominal aortic aneurysms. *J Am Coll Surg*. 2004;**199**(5):709–15. doi: 10.1016/j.jamcollsurg.2004.07.031.

22. Brady AR, Thompson SG, Fowkes FGR, Greenhalgh RM, Powell JT. Abdominal aortic aneurysm expansion: risk factors and time intervals for surveillance. *Circulation*. 2004;**110**(1):16–21. doi: 10.1161/01.CIR.0000133279.07468.9F.

23. Basciano C, Kleinstreuer C, Hyun S, Finol EA. A relation between near-wall particle-hemodynamics and onset of thrombus formation in abdominal aortic aneurysms. *Ann Biomed Eng*. 2011;**39**(7):2010–26. doi: 10.1007/s10439-011-0285-6.

24. Holzapfel GA, Gasser TC, Ogden RW. A new constitutive framework for arterial wall mechanics and a comparative study of material models. *J Elast*. 2000;**61**:1–48.

25. Gasser TC, Ogden RW, Holzapfel GA. Hyperelastic modelling of arterial layers with distributed collagen fibre orientations. *J R Soc Interface*. 2006;**3**(6):15–35. doi: 10.1098/rsif.2005.0073.

26. Rodriguez EK, Hoger A, McCulloch AD. Stress-dependent finite-growth in soft elastic tissues. *J Biomech*. 1994;**27**(4):455–467.

27. Taber LA, Eggers DW. Theoretical study of stress-modulated growth in the aorta. *J Theor Biol*. 1996;**180**(4):343–57. doi: 10.1006/jtbi.1996.0107.

28. Rachev A. A model of arterial adaptation to alterations in blood flow. *J Elast*. 2000;**61**:83–111.

29. Humphrey JD, Rajagopal KR. A constrained mixture model for growth and remodeling of soft tissues. *Math Model Methods Appl Sci*. 2002;**12**(3):407–430. doi: 10.1142/S0218202502001714.

30. Baek S, Rajagopal KR, Humphrey JD. Competition between radial expansion and thickening in the enlargement of an intracranial saccular aneurysm. *J Elast*. 2005;**80**(1–3):13–31. doi: 10.1007/s10659-005-9004-6.

31. Valentín A, Humphrey JD. Parameter sensitivity study of a constrained mixture model of arterial growth and remodeling. *J Biomech Eng*. 2009;**131**(10):101006. doi: 10.1115/1.3192144.

32. Wan W, Hansen L, Gleason RL. A 3-D constrained mixture model for mechanically

mediated vascular growth and remodeling. *Biomech Model Mechanobiol*. 2010;**9**(4):403–19. doi: 10.1007/s10237-009-0184-z.

33. Karšaj I, Sorić J, Humphrey JD. A 3-D framework for arterial growth and remodeling in response to altered hemodynamics. *Int J Eng Sci*. 2011;**48**(11):1357–1372. doi: 10.1016/j.ijengsci.2010.06.033.A.

34. Karšaj I, Humphrey JD. A multilayered wall model of arterial growth and remodeling. *Mech Mater*. 2012;**44**:110–119. doi: 10.1016/j.mechmat.2011.05.006.

35. Vande Geest JP, Sacks MS, Vorp DA. Age Dependency of the Biaxial Biomechanical Behavior of Human Abdominal Aorta. *J Biomech Eng*. 2004;**126**(6):815–822. doi: 10.1115/1.1824121.

36. Volokh KY, Vorp DA. A model of growth and rupture of abdominal aortic aneurysm. *J Biomech*. 2008;**41**(5):1015–21. doi: 10.1016/j.jbiomech.2007.12.014.

37. Rodríguez JF, Martufi G, Doblaré M, Finol E a. The effect of material model formulation in the stress analysis of abdominal aortic aneurysms. *Ann Biomed Eng*. 2009;**37**(11):2218–21. doi: 10.1007/s10439-009-9767-1.

38. Rissland P, Alemu Y, Einav S, Ricotta J, Bluestein D. Abdominal aortic aneurysm risk of rupture: patient-specific FSI simulations using anisotropic model. *J Biomech Eng*. 2009;**131**(3):31001. doi: 10.1115/1.3005200.

39. Ferruzzi J, Vorp DA, Humphrey JD. On constitutive descriptors of the biaxial mechanical behaviour of human abdominal aorta and aneurysms. *J R Soc Interface*. 2011;**8**(56):435–50. doi: 10.1098/rsif.2010.0299.

40. Watton PN, Hill NA, Heil M. A mathematical model for the growth of the abdominal aortic aneurysm. *Biomech Model Mechanobiol*. 2004;**3**(2):98–113. doi: 10.1007/s10237-004-0052-9.

41. Zeinali-Davarani S, Raguin LG, Vorp DA, Baek S. Identification of in vivo material and geometric parameters of a human aorta: toward patient-specific modeling of abdominal aortic aneurysm. *Biomech Model Mechanobiol*. 2011;**10**(5):689–99. doi: 10.1007/s10237-010-0266-y.

42. Sheidaei A, Hunley SC, Zeinali-Davarani S, Raguin LG, Baek S. Simulation of abdominal aortic aneurysm growth with updating hemodynamic loads using a realistic geometry. *Med Eng Phys*. 2011;**33**(1):80–8. doi: 10.1016/j.medengphy.2010.09.012.

43. Wilson JS, Baek S, Humphrey JD. Importance of initial aortic properties on the evolving regional anisotropy, stiffness and wall thickness of human abdominal aortic aneurysms. *J R Soc Interface*. 2012;**9**(74):2047–58. doi: 10.1098/rsif.2012.0097.

44. Watton PN, Hill NA. Evolving mechanical properties of a model of abdominal aortic aneurysm. *Biomech Model Mechanobiol*. 2009;**8**(1):25–42. doi: 10.1007/s10237-007-0115-9.

45. Lobanov AI, Starozhilova TK. The effect of convective flows on blood coagulation processes. *Pathophysiol Haemost Thromb*. 2005;**34**(2–3):121–34. doi: 10.1159/000089932.

46. Anand M, Rajagopal K, Rajagopal KR. A model for the formation and lysis of blood clots. *Pathophysiol Haemost Thromb*. 2005;**34**(2–3):109–20. doi: 10.1159/000089931.

47. Wang J, Slattery MJ, Hoskins MH, Liang S, Dong C, Du Q. Monte Carlo simulation of heterotypic cell aggregation in nonlinear shear flow. *Math Biosci Eng*. 2006;**3**(4):683–696.

48. Xu Z, Chen N, Kamocka MM, Rosen ED, Alber M. A multiscale model of thrombus development. *J R Soc Interface*. 2008;**5**(24):705–22. doi: 10.1098/rsif.2007.1202.

49. Xu Z, Chen N, Shadden SC, *et al.* Study of blood flow impact on growth of thrombi using a multiscale model. *Soft Matter*. 2009;**5**:769–779.

50. Xu Z, Lioi J, Mu J, *et al.* A multiscale model of venous thrombus formation with surface-mediated control of blood coagulation cascade. *Biophys J*. 2010;**98**(9):1723–32. doi: 10.1016/j.bpj.2009.12.4331.

51. Leiderman K, Fogelson AL. Grow with the flow: a spatial-temporal model of platelet deposition and blood coagulation under flow. *Math Med Biol*. 2011;**28**(1):47–84. doi: 10.1093/imammb/dqq005.

52. Scianna M, Preziosi L. Multiscale developments of the cellular Potts model. *Soc Ind Appl Math*. 2012;**10**(2):342–382.

53. Flamm MH, Diamond SL. Multiscale systems biology and physics of thrombosis under flow. *Ann Biomed Eng*. 2012;**40**(11):2355–64. doi: 10.1007/s10439-012-0557-9.

54. Karšaj I, Humphrey JD. A mathematical model of evolving mechanical properties of intraluminal thrombus. *Biorheology*. 2009;**46**(6):509–527. doi: 10.3233/BIR-2009-0556.A.

55. Fontaine V, Touat Z, Mtairag EM, *et al.* Role of leukocyte elastase in preventing cellular re-colonization of the mural thrombus. *Am J Pathol*. 2004;**164**(6):2077–87.

56. Scott DJA, Prasad P, Philippou H, *et al.* Clot architecture is altered in abdominal aortic aneurysms and correlates with aneurysm size. *Arterioscler Thromb Vasc Biol*. 2011;**31**(12):3004–10. doi: 10.1161/ATVBAHA.111.236786.

57. Weisel JW. The mechanical properties of fibrin for basic scientists and clinicians. *Biophys Chem*. 2004;**112**(2–3):267–76. doi: 10.1016/j.bpc.2004.07.029.

58. Weisel JW. Structure of fibrin: impact on clot stability. *J Thromb Haemost*. 2007;**5 Suppl 1**:116–24. doi: 10.1111/j.1538-7836.2007.02504.x.

59. Furie B, Furie BC. In vivo thrombus formation. *J Thromb Haemost*. 2007;**5**:12–17.

60. Gersh KC, Nagaswami C, Weisel JW. Fibrin network structure and clot mechanical properties are altered by incorporation of erythrocytes. *Thromb Haemost*. 2010;**102**(6):1169–1175. doi: 10.1160/TH09-03-0199.Fibrin.

61. Gersh KC, Edmondson KE, Weisel JW. Flow rate and fibrin fiber alignment. *J Thromb Haemost*. 2010;**8**(12):2826–8. doi: 10.1111/j.1538-7836.2010.04118.x.

62. Varjú I, Sótonyi P, Machovich R, *et al.* Hindered dissolution of fibrin formed under mechanical stress. *J Thromb Haemost*. 2011;**9**(5):979–86. doi: 10.1111/j.1538-7836.2011.04203.x.

63. Vorp DA, Mandarino WA, Webster MW, Gorcsan III J. Potential influence of intraluminal thrmbus on abdominal aortic aneurysm as assessed by a new non-invasive method. *Cardiovasc Surg*. 1996;**4**(6):732–739.

64. Ashton JH, Vande Geest JP, Simon BR, Haskett DG. Compressive mechanical properties of the intraluminal thrombus in abdominal aortic aneurysms and fibrin-based thrombus mimics. *J Biomech*. 2009;**42**(3):197–201. doi: 10.1016/j.jbiomech.2008.10.024.

65. Michel J-B, Martin-Ventura J-L, Egido J, *et al.* Novel aspects of the pathogenesis of aneurysms of the abdominal aorta in humans. *Cardiovasc Res*. 2010;**90**(1):18–27. doi: 10.1093/cvr/cvq337.

66. Wiernicki I, Stachowska E, Safranow K, *et al.* Enhanced matrix-degrading proteolytic activity within the thin thrombus-covered wall of human abdominal aortic aneurysms. *Atherosclerosis*. 2010;**212**(1):161–5. doi: 10.1016/j.atherosclerosis.2010.04.033.

67. Khan JA, Abdul Rahman MN a, Mazari F a K, *et al.* Intraluminal thrombus has a selective influence on matrix metalloproteinases and their inhibitors (tissue inhibitors of matrix metalloproteinases) in the wall of abdominal aortic aneurysms. *Ann Vasc Surg*. 2012;**26**(3):322–9. doi: 10.1016/j.avsg.2011.08.015.

68. Touat Z, Ollivier V, Dai J, *et al.* Renewal of mural thrombus releases plasma markers and is involved in aortic abdominal aneurysm evolution. *Am J Pathol*. 2006;**168**(3):1022–30. doi: 10.2353/ajpath.2006.050868.

69. Folkesson M, Silveira A, Eriksson P, Swedenborg J. Protease activity in the multi-layered intra-luminal thrombus of abdominal aortic aneurysms. *Atherosclerosis*. 2011;**218**(2):294–9. doi: 10.1016/j.atherosclerosis.2011.05.002.

70. Kazi M, Thyberg J, Religa P, *et al.* Influence of intraluminal thrombus on structural and cellular composition of abdominal aortic aneurysm wall. *J Vasc Surg*. 2003;**38**(6):1283–1292. doi: 10.1016/S0741-5214(03)00791-2.

71. Vorp DA. Biomechanics of abdominal aortic aneurysm. *J Biomech*. 2007;**40**(9):1887–902. doi: 10.1016/j.jbiomech.2006.09.003.

72. Labruto F, Blomqvist L, Swedenborg J. Imaging the intraluminal thrombus of abdominal aortic aneurysms: Techniques, findings, and clinical implications. *J Vasc Interv Radiol*. 2011;**22**(8):1069–1075. doi: 10.1016/j.jvir.2011.01.454.

73. Wilson JS, Baek S, Humphrey JD. Parametric study of effects of collagen turnover on the natural history of abdominal aortic aneurysms. *Proc Math Phys Eng Sci*. 2013;**469**(2150):20120556. doi: 10.1098/rspa.2012.0556.

74. Vorp DA, Lee PC, Wang DH, *et al.* Association of intraluminal thrombus in abdominal aortic aneurysm with local hypoxia and wall weakening. *J Vasc Surg*. 2002;**34**(2):291–9. doi: 10.1067/mva.2001.114813.

75. Anidjar S, Salzmann JL, Gentric D, Lagneau P, Camilleri JP, Michel JB. Elastase-induced experimental aneurysms in rats. *Circulation*. 1990;**82**(3):973–981. doi: 10.1161/01.CIR.82.3.973.

76. Abdul-Hussien H, Soekhoe RGV, Weber E, *et al.* Collagen Degradation in the Abdominal Aneurysm. *Am J Pathol*. 2007;**170**(3):809–817. doi: 10.2353/ajpath.2007.060522.

77. Mahmud A, Feely J. Effect of smoking on arterial stiffness and pulse pressure amplification. *Hypertension*. 2003;**41**(1):183–187. doi: 10.1161/01.HYP.0000047464.66901.60.

78. Jatoi NA, Jerrard-Dunne P, Feely J, Mahmud A. Impact of smoking and smoking cessation on arterial stiffness and aortic wave reflection in hypertension. *Hypertension*. 2007;**49**(5):981–985. doi: 10.1161/HYPERTENSIONAHA.107.087338.

79. Bhak RH, Wininger M, Johnson GR, *et al.* Factors associated with small abdominal aortic aneurysm expansion rate. *JAMA Surg*. 2015;**150**(1):44–50. doi: 10.1001/jamasurg.2014.2025.

80. Lasheras JC. The Biomechanics of Arterial Aneurysms. *Annu Rev Fluid Mech*. 2007;**39**(1):293–319. doi: 10.1146/annurev.fluid.39.050905.110128.

81. Vande Geest JP, Schmidt DE, Sacks MS, Vorp DA. The effects of anisotropy on the stress analyses of patient-specific abdominal aortic aneurysms. *Ann Biomed Eng*. 2008;**36**(6):921–32. doi: 10.1007/s10439-008-9490-3.

82. Virmani R, Avolio AP, Mergner WJ, *et al.* Effect of Aging on Aortic Morphology in Populations with High and Low Prevalence of Hypertension and Atherosclerosis Communities. *Am J Pathol*. 1991;**139**(5):1119–1129.

83. Houard X, Leclercq A, Fontaine V, *et al.* Retention and Activation of Blood-Borne Proteases in the Arterial Wall. *J Am Coll Cardiol*. 2006;**48**(9):A3–A9. doi: 10.1016/j.jacc.2006.04.098.

84. Wilson JS, Virag L, Di Achille P, Karšaj I, Humphrey JD. Biochemomechanics of intraluminal thrombus in abdominal aortic aneurysms. *J Biomech Eng*. 2013;**135**(2):21011-1-21011–14. doi: 10.1115/1.4023437.

85. Baek S, Rajagopal KR, Humphrey JD. A theoretical model of enlarging intracranial fusiform eneurysms. *J Biomech Eng*. 2006;**128**(1):142. doi: 10.1115/1.2132374.

86. Schriefl AJ, Zeindlinger G, Pierce DM, Regitnig P, Holzapfel GA. Determination of the layer-specific distributed collagen fibre orientations in human thoracic and abdominal aortas and common iliac arteries. *J R Soc Interface*. 2012;**9**(71):1275–86. doi: 10.1098/rsif.2011.0727.

87. Humphrey JD. *Cardiovascular solid mechanics: cells, tissues, and organs*. Springer, 2002.

88. Rachev A, Hayashi K. Theoretical study of the effects of vascular smooth muscle contraction on strain and stress distributions in arteries. *Ann Biomed Eng*. 1999;**27**(4):459–468.

89. Baek S, Valentín A, Humphrey JD. Biochemomechanics of cerebral vasospasm and its resolution: II. Constitutive relations and model simulations. *Ann Biomed Eng*. 2007;**35**(9):1498–509. doi: 10.1007/s10439-007-9322-x.

90. Sansour C. On the physical assumptions underlying the volumetric-isochoric split and the case of anisotropy. *Eur J Mech - A/Solids*. 2008;**27**(1):28–39. doi: 10.1016/j.euromechsol.2007.04.001.

91. Federico S. Volumetric-Distortional Decomposition of Deformation and Elasticity Tensor. *Math Mech Solids*. 2009;**15**(6):672–690. doi: 10.1177/1081286509105591.

92. Helfenstein J, Jabareen M, Mazza E, Govindjee S. On non-physical response in models for fiber-reinforced hyperelastic materials. *Int J Solids Struct*. 2010;**47**(16):2056–2061. doi: 10.1016/j.ijsolstr.2010.04.005.

93. Valentín A, Humphrey JD, Holzapfel GA. A finite element-based constrained mixture implementation for arterial growth , remodeling , and adaptation : Theory and numerical verification. *Int J Numer Meth Biomed Engng*. 2013;**29**(8):822–49. doi: 10.1002/cnm.

94. Länne T, Sonesson B, Bergqvist D, Bengtsson H, Gustafsson D. Diameter and compliance in the male human abdominal aorta: influence of age and aortic aneurysm. *Eur J Vasc Surg*. 1992;**6**(2):178–84.

95. Wu J, Shadden SC. Coupled Simulation of Hemodynamics and Vascular Growth and Remodeling in a Subject-Specific Geometry. *Ann Biomed Eng (in Press 2015)*. 2015. doi: 10.1007/s10439-015-1287-6.

96. Valentín A, Humphrey JD, Holzapfel GA. A multi-layered computational model of coupled elastin degradation, vasoactive dysfunction, and collagenous stiffening in aortic aging. *Ann Biomed Eng*. 2011;**39**(7):2027–2045. doi: 10.1007/s10439-011-0287-4.

97. Cardamone L, Valentín A, Eberth JF, Humphrey JD. Origin of axial prestretch and residual stress in arteries. *Biomech Model Mechanobiol*. 2009;**8**(6):431–446. doi: 10.1007/s10237-008-0146-x.

98. Hjort PF, Paputchis H. Platelet life span in normal, splenectomized and hypersplenic rats. *Blood*. 1950;**15**:45–51.

99. Kline DL, Cliffton EE. Lifespan of leucocytes in man. *J Appl Physiol*. 1952;**5**:79–84.

100. Isenberg BC, Tranquillo RT. Long-Term Cyclic Distention Enhances the Mechanical Properties of Collagen-Based Media-Equivalents. *Ann Biomed Eng*. 2003;**31**(8):937–949. doi: 10.1114/1.1590662.

101. Cyron CJ, Wilson JS, Humphrey JD. Mechanobiological stability : a new paradigm to understand the enlargement of aneurysms ? Mechanobiological stability : a new paradigm to understand the enlargement of aneurysms ? *J R Soc Interface*. 2014;**11**:20140680.

102. Zeinali-Davarani S, Sheidaei A, Baek S. A finite element model of stress-mediated vascular adaptation: application to abdominal aortic aneurysms. *Comput Methods Biomech Biomed Engin*. 2011;**14**(9):803–817. doi: 10.1080/10255842.2010.495344.

103. Crowther M, Goodall S, Jones JL, Bell PR, Thompson MM. Localization of matrix metalloproteinase 2 within the aneurysmal and normal aortic wall. *Br J Surg*. 2000;**87**(10):1391–400. doi: 10.1046/j.1365-2168.2000.01554.x.

104. Fridez P, Zulliger M, Bobard F, *et al.* Geometrical, functional, and histomorphometric adaptation of rat carotid artery in induced hypertension. *J Biomech*. 2003;**36**(5):671–680. doi: 10.1016/S0021-9290(02)00445-1.

105. Hu JJ, Fossum TW, Miller MW, Xu H, Liu JC, Humphrey JD. Biomechanics of the porcine basilar artery in hypertension. *Ann Biomed Eng*. 2007;**35**(1):19–29. doi: 10.1007/s10439-006-9186-5.

106. Franck G, Dai J, Fifre A, *et al.* Reestablishment of the endothelial lining by endothelial cell therapy stabilizes experimental abdominal aortic aneurysms. *Circulation*. 2013;**127**(18):1877–1887. doi: 10.1161/CIRCULATIONAHA.113.001677.

107. Raut SS, Chandra S, Shum J, Finol E a. The role of geometric and biomechanical factors in abdominal aortic aneurysm rupture risk assessment. *Ann Biomed Eng*. 2013;**41**(7):1459–77. doi: 10.1007/s10439-013-0786-6.

108. Di Achille P, Tellides G, Figueroa CA, Humphrey JD. A haemodynamic predictor of intraluminal thrombus formation in abdominal aortic aneurysms. *Proc R Soc A*. 2014;**470**:20140163. doi: 10.1098/rspa.2014.0163.

109. Les AS, Shadden SC, Figueroa CA, *et al.* Quantification of hemodynamics in abdominal aortic aneurysms during rest and exercise using magnetic resonance imaging and computational fluid dynamics. *Ann Biomed Eng*. 2010;**38**(4):1288–1313. doi: 10.1007/s10439-010-9949-x.

110. Xu Z, Kamocka M, Alber M, Rosen ED. Computational approaches to studying thrombus development. *Arterioscler Thromb Vasc Biol*. 2011;**31**(3):500–505. doi: 10.1161/ATVBAHA.110.213397.

111. Biasetti J, Spazzini PG, Swedenborg J, Gasser TC. An integrated fluid-chemical model toward modeling the formation of intra-luminal thrombus in abdominal aortic aneurysms. *Front Physiol*. 2012;**3**(July):266. doi: 10.3389/fphys.2012.00266.

112. Whittaker P, Przyklenk K. Fibrin architecture in clots: a quantitative polarized light microscopy analysis. *Blood Cells Mol Dis*. 2009;**42**(1):51–6. doi: 10.1016/j.bcmd.2008.10.014.

113. Di Martino E, Mantero S, Inzoli F, *et al.* Biomechanics of abdominal aortic aneurysm in the presence of endoluminal thrombus: experimental characterisation and structural static computational analysis. *Eur J Vasc Endovasc Surg*. 1998;**15**(4):290–9.

114. van Dam E a, Dams SD, Peters GWM, *et al.* Non-linear viscoelastic behavior of

abdominal aortic aneurysm thrombus. *Biomech Model Mechanobiol*. 2008;**7**(2):127–37. doi: 10.1007/s10237-007-0080-3.

115. Georgakarakos E, Ioannou C V, Kamarianakis Y, *et al.* The role of geometric parameters in the prediction of abdominal aortic aneurysm wall stress. *Eur J Vasc Endovasc Surg*. 2010;**39**(1):42–8. doi: 10.1016/j.ejvs.2009.09.026.

116. Speelman L, Schurink GWH, Bosboom EMH, *et al.* The mechanical role of thrombus on the growth rate of an abdominal aortic aneurysm. *J Vasc Surg*. 2010;**51**(1):19–26. doi: 10.1016/j.jvs.2009.08.075.

117. VandeGeest JP, Sacks MS, Vorp DA. A planar biaxial constitutive relation for the luminal layer of intra-luminal thrombus in abdominal aortic aneurysms. *J Biomech*. 2006;**39**(13):2347–54. doi: 10.1016/j.jbiomech.2006.05.011.

118. Houard X, Touat Z, Ollivier V, *et al.* Mediators of neutrophil recruitment in human abdominal aortic aneurysms. *Cardiovasc Res*. 2009;**82**(3):532–41. doi: 10.1093/cvr/cvp048.

119. Houard X, Ollivier V, Louedec L, Michel J-B, Bäck M. Differential inflammatory activity across human abdominal aortic aneurysms reveals neutrophil-derived leukotriene B4 as a major chemotactic factor released from the intraluminal thrombus. *FASEB J*. 2009;**23**(5):1376–83. doi: 10.1096/fj.08-116202.

120. Curci JA, Liao S, Huffman MD, Shapiro SD, Thompson RW. Expression and localization of macrophage elastase (matrix metalloproteinase-12) in abdominal aortic aneurysms. *J Clin Invest*. 1998;**102**(11):1900–1910. doi: 10.1172/JCI2182.

121. Rizas KD, Ippagunta N, Tilson MD. Immune cells and molecular mediators in the pathogenesis of the abdominal aortic aneurysm. *Cardiol Rev*. 2009;**17**(5):201–210. doi: 10.1097/CRD.0b013e3181b04698.

122. Siegel CL, Leder A. Abdominal Morphology : with Ruptured Aneurysms Aortic Aneurysm CT Features in Patients.

123. Schriefl A J, Collins MJ, Pierce DM, Holzapfel GA, Niklason LE, Humphrey JD. Remodeling of intramural thrombus and collagen in an Ang-II infusion ApoE-/- model of dissecting aortic aneurysms. *Thromb Res*. 2012;**130**(3):e139-46. doi: 10.1016/j.thromres.2012.04.009.

124. Houard X, Rouzet F, Touat Z, *et al.* Topology of the fibrinolytic system within the mural thrombus of human abdominal aortic aneurysms. *J Pathol*. 2007;**212**:20–28. doi: 10.1002/path2148.

125. Carrell TW, Burnand KG, Booth N a, Humphries J, Smith A. Intraluminal thrombus enhances proteolysis in abdominal aortic aneurysms. *Vascular*. 2006;**14**(1):9–16. doi: 10.2310/6670.2006.00008.

126. Knox JB, Sukhova GK, Whittemore AD, Libby P. Evidence for Altered Balance Between Matrix Metalloproteinases and Their Inhibitors in Human Aortic Diseases. *Circulation*. 2007;**95**:205–212.

127. Diehm N, Di Santo S, Schaffner T, *et al.* Severe structural damage of the seemingly non-diseased infrarenal aortic aneurysm neck. *J Vasc Surg*. 2008;**48**(2):425–34. doi: 10.1016/j.jvs.2008.03.001.

128. Gong Y, Hart E, Shchurin A, Hoover-Plow J. Inflammatory macrophage migration requires MMP-9 activation by plasminogen in mice. *J Clin Invest*. 2008;**118**(9):3012–3024. doi: 10.1172/JCI32750.

129. Plow EF, Hoover-Plow J. The functions of plasminogen in cardiovascular disease.

Trends Cardiovasc Med. 2004;**14**(5):180–186. doi: 10.1016/j.tcm.2004.04.001.

130. Falcone DJ, McCaffrey TA, Haimovitz-Friedman A, Vergilio JA, Nicholson AC. Macrophage and foam cell release of matrix-bound growth factors: Role of plasminogen activation. *J Biol Chem*. 1993;**268**(16):11951–11958.

131. Meilhac O, Ho-Tin-Noé B, Houard X, Philippe M, Michel J-B, Anglés-Cano E. Pericellular plasmin induces smooth muscle cell anoikis. *FASEB J*. 2003;**17**(10):1301–3. doi: 10.1096/fj.02-0687fje.

132. Coutard M, Touat Z, Houard X, Leclercq A, Michel J-B. Thrombus versus wall biological activities in experimental aortic aneurysms. *J Vasc Res*. 2010;**47**(4):355–66. doi: 10.1159/000265569.

133. Antonicelli F, Bellon G, Debelle L, Hornebeck W. Elastin-elastases and inflamm-aging. *Curr Top Dev Biol*. 2007;**79**(6):99–155. doi: 10.1016/S0070-2153(06)79005-6.

134. Faisal Khan KM, Laurie GW, McCaffrey TA, Falcone DJ. Exposure of cryptic domains in the ??1-chain of laminin-1 by elastase stimulates macrophages urokinase and matrix metalloproteinase-9 expression. *J Biol Chem*. 2002;**277**(16):13778–13786. doi: 10.1074/jbc.M111290200.

135. Weitz JI, Leslie B, Ginsberg J. Soluble fibrin degradation products potentiate tissue plasminogen activator-induced fibrinogen proteolysis. *J Clin Invest*. 1991;**87**(3):1082–1090. doi: 10.1172/JCI115069.

136. Nackman GB, Karkowski FJ, Halpern VJ, Gaetz HP, Tilson MD. Elastin degradation products induce adventitial angiogenesis in the Anidjar/Dobrin rat aneurysm model. *Surgery*. 1997;**122**(1):39–44.

137. Chen ZL, Strickland S. Neuronal death in the hippocampus is promoted by plasmin-catalyzed degradation of laminin. *Cell*. 1997;**91**(7):917–925. doi: 10.1016/S0092-8674(00)80483-3.

138. Michel J-B, Thaunat O, Houard X, Meilhac O, Caligiuri G, Nicoletti A. Topological determinants and consequences of adventitial responses to arterial wall injury. *Arterioscler Thromb Vasc Biol*. 2007;**27**(6):1259–68. doi: 10.1161/ATVBAHA.106.137851.

139. Dal Canto AJ, Swanson PE, O'Guin AK, Speck SH, Virgin HW. IFN-?? action in the media of the great elastic arteries, a novel immunoprivileged site. *J Clin Invest*. 2001;**107**(2):15–22. doi: 10.1172/JCI11540.

140. Burns WR, Wang Y, Tang PCY, *et al.* Recruitment of CXCR3+ and CCR5+ T cells and production of interferon-??-inducible chemokines in rejecting human arteries. *Am J Transplant*. 2005;**5**(6):1226–1236. doi: 10.1111/j.1600-6143.2005.00892.x.

141. Odekon LE, Blasi F, Rifkin DB. Requirement for receptor-bound urokinase in plasmin-dependent cellular conversion of latent TGF-beta to TGF-beta. *J Cell Physiol*. 1994;**158**(3):398–407. doi: 10.1002/jcp.1041580303.

142. Baxter BT, Davis VA, Minion DJ, Wang YP, Lynch TG, Mcmanus BM. Abdominal aortic aneurysms are associated with altered matrix proteins of the non aneurysmal aortic segments. *J Vasc Surg*. 1994;**19**:797–803.

143. Goodall S, Crowther M, Hemingway DM, Bell PR, Thompson MM. Ubiquitous Elevation of Matrix Metalloproteinase-2 Expression in the Vasculature of Patients With Abdominal Aneurysms. *Circulation*. 2001;**104**(3):304–309. doi: 10.1161/01.CIR.104.3.304.

144. Ayyalasomayajula A, Vande Geest JP, Simon BR. Porohyperelastic finite element modeling of abdominal aortic aneurysms. *J Biomech Eng*. 2010;**132**(10):104502. doi:

10.1115/1.4002370.

145. Vande Geest JP, Simon BR, Mortazavi A. Toward a model for local drug delivery in abdominal aortic aneurysms. *Ann N Y Acad Sci*. 2006;**1085**:396–399. doi: 10.1196/annals.1383.047.

146. Daugherty A., Manning MW. C LA. Angiotensin II promotes atherosclerotic lesions and aneurysm in apoliprotein E-deficient mice. *J Clin Invest*. 2000;**105(**11):1605–12.

147. Kazi M. Difference in Matrix-Degrading Protease Expression and Activity Between Thrombus-Free and Thrombus-Covered Wall of Abdominal Aortic Aneurysm. *Arterioscler Thromb Vasc Biol*. 2005;**25(**7):1341–1346. doi: 10.1161/01.ATV.0000166601.49954.21.

148. Stenbaek J, Kalin B, Swedenborg J. Growth of thrombus may be a better predictor of rupture than diameter in patients with abdominal aortic aneurysms. *Eur J Vasc Endovasc Surg*. 2000;**20**(5):466–9. doi: 10.1053/ejvs.2000.1217.

149. Hans SS, Jareunpoon O, Balasubramaniam M, Zelenock GB. Size and location of thrombus in intact and ruptured abdominal aortic aneurysms. *J Vasc Surg*. 2005;**41**(4):584–8. doi: 10.1016/j.jvs.2005.01.004.

150. Sun N, Leung JH, Wood NB, *et al.* Computational analysis of oxygen transport in a patient-specific model of abdominal aortic aneurysm with intraluminal thrombus. *Br J Radiol*. 2009;**82 Spec No**:S18-23. doi: 10.1259/bjr/89466318.

151. Yoshimura K, Ikeda Y, Aoki H. Innocent bystander? Intraluminal thrombus in abdominal aortic aneurysm. *Atherosclerosis*. 2011;**218(**2):285–286. doi: 10.1016/j.atherosclerosis.2011.06.027.

152. Satoh H, Nakamura M, Satoh M, *et al.* Expression and localization of tumour necrosis factor-alpha and its converting enzyme in human abdominal aortic aneurysm. *Clin Sci (Lond)*. 2004;**106**(3):301–6. doi: 10.1042/CS20030189.

153. Li Z-Y, Sadat U, U-King-Im J, *et al.* Association between aneurysm shoulder stress and abdominal aortic aneurysm expansion: a longitudinal follow-up study. *Circulation*. 2010;**122**(18):1815–22. doi: 10.1161/CIRCULATIONAHA.110.939819.

154. Mower WD, Baraff LJ, Sneyd J. Stress Distributions in Vascular Aneurysms - Factors Affecting Risk of Aneurysm Rupture. *J Surg Res*. 1993;**55**(2):155–161.

155. Wang DHJ, Makaroun MS, Webster MW, Vorp DA. Effect of intraluminal thrombus on wall stress in patient-specific models of abdominal aortic aneurysm. *J Vasc Surg*. 2002;**36**(3):598–604. doi: 10.1067/mva.2002.126087.

156. Gasser TC, Auer M, Labruto F, Swedenborg J, Roy J. Biomechanical rupture risk assessment of abdominal aortic aneurysms: model complexity versus predictability of finite element simulations. *Eur J Vasc Endovasc Surg*. 2010;**40**(2):176–85. doi: 10.1016/j.ejvs.2010.04.003.

157. Larsson E, Labruto F, Gasser TC, Swedenborg J, Hultgren R. Analysis of aortic wall stress and rupture risk in patients with abdominal aortic aneurysm with a gender perspective. *J Vasc Surg*. 2011;**54**(2):295–299. doi: 10.1016/j.jvs.2010.12.053.

158. Brown AEX, Litvinov RI, Discher DE, Purohit PK, Weisel JW. Multiscale mechanics of fibrin polymer: gel stretching with protein unfolding and loss of water. *Science*. 2009;**325**(5941):741–4. doi: 10.1126/science.1172484.

159. Truijers M, Fillinger MF, Renema KW, *et al.* In-vivo imaging of changes in abdominal aortic aneurysm thrombus volume during the cardiac cycle. *J Endovasc Ther*. 2009;**16**(3):314–9. doi: 10.1583/08-2625.1.

160. Vande Geest JP, Di Martino ES, Bohra A, Makaroun MS, Vorp D a. A biomechanics-based rupture potential index for abdominal aortic aneurysm risk assessment: Demonstrative application. *Ann N Y Acad Sci*. 2006;**1085**:11–21. doi: 10.1196/annals.1383.046.

161. Gasser TC, Görgülü G, Folkesson M, Swedenborg J. Failure properties of intraluminal thrombus in abdominal aortic aneurysm under static and pulsating mechanical loads. *J Vasc Surg*. 2008;**48**(1):179–88. doi: 10.1016/j.jvs.2008.01.036.

162. Nchimi A, Defawe O, Brisbois D, Broussaud TKY, Magotteaux P, Massart B. MR Imaging of Iron Phagocytosis in Intraluminal Thrombi of Abdominal Aortic Aneurysms. *Radiology*. 2010;**254**(3):973–981. doi: 10.1148/radiol.09090657/-/DC1.

163. Richards JMJ, Semple SI, MacGillivray TJ, *et al.* Abdominal aortic aneurysm growth predicted by uptake of ultrasmall superparamagnetic particles of Iron oxide : A pilot study. *Circ Cardiovasc Imaging*. 2011;**4**(3):274–281. doi: 10.1161/CIRCIMAGING.110.959866.

164. Zambrano BA, Gharahi H, Lim C, *et al.* Association of intraluminal thrombus, hemodynamic forces, and abdominal aortic aneurysm expansion using longitudinal CT images. *Ann Biomed Eng*. 2015:1–13. doi: 10.1007/s10439-015-1461-x.

165. Hinnen J-W, Koning OHJ, Visser MJT, Van Bockel HJ. Effect of intraluminal thrombus on pressure transmission in the abdominal aortic aneurysm. *J Vasc Surg*. 2005;**42**(6):1176–82. doi: 10.1016/j.jvs.2005.08.027.

166. Choke E, Cockerill G, Wilson WRW, *et al.* A review of biological factors implicated in abdominal aortic aneurysm rupture. *Eur J Vasc Endovasc Surg*. 2005;**30**(3):227–44. doi: 10.1016/j.ejvs.2005.03.009.

167. Fillinger MF, Marra SP, Raghavan ML, Kennedy FE. Prediction of rupture risk in abdominal aortic aneurysm during observation: Wall stress versus diameter. *J Vasc Surg*. 2003;**37**(4):724–732. doi: 10.1067/mva.2003.213.

168. Burke A, Fitzgerald GA. Oxidative stress and smoking-induced vascular injury. *Prog Cardiovasc Dis*. 2003;**46**(1):79–90. doi: 10.1016/S0033-0620(03)00076-8.

169. Powell JT. Vascular damage from smoking: disease mechanisms at the arterial wall. *Vasc Med*. 1998;**3**(1):21–28. doi: 10.1191/135886398670269973.

170. Enevoldsen MS, Henneberg KA, Jensen JA, Lönn L, Humphrey JD. New interpretation of arterial stiffening due to cigarette smoking using a structurally motivated constitutive model. *J Biomech*. 2011;**44**(6):1209–1211. doi: 10.1016/j.jbiomech.2011.01.032.

171. Behr-Rasmussen C, Grøndal N, Bramsen MB, Thomsen MD, Lindholt JS. Mural thrombus and the progression of abdominal aortic aneurysms: a large population-based prospective cohort study. *Eur J Vasc Endovasc Surg*. 2014;**48**(3):301–7. doi: 10.1016/j.ejvs.2014.05.014.

172. Al-Barjas HS, Ariëns R, Grant P, Scott JA. Raised plasma fibrinogen concentration in patients with abdominal aortic aneurysm. *Angiology*. 2006;**57**(5):607–14. doi: 10.1177/0003319706293132.

173. van den Berkmortel FWPJ, Wollersheim H, van Langen H, Smilde TJ, den Arend J, Thien T. Two years of smoking cessation does not reduce arterial wall thickness and stiffness. *Neth J Med*. 2004;**62**(7):235–241.

174. Meade TW, Imeson J, Stirling Y. Effects of changes in smoking and other characteristics on clotting factors and the risk of ischaemic heart disease. *Lancet*. 1987;**330**(8566):986–988.

175. Deuel TF, Senior RM, Chang D, Griffin GL, Heinrikson RL, Kaiser ET. Platelet factor 4 is chemotactic for neutrophils and monocytes. *Proc Natl Acad Sci U S A*. 1981;**78**(7):4584–

4587. doi: 10.1073/pnas.78.7.4584.

176. Parodi FE, Mao D, Ennis TL, Bartoli MA, Thompson RW. Suppression of experimental abdominal aortic aneurysms in mice by treatment with pyrrolidine dithiocarbamate, an antioxidant inhibitor of nuclear factor-kB. *J Vasc Surg*. 2005;**41**(3):479–489. doi: 10.1016/j.jvs.2004.12.030.

177. Steinmetz EF, Buckley C, Shames ML, *et al.* Treatment with simvastatin suppresses the development of experimental abdominal aortic aneurysms in normal and hypercholesterolemic mice. *Ann Surg*. 2005;**241**(1):92–101. doi: 10.1097/01.sla.0000150258.36236.e0.

178. Owens AP, Edwards TL, Antoniak S, *et al.* Platelet inhibitors reduce rupture in a mouse model of established abdominal aortic aneurysm. *Arterioscler Thromb Vasc Biol*. 2015;**35**(9):2032–2041. doi: 10.1161/ATVBAHA.115.305537.

179. Lawrence DM, Singh RS, Franklin DP, Carey DJ, Elmore JR. Rapamycin suppresses experimental aortic aneurysm growth. *J Vasc Surg*. 2004;**40**(2):334–338. doi: 10.1016/j.jvs.2004.05.020.

180. Arnoud Meijer C, Stijnen T, Wasser MNJM, Hamming JF, Van Bockel JH, Lindeman JHN. Doxycycline for stabilization of abdominal aortic aneurysms: A randomized trial. *Ann Intern Med*. 2013;**159**(12):815–823. doi: 10.1016/j.jvs.2014.02.035.

181. Brown PM, Zelt DT, Sobolev B. The risk of rupture in untreated aneurysms: The impact of size, gender, and expansion rate. *J Vasc Surg*. 2003;**37**(2):280–284. doi: 10.1067/mva.2003.119.

182. Ahimastos AA, Formosa M, Dart AM, Kingwell BA. Gender differences in large artery stiffness pre- and post puberty. *J Clin Endocrinol Metab*. 2003;**88**(11):5375–5380. doi: 10.1210/jc.2003-030722.

183. Celermajer DS, Sorensen KE, Spiegelhalter DJ, Georgakopoulos D, Robinson J, Deanfield JE. Aging is associated with endothelial dysfunction in healthy men years before the age-related decline in women. *J Am Coll Cardiol*. 1994;**24**(2):471–6.

184. Blanchard JF, Armenian HK, Friesen PP. Risk factors for abdominal aortic aneurysm: results of a case-control study. *Am J Epidemiol*. 2000;**151**(6):575–583. doi: 10.1093/oxfordjournals.aje.a010245.

185. Tong J, Schriefl AJ, Cohnert T, Holzapfel GA. Gender differences in biomechanical properties, thrombus age, mass fraction and clinical factors of abdominal aortic aneurysms. *Eur J Vasc Endovasc Surg*. 2013;**45**(4):364–72. doi: 10.1016/j.ejvs.2013.01.003.

186. Brown LC, Powell JT. Risk factors for aneurysm rupture in patients kept under ultrasound surveillance. *Ann Surg*. 1999;**230**(3):289–297.

187. Chobanian A V., Bakris GL, Black HR, *et al.* Seventh report of the Joint National Committee on Prevention, Detection, Evaluation, and Treatment of High Blood Pressure. *Hypertension*. 2003;**42**(6):1206–1252. doi: 10.1161/01.HYP.0000107251.49515.c2.

188. Parr A, McCann M, Bradshaw B, Shahzad A, Buttner P, Golledge J. Thrombus volume is associated with cardiovascular events and aneurysm growth in patients who have abdominal aortic aneurysms. *J Vasc Surg*. 2011;**53**(1):28–35. doi: 10.1016/j.jvs.2010.08.013.

189. Golledge J, Iyer V, Jenkins J, Bradshaw B, Cronin O, Walker PJ. Thrombus volume is similar in patients with ruptured and intact abdominal aortic aneurysms. *J Vasc Surg*. 2014;**59**(2):315–20. doi: 10.1016/j.jvs.2013.08.036.

190. Krievins D, Thora S, Zarins CK. Gigantic 25-cm abdominal aortic aneurysm. *J Vasc*

Surg. 2015;**61**(4):1067. doi: 10.1016/j.jvs.2014.09.005.

191. Santilli SM, Littooy FN, Cambria R a., *et al.* Expansion rates and outcomes for the 3.0-cm to the 3.9-cm infrarenal abdominal aortic aneurysm. *J Vasc Surg*. 2002;**35**(4):666–671. doi: 10.1067/mva.2002.121572.

192. Reeps C, Pelisek J, Seidl S, *et al.* Inflammatory infiltrates and neovessels are relevant sources of MMPs in abdominal aortic aneurysm wall. *Pathobiology*. 2009;**76**(5):243–52. doi: 10.1159/000228900.

193. Brophy CM, Reilly JM, Smith GJ, Tilson MD. The role of inflammation in nonspecific abdominal aortic aneurysm disease. *Ann Vasc Surg*. 1991;**5**(3):229–33.

194. Treska V, Kocova J, Boudova L, *et al.* Inflammation in the wall of abdominal aortic aneurysm and its role in the symptomatology of aneurysm. *Cytokines Cell Mol Ther*. 2002;**7**(3):91–7. doi: 10.1080/13684730310001652.

195. Humphrey JD, Taylor CA. Intracranial and abdominal aortic aneurysms: similarities, differences and need for a new class of computational models. *Annu Rev Biomed Eng*. 2008;**10**:221–246. doi: 10.1146/annurev.bioeng.10.061807.160439.